

**THE INFLUENCE OF SEQUENCE VARIATION ON VON  
WILLEBRAND FACTOR BIOSYNTHESIS, PROTEOLYTIC  
PROCESSING AND CLEARANCE**

by

Cynthia Marie Pruss

A thesis submitted to the Department of Pathology and Molecular Medicine

In conformity with the requirements for

the degree of Doctor of Philosophy

Queen's University

Kingston, Ontario, Canada

(July, 2010)

Copyright © Cynthia Marie Pruss, 2010

## Abstract

Von Willebrand factor (VWF) promotes platelet adhesion and aggregation at sites of vascular damage. This function is directly related to the multimer size of VWF. The VWF-specific metalloprotease ADAMTS13 decreases VWF multimer size by cleaving at Y1605-M1606 in the VWF A2 domain.

This thesis examined the sensitivity of ADAMTS13 cleavage to mutagenesis of the full-length multimerized VWF substrate, and a small VWF A2 domain fragment, VWF115. The ADAMTS13 cleavage site at Y1605-M1606 was mutated with the most severe loss of cleavage observed in Y1605A/M1606A. In addition, 4 single nucleotide polymorphisms were examined, with D1472H, Q1571H, P1601T proteins all showing increased resistance to cleavage. In contrast, G1643S has enhanced cleavage in the full-length VWF substrate but shows cleavage resistance in VWF115. Three von Willebrand disease mutations were also examined. In patients, R1597W has enhanced ADAMTS13 cleavage and a loss of high molecular weight multimers, while R1205H has enhanced protein clearance resulting in very low VWF levels and Y1584C patients have moderately low VWF levels. R1597W has enhanced cleavage of full-length VWF, while a slight cleavage increase is observed in VWF115 for Y1584C, and no change is seen with R1205H.

The VWF mutations R1597W, Y1605A/M1606A, R1205H and Y1584C were further examined in the VWF knockout mouse using recombinant VWF protein infusion and hydrodynamic delivery of VWF cDNA to determine the effects these mutations produce on VWF antigen levels, multimer structure, secretion, clearance and function in a thrombotic injury model. All four mutations had different pathogenic mechanisms. R1597W showed accelerated clearance with loss of multimer structure, and greatly increased time to thrombotic occlusion. Y1605A/M1606A showed accelerated clearance with normal or supranormal multimer structure,

a loss of thrombotic occlusion but increased platelet accumulation. Y1584C showed no change in protein clearance, with decreased VWF antigen level, reduced multimer structure, and reduced thrombotic potential. R1205H demonstrated a synthetic defect in vitro and in vivo increased clearance with a decrease in VWF antigen levels and normal multimer structure and a variable thrombotic potential. These results validate the use of the genetically-modified VWF knockout mouse model for evaluating the pathogenic mechanisms of putative VWF mutations.

## Co-Authorship

Dr. David Lillicrap oversaw research, and assisted in the editing and writing of the manuscripts.

Mia Golder performed data collection for the hydrodynamic injection mice and analysis of the wild type animals for intravital microscopy.

Carol Hegadorn and Erin Burnett performed the multimer profile analysis of VWF.

Colleen Notley purified the VWF115 proteins and performed the VWF115 digest assays.

Aly Dhala performed the mutagenesis of mouse VWF for Y1584C and performed mouse full-length and VWF115 digest assays as part of his fourth year thesis.

Erin Burnett, Kim Lavery and Kate Sponagle performed protein infusions, hydrodynamic injections, and mouse sampling.

Andrea Bryant performed animal experiments, including the surgeries for intravital microscopy.

Lee O'Brien designed the single amino acid substitutions at Y1605-M1606.

All other work is my own.

## Acknowledgements

I would like to thank Dr. David Lillicrap, my supervisor. His vision and clear guidance have been a great help in my pursuit of my degree. I have learned much about writing, critical thinking, and how to teach from him.

I thank my thesis committee, coworkers and fellow graduate students in the Lillilab. Without them, I would not have been able to finish this work. The veterinary technicians Andrea, Erin, Kim, and Kate: my deepest thanks for dealing with my angry little knockout mice. Carol and Erin, thank you so much for all of the time you spent running my multimers. Colleen, thank you for your work on the VWF115 assay. Christine Brown, thank you for your sense of humor and help in making the recombinant proteins and assistance in plasmid cloning and purification. Mia, thank you for sharing the mouse data collection and analysis with me. I also appreciate your data collection and analysis for the “Seminar time to unconsciousness study.” Angie and Mia, thank you for all of the snacks, coffees, and extra assistance with day-to-day life in the lab.

I thank my family for never once wondering why I was working so hard for this. My parents, Bill and Chris, and my in-laws, John and Kay, were fabulous for watching Sophie when Rob and I needed a helping hand, especially after her surgery so I could keep working in the lab.

I would like to show my deepest gratitude to my husband, Rob. We were married three weeks before the start of graduate school, and I would have been lost without you. Your enthusiasm and support are fantastic. Even more incredible is your ability to still love me even when I am a grumpy mess.

I dedicate this thesis to my daughter Sophie, who has learned more in her three years than I have in the almost six years I have worked on my degree.

# Table of Contents

|  |      |
|--|------|
| Abstract.....  | ii   |
| Co-Authorship .....  | iv   |
| Acknowledgements.....  | v    |
| Table of Contents.....   | vi   |
| List of Figures.....   | xi   |
| List of Tables .....   | xiii |
| List of Abbreviations .....  | xiv  |
| Chapter 1 Introduction to Von Willebrand Factor and ADAMTS13 ..... | 1    |
| 1.1 Introduction to von Willebrand Factor and ADAMTS13 .....       | 1    |
| 1.2 VWF Organization and Structure .....                           | 1    |
| 1.3 Biosynthesis, Intracellular Modification, and Trafficking..... | 2    |
| 1.4 VWF Clearance Mechanisms .....                                 | 7    |
| 1.4.1 Determination of accelerated clearance .....                 | 9    |
| 1.5 Biological activities of VWF .....                             | 10   |
| 1.5.1 Factor VIII .....  | 10   |
| 1.5.2 Subendothelial Matrix.....                                   | 10   |
| 1.5.3 Platelets.....   | 11   |
| 1.5.4 Thrombospondin-1.....  | 11   |
| 1.5.5 Osteoprotegerin.....   | 12   |
| 1.5.6 Additional VWF Interactions.....                             | 13   |
| 1.6 VWF Levels and Activity Assays.....                            | 13   |
| 1.7 ADAMTS13.....  | 14   |
| 1.7.1 ADAMTS13 Production and Levels.....                          | 15   |
| 1.7.2 ADAMTS13-Mediated Cleavage of VWF .....                      | 16   |
| 1.7.3 ADAMTS13 Activity Assays .....                               | 17   |
| 1.8 Von Willebrand Disease .....                                   | 18   |
| 1.8.1 Type 1 VWD.....  | 18   |
| 1.8.2 Type 2 VWD.....  | 18   |
| 1.8.3 Type 3 VWD.....  | 19   |
| 1.9 Thrombotic Thrombocytopenic Purpura.....                       | 19   |
| 1.10 Animal models of von Willebrand Factor and ADAMTS13 .....     | 19   |

|  |    |
|--|----|
| 1.10.1 VWF knockout mouse and mouse VWF .....  | 20 |
| 1.10.2 ADAMTS13 knockout mouse and mouse ADAMTS13 .....  | 20 |
| 1.10.3 Hydrodynamic Delivery.....  | 21 |
| 1.10.4 Intravital Microscopy Experimental Models of Thrombosis .....   | 22 |
| 1.11 Thesis Hypotheses .....   | 22 |
| 1.12 Thesis Objectives .....   | 23 |
| 1.12.1 ADAMTS13-mediated cleavage of von Willebrand Factor .....   | 23 |
| 1.12.2 Mouse models of VWF changes that alter ADAMTS13 mediated cleavage.....  | 23 |
| 1.12.3 In vitro and in vivo models of the type 1 VWD mutations R1205H and Y1584C .....   | 23 |
| Chapter 2 ADAMTS13 cleavage efficiency is altered by mutation and, to a lesser extent,<br>polymorphic sequence changes in the A1 and A2 domains of von Willebrand factor ..... | 24 |
| 2.1 Summary .....  | 24 |
| 2.2 Introduction.....  | 25 |
| 2.3 Materials and Methods.....   | 25 |
| 2.3.1 Plasmid mutagenesis and recombinant protein production.....  | 25 |
| 2.3.2 Proteolysis of rVWF and VWF115 by rADAMTS13.....   | 28 |
| 2.4 Results.....   | 29 |
| 2.4.1 Expression and characterization of VWF and ADAMTS13 protein.....   | 29 |
| 2.4.2 Proteolysis of full-length rVWF by rADAMTS13 .....   | 30 |
| 2.4.3 VWF115 proteolysis by rADAMTS13 .....  | 34 |
| 2.4.4 Effect of Y1605-M1606 cleavage site mutations on ADAMTS13 cleavage.....  | 36 |
| 2.4.5 Effect of VWF Single Nucleotide Polymorphisms on ADAMTS13 Cleavage .....   | 36 |
| 2.4.6 The effect of ADAMTS13 cleavage controls .....   | 37 |
| 2.5 Discussion .....   | 38 |
| 2.6 Acknowledgements.....  | 40 |
| Chapter 3 Evaluation of von Willebrand Factor mutations influencing ADAMTS13-mediated<br>cleavage in a mouse model system: R1597W and Y1605A/M1606A.....                       | 42 |
| 3.1 Summary .....  | 42 |
| 3.2 Introduction.....  | 43 |
| 3.3 Materials and Methods.....   | 44 |
| 3.3.1 Plasmid construction and mutagenesis .....   | 44 |
| 3.3.2 Recombinant protein production and cell culture .....  | 45 |
| 3.3.3 VWF antigen, propeptide and multimer quantitation .....  | 45 |

|  |    |
|--|----|
| 3.3.4 In vitro ADAMTS13 digests.....   | 46 |
| 3.3.5 von Willebrand Factor Studies in VWF Knockout Mice.....                                | 47 |
| 3.3.6 Hydrodynamic injections.....   | 47 |
| 3.3.7 Blood collection.....  | 47 |
| 3.3.8 Recombinant Protein Infusions.....   | 47 |
| 3.3.9 Intravital Microscopy for the Ferric Chloride Injury Model of Thrombosis.....          | 48 |
| 3.3.10 Graphing and Statistical Analysis.....  | 48 |
| 3.4 Results.....   | 49 |
| 3.4.1 Expression and characterization of recombinant proteins.....                           | 49 |
| 3.4.2 ADAMTS13 digests of full-length mouse VWF.....   | 49 |
| 3.4.3 Mouse ADAMTS13 digestion of the mVWF115 substrates.....                                | 51 |
| 3.4.4 Recombinant protein Infusions.....   | 51 |
| 3.4.5 VWF expression via hydrodynamic transgene delivery.....                                | 52 |
| 3.4.6 VWF antigen levels.....  | 53 |
| 3.4.7 VWFpp/VWF:Ag ratio determination.....  | 54 |
| 3.4.8 Multimer Analysis.....   | 55 |
| 3.4.9 Evaluation of in vivo thrombogenesis.....  | 57 |
| 3.5 Discussion:.....   | 58 |
| <b>Chapter 4 Investigating the pathologic mechanisms of the common Type 1 von Willebrand</b> |    |
| <b>Disease mutations R1205H and Y1584C through in vitro and in vivo mouse models.....</b>    |    |
| 4.1 Summary.....   | 63 |
| 4.2 Introduction.....  | 64 |
| 4.3 Materials and Methods.....   | 66 |
| 4.3.1 Plasmid construction and mutagenesis.....  | 66 |
| 4.3.2 Recombinant protein production and cell culture.....                                   | 66 |
| 4.3.3 VWF antigen, propeptide and multimer quantitation.....                                 | 67 |
| 4.3.4 In vitro ADAMTS13 digests of recombinant VWF.....                                      | 68 |
| 4.3.5 Von Willebrand Factor studies in VWF Knockout Mice.....                                | 69 |
| 4.3.6 Hydrodynamic injections.....   | 69 |
| 4.3.7 Blood collection.....  | 69 |
| 4.3.8 Recombinant mVWF Protein Infusions.....  | 70 |
| 4.3.9 Intravital Microscopy for the Ferric Chloride Injury Model of Thrombosis.....          | 70 |
| 4.3.10 Graphing and Statistical Analysis.....  | 71 |

|   |     |
|---|-----|
| 4.4 Results.....  | 71  |
| 4.4.1 Expression and characterization of recombinant proteins .....   | 71  |
| 4.4.2 In vitro ADAMTS13 digests of recombinant VWF.....   | 73  |
| 4.4.3 Recombinant Mouse VWF Protein Infusions .....   | 75  |
| 4.4.4 Hydrodynamic Injections.....  | 76  |
| 4.4.5 VWF Antigen Levels .....  | 76  |
| 4.4.6 VWF propeptide to VWF Antigen Ratios.....   | 78  |
| 4.4.7 Multimeric structure.....   | 79  |
| 4.4.8 Evaluation of in vivo thrombogenesis .....  | 81  |
| 4.5 Discussion .....  | 82  |
| Chapter 5 Thesis Discussion.....  | 88  |
| 5.1 Summary .....   | 88  |
| 5.2 ADAMTS13-mediated cleavage is altered by VWF Variants .....   | 89  |
| 5.2.1 VWF Polymorphisms.....  | 95  |
| 5.2.2 ADAMTS13 cleavage site mutations .....  | 96  |
| 5.2.3 Known von Willebrand Disease Mutations .....  | 98  |
| 5.2.4 In vitro mouse ADAMTS13 studies .....   | 99  |
| 5.3 In Vivo Mouse Studies.....  | 100 |
| 5.4 Future applications and Conclusions .....   | 104 |
| References.....   | 106 |
| Appendix A VWF knockout mice have a low incidence rate of high-titre anti-VWF antibodies<br>post-hydrodynamic injection ..... | 126 |
| A.1 Summary .....   | 126 |
| A.2 Introduction.....   | 127 |
| A.3 Materials and Methods.....  | 128 |
| A.3.1 Mice .....  | 128 |
| A.3.2 Hydrodynamic injections .....   | 128 |
| A.3.3 Blood collection .....  | 128 |
| A.3.4 ELISA Assays.....   | 129 |
| A.3.5 Control Plasmas .....   | 130 |
| A.3.6 Graphing and Statistical Analysis .....   | 130 |
| A.4 Results.....  | 130 |
| A.5 Discussion .....  | 134 |

|  |     |
|--|-----|
| Appendix B Thesis Protocols.....                 | 137 |
| B.1 HEK293T Calcium Phosphate Transfections..... | 137 |
| Day -1: Plating Cells.....                       | 138 |
| Day 0: Transfection.....                         | 138 |
| Day 1: Medium Change.....                        | 139 |
| Day 4: Medium and cell harvest.....              | 139 |
| B.2 VWF Antigen ELISA Assay.....                 | 140 |
| B.3 Mouse VWF Propeptide ELISA protocol.....     | 143 |
| B.4 Anti-VWF Antibody ELISA Protocol.....        | 145 |
| B.5 ADAMTS13 Activity ELISA Protocol.....        | 147 |

## List of Figures

|   |     |
|---|-----|
| Figure 1.1 A diagram of the functional domains of VWF. ....   | 2   |
| Figure 1.2. The processing steps involved in the biosynthesis of VWF. ....  | 3   |
| Figure 1.3 Schematic diagram of ADAMTS13. ....  | 15  |
| Figure 2.1 Recombinant VWF has ultra-large (UL) VWF multimers in both wild type and mutant forms. ....  | 30  |
| Figure 2.2 Multimer Analysis of ADAMTS13 Digestion of Full-Length Wild Type VWF. ....   | 31  |
| Figure 2.3 Analysis of ADAMTS13 Digestion of Full-Length VWF. ....  | 32  |
| Figure 2.4 Data for Analysis of ADAMTS13 Digestion of Full-Length VWF. ....   | 33  |
| Figure 2.5 ADAMTS13 concentrations necessary for 50% loss of intact VWF115. ....  | 34  |
| Figure 2.6 Data for the Analysis of the ADAMTS13 concentrations necessary for 50% loss of intact VWF115. ....                                 | 35  |
| Figure 3.1 ADAMTS13 Digestion of Full-Length mVWF and mVWF115. ....   | 50  |
| Figure 3.2 Recombinant Mouse VWF Protein Clearance. ....  | 52  |
| Figure 3.3 Mouse VWF antigen levels post-hydrodynamic injection. ....   | 53  |
| Figure 3.4 VWFpp/VWF:Ag ratio determination. ....   | 54  |
| Figure 3.5 Hydrodynamic VWF Multimer Structure. ....  | 56  |
| Figure 3.6 Thrombogenesis in response to ferric chloride injury. ....   | 58  |
| Figure 4.1 Expression of human and mouse recombinant VWF. ....  | 72  |
| Figure 4.2 Analysis of ADAMTS13 Digestion of Full-Length mVWF and mVWF115. ....   | 74  |
| Figure 4.3 Recombinant Mouse Protein Clearance. ....  | 75  |
| Figure 4.4 Mouse VWF antigen levels post-hydrodynamic injection. ....   | 77  |
| Figure 4.5 VWFpp/VWF:Ag ratios for hydrodynamic mVWF. ....  | 78  |
| Figure 4.6 Hydrodynamic mVWF Multimer Structure. ....   | 80  |
| Figure 4.7 Thrombogenesis in response to ferric chloride injury. ....   | 81  |
| Figure 5.1 Sketch of the A2 domain illustrates the secondary structural organization. ....  | 90  |
| Figure 5.2 Crystal structure of the A2 domain showing amino acids of interest. ....   | 91  |
| Figure 5.3 ADAMTS13-VWF interactions. ....  | 92  |
| Figure A 1 Anti-VWF antibody ELISA control plasma results. ....   | 131 |
| Figure A 2 Anti-VWF antibody and VWF antigen levels for antibody-positive VWF <sup>(-/-)</sup> mice receiving wild type <i>Vwf</i> cDNA. .... | 132 |

Figure A 3 Anti-VWF antibody and VWF antigen levels for antibody-positive VWF<sup>(-/-)</sup> mice  
receiving mutant *Vwf* cDNA..... 133

Figure A 4 Anti-VWF antibody and VWF antigen levels for antibody-positive VWF<sup>(-/-)</sup> mice  
receiving mutant R1205H *Vwf* cDNA. .... 134

## List of Tables

|   |     |
|---|-----|
| Table 2.1 Summarized results of rADAMTS13-mediated digestion.....                       | 27  |
| Table 5.1 Summary of <i>VWF</i> mutations and polymorphisms examined in the thesis..... | 94  |
| Table 5.2 Summary of mouse ADAMTS13 digest results. ....                                | 100 |

## List of Abbreviations

|                 |  |
|-----------------|--|
| $\mu$           | micro  |
| ADAMTS13        | <b>A</b> <b>d</b> isintegrin-like <b>and</b> <b>m</b> etalloprotease with <b>t</b> hrombos <b>s</b> pondin type 1 motif, 13 <sup>th</sup> member |
| <i>ADAMTS13</i> | human ADAMTS13 gene  |
| <i>Adamts13</i> | mouse ADAMTS13 gene  |
| aVWS            | acquired von Willebrand syndrome   |
| ET              | a synthetic hepatocyte-specific enhancer and murine transthyretin promoter   |
| FVIII           | coagulation factor VIII  |
| GPIb $\alpha$   | glycoprotein Ib $\alpha$ receptor on platelets   |
| GST             | glutathione-S-transferase  |
| HMW             | high molecular weight  |
| L               | liter  |
| m               | milli  |
| M               | molar (moles/liter)  |
| OPG             | osteoprotegerin  |
| Pa              | Pascals  |
| proVWF          | unprocessed protein consisting of VWF propeptide and mature VWF protein.   |
| TSP1            | thrombospondin-1   |
| TTP             | thrombotic thrombocytopenic purpura  |
| ULVWF           | ultralarge von Willebrand factor multimers   |
| VWD             | von Willebrand disease   |
| VWF             | von Willebrand factor  |
| <i>VWF</i>      | human von Willebrand factor gene   |
| <i>Vwf</i>      | mouse von Willebrand factor gene   |
| VWF73           | GST- and histidine-tagged 73 amino acid VWF A2 fragment, D1596-R1668   |
| VWF115          | GST- and histidine-tagged 115 amino acid VWF A2 fragment, E1554-R1668  |
| VWF:Ag          | von Willebrand factor antigen  |
| VWFpp           | von Willebrand factor propeptide (VWF antigen II)  |
| VWFpp/VWF:Ag    | ratio of VWF propeptide levels to VWF antigen levels   |
| VWF:RCo         | von Willebrand factor ristocetin cofactor activity   |

# Chapter 1

## Introduction to Von Willebrand Factor and ADAMTS13

### 1.1 Introduction to von Willebrand Factor and ADAMTS13

Von Willebrand factor (VWF) is a large multimeric glycoprotein with a critical role in maintaining hemostasis. VWF serves as the carrier protein for the plasma coagulation protein factor VIII (FVIII) and promotes platelet adhesion and aggregation at the sites of vascular damage.<sup>1</sup> The hemostatic potential of VWF greatly increases with the multimer size, which is tightly regulated *in vivo* by the metalloprotease ADAMTS13.<sup>2-4</sup> A qualitative or quantitative defect in VWF results in von Willebrand disease, the most common inherited bleeding disorder, with a prevalence rate of approximately 1 in 1000.<sup>5</sup> This chapter explains how VWF is produced and cleared, VWF protein interactions, and how ADAMTS13-mediated cleavage takes place. In addition, animal models of VWF and pathological conditions are explored.

### 1.2 VWF Organization and Structure

The *VWF* gene is located on chromosome 12p13.2, and contains 52 exons and spans approximately 180 kb.<sup>6</sup> The VWF propeptide consists of the D1 and D2 domains, while the mature VWF monomer consists of D'-D3-A1-A2-A3-D4-B1-B2-B3-C1-C2-CK (cysteine knot motif) (Figure 1.1). These domains allow VWF to interact with other molecules both within the cell as well as in the circulation. These interactions may require conformational changes in VWF domains, that occur at a specific pH or when VWF is interacting with other binding partners, as elaborated in greater detail below.

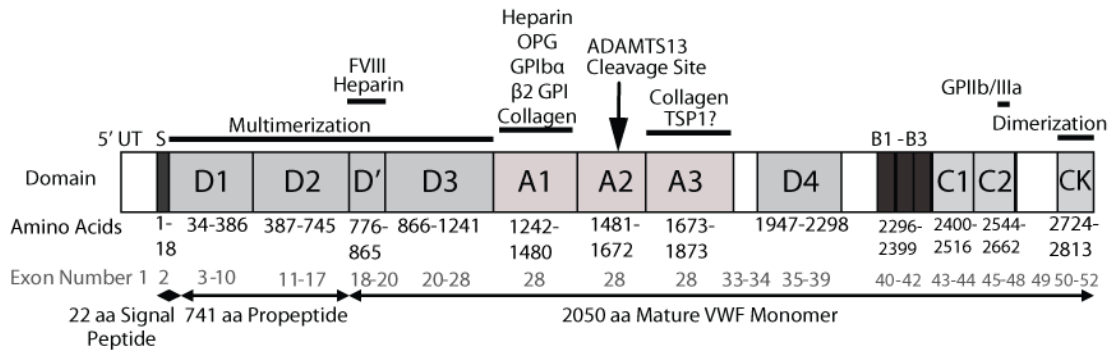


**Figure 1.1 A diagram of the functional domains of VWF.**

Areas of VWF are listed above that interact with other proteins, while the exons corresponding to the different domains are listed below in gray. Adapted from the International Society on Thrombosis and Haemostasis Scientific and Standardization Committee (ISTH SSC) VWF database (<http://www.vwf.group.shef.ac.uk/>).<sup>7, 8</sup>

### 1.3 Biosynthesis, Intracellular Modification, and Trafficking

VWF is produced in both endothelial cells and megakaryocytes, and originates from the precursor VWF protein, proVWF. The processing of proVWF produces both the mature VWF protein, as well as the VWF propeptide (VWFpp), also referred to as VWF antigen II. A loss of the biosynthetic processing or post translational modification can be caused by mutations which lead to a qualitative loss of function or a quantitative reduction of VWF, producing a form of von Willebrand Disease (VWD).<sup>1</sup>

VWF is a typical example of a secreted protein, since the molecular events associated with the biosynthesis and secretion follow a pathway generally used by many other proteins that are externalized from the cell. However, a portion of VWF follows a different pathway by the very specific storage in the Weibel-Palade bodies of endothelial cells and the  $\alpha$ -granules of megakaryocytes.<sup>9</sup> This biosynthetic pathway is outlined in Figure 1.2.

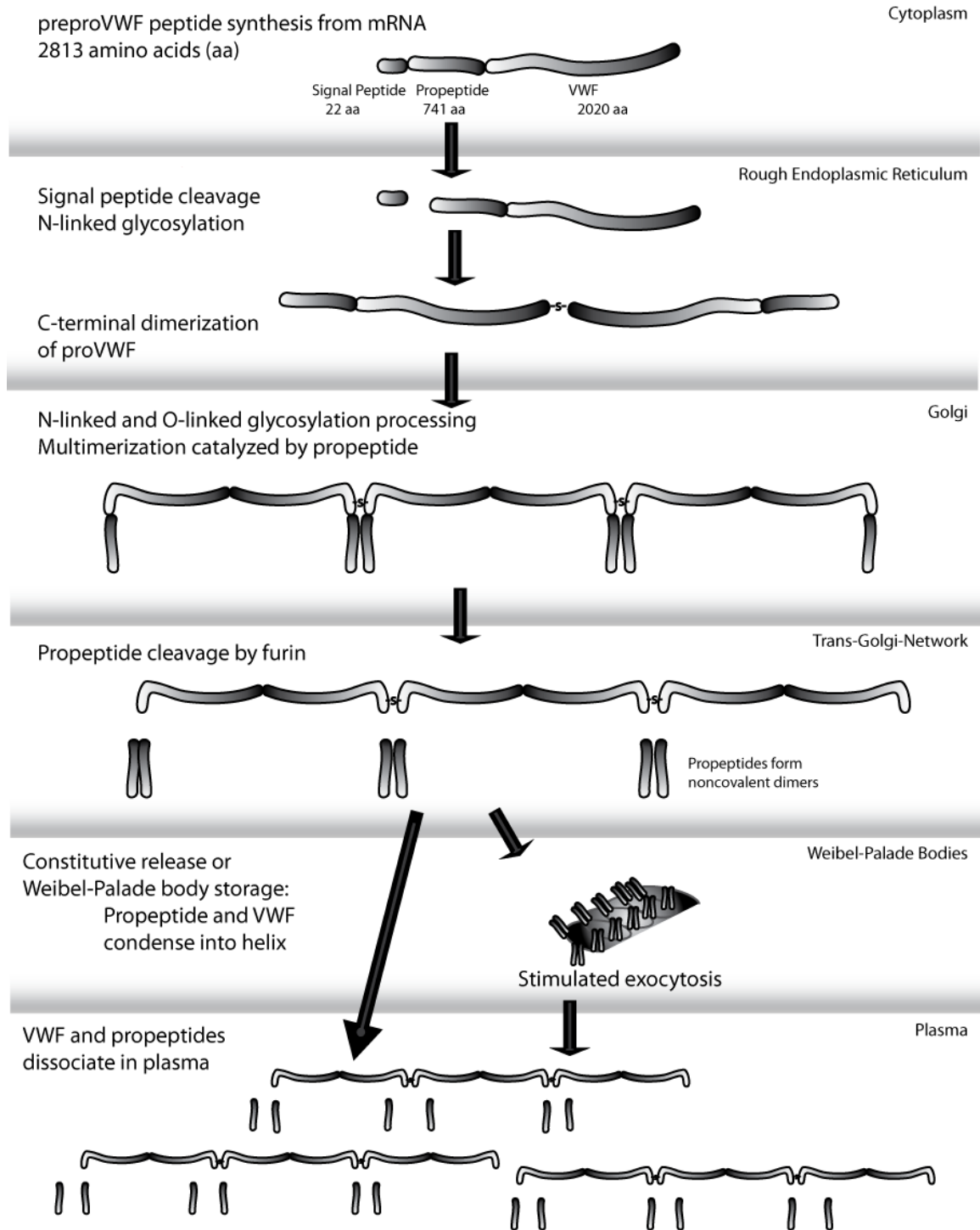


**Figure 1.2. The processing steps involved in the biosynthesis of VWF.**

–S– represents disulfide bonds. Adapted from Romani de Wit and van Mourik, 2001.<sup>9</sup>

The molecular events in VWF biosynthesis are well organized. The mRNA is translated at the rough endoplasmic reticulum as a 2,813 amino acid precursor protein, which is composed of a 22 amino acid signal peptide, a 741 amino acid propeptide, and the mature VWF molecule of 2,050 amino acids, known as preproVWF. The protein consists of several repeated domain types, which provide the framework for VWF's secondary and tertiary structure, as well as its many functional domains (see Figure 1.1).<sup>1</sup>

After translocation into the endoplasmic reticulum (ER), the signal peptide is removed by signal peptidases. At this point, the primary translation product undergoes N-linked glycosylation at 12 sites. VWF is unusual because unlike other plasma glycoproteins, VWF contains ABO blood group asparagine-linked oligosaccharides.<sup>10</sup> Inhibition of N-glycosylation by tunicamycin causes proVWF monomers to accumulate in the ER, showing that this event occurs before dimerization.<sup>11</sup>

The dimerization of VWF occurs through disulfide bonds near the carboxyl termini of proVWF monomers. This "tail-to-tail" linkage requires sequences in only the last 150 amino acids.<sup>12,13</sup> The carboxyl-terminal 90 amino acids comprise the "CK" domain that is homologous to the "cysteine knot" superfamily of glycoproteins.

At this point the proVWF dimers are transported to the Golgi apparatus. In the Golgi, the completion of O- and N-linked glycosylation occurs. The majority of the O-linked glycans consist of sialylated T-antigen, a mucin-type core 1 structure.<sup>14</sup> This is followed by multimerization and removal of the VWF propeptide.<sup>1</sup> Sulfation of certain N-linked glycosyl groups probably occurs in the trans-Golgi network.<sup>1</sup>

The acidic pH of the Golgi apparatus is necessary to form the additional "head-to-head" disulfide bonds in the D3 domains near the amino termini of the subunits, yielding multimers that may exceed 20,000 kDa in size. The D1 domain in the propeptide has been established to be important in this process.<sup>15,16</sup> Furthermore, it appears that the D1-D2 domains form transient intrachain disulfide bonds with the D'-D3 domains, providing a covalent oxidoreductase

intermediate. The VWF propeptide contains two *CXXC* domains, the signature sequence for oxidoreductases, which are necessary for disulfide bond formation under the acidic conditions of the Golgi apparatus.<sup>16</sup> Efficient multimerization is critical to the proper secretion and function of VWF.

Additional modifications in the Golgi apparatus or trans-Golgi network include the proteolytic removal of the large propeptide after a pair of dibasic amino acids (Lys-Arg) at residue 763 by a member of the subtilisin-related propeptide-processing enzyme family. Members which cleave VWF include the protease furin, also known as PACE, or another member of the same protease family, like PACE4, both of which have been demonstrated to cleave VWF *in vitro*.<sup>17, 18</sup> Mutations of either of the VWF dibasic residues before the cleavage site, amino acid 763, results in a reduction of the cleavage rate of furin, showing that the site requires conservation.<sup>19</sup> Moreover, an Arg760Cys mutation in a patient results in a loss of cleavage as well. The heterozygous patient showed both processed and unprocessed VWF in the plasma, with a reduction in VWF multimers, a mild decrease in plasma VWF and FVIII, as well as a decrease in the affinity for VWF to bind FVIII.<sup>20</sup> This decrease in FVIII binding is due to the FVIII binding site being physically blocked by the propeptide not being removed, resulting in steric hindrance.

In general, the majority of VWF is constitutively secreted from the cell. This is normally a smaller molecular weight population of VWF molecules that often has not been fully processed, with the VWF propeptide still attached to the mature VWF peptide in some molecules.<sup>21</sup> The higher molecular weight, functionally more potent, VWF is instead transported into storage bodies. At this point the VWFpp serves as a molecular chaperone for sorting VWF to the storage granules by binding with noncovalent linkages in equimolar concentrations.<sup>22, 23</sup> This stimulates condensation of the VWF multimer into a right turn helix using noncovalently paired VWF propeptides associated with pairs of VWF D<sup>2</sup>-D3 domains to facilitate the packing at the acidic pH of the trans-Golgi network.<sup>23</sup> In fact, when the VWFpp is expressed alone, it will segregate to these storage granules, whereas mature VWF expressed in the absence of VWFpp does not.

However, if expressed *in cis* or *in trans*, the mature VWF and the VWFpp are co-localized in the storage granule.<sup>24</sup> The areas of interaction are between amino acids 386-477 of the VWF propeptide, in the start of the D2 domain, and between amino acids 866-907 of the D3 domain of mature VWF.<sup>25</sup> The Weibel-Palade bodies appear to bud off from the Golgi network, and VWFpp and VWF are the driving force behind this formation.<sup>22</sup>

Besides VWF and the VWF propeptide, other proteins in the Weibel-Palade bodies include osteoprotegerin, which binds to VWF A1 domain,<sup>26</sup> P-selectin for leukocyte adhesion, endothelin for vasoconstriction, CD63 for cell adhesion and migration, interleukin-8 for inflammatory reactions, the primarily antagonistic, vessel-destabilizing Tie-2 ligand Angiopoietin-2,<sup>27</sup> and tissue-type plasminogen activator which initiates fibrinolysis.<sup>22</sup> These all contribute to the thrombotic and inflammatory responses that occur upon release of the contents of Weibel-Palade bodies.

Weibel-Palade body exocytosis is stimulated by shear forces or molecular signaling. In vitro studies have established that short term increases in shear rate, similar to forces found in a damaged vessel with a growing thrombus, will stimulate exocytosis.<sup>28,29</sup> This release is proportional to the force applied, with shear rates of 1.2 Pa producing greater than 400% more VWF compared to the static control, compared to that of 0.2 Pa at 140% above control.<sup>28</sup> Longer term application of higher shear rates will lead to greater overall VWF expression in the cell, a state mimicking that of the arterial vasculature.<sup>29</sup> For a short-time shear stimulation, both 0.2 Pa and 1.0 Pa shear stresses induced a release of VWF from the endothelial cells. In contrast, after 24 hours, VWF levels were much higher in the cells receiving exposure to 1.0 Pa shear flow than that in the cells exposed to 0.2 Pa for 24 hours.<sup>29</sup>

Weibel-Palade body exocytosis has been shown to be stimulated by a large number of molecules. Divalent cationic calcium secretagogues such as histamine and thrombin stimulate release of VWF from Weibel-Palade bodies.<sup>1</sup> Xanthine oxidase treatment, which generates superoxide radicals, creates a rapid, sustained increase of intracellular free calcium. This

suggests that the release of VWF from storage granules is caused by calcium mobilization from intracellular stores.<sup>30</sup> The cAMP-raising substances also cause exocytosis, and include epinephrine and vasopressin.<sup>1</sup> The drug desmopressin (1-deamino-8-D-arginine vasopressin [DDAVP]), a vasopressin analog, also produces a rapid release of VWF from the Weibel-Palade bodies into the blood stream, by activating the vasopressin V2 receptor.<sup>9</sup> The small GTP-binding protein Ra1 has been shown to participate further down the pathway that regulates cAMP-mediated exocytosis.<sup>31</sup> Sphingosine 1-phosphate, a lysophospholipid secreted by platelets, monocytes, and mast cells not only regulates angiogenesis, vascular permeability, and vascular tone, but also promotes vascular inflammation via Weibel-Palade body exocytosis which releases factors like VWF that cause thrombosis and other factors that leads to inflammation.<sup>32</sup> Similar molecular processes have also been shown with ceramide and vascular endothelial growth factor (VEGF) leading to Weibel-Palade body exocytosis.<sup>33, 34</sup> Upon release from the cell, the tightly packed VWF multimer-propeptide helix dissociates under physiologic pH.<sup>23</sup> VWF circulates at approximately 10 µg/ml, defined at 1 unit/ml, and has a half life of 8-12 hours.<sup>1</sup>

VWF is cleaved in the plasma after release from the cell. Partially processed proVWF substrates that are constitutively expressed are processed by thrombin and its precursor, meizothrombin, which removes any remaining VWF propeptide.<sup>21</sup> Thrombin inhibitors do not entirely halt this process *in vivo* in a mouse model, so it is likely that other proteases are also involved.<sup>21</sup> VWF is degraded by the serine proteases plasmin and elastase, which have a high activity to bound VWF, and a more limited activity to VWF in medium.<sup>35</sup> VWF is also cleaved in circulation by the protease, ADAMTS13.<sup>3, 4</sup>

#### **1.4 VWF Clearance Mechanisms**

The exact mechanisms that clear VWF from the circulation are not currently understood. However, some aspects of this process have been explored experimentally. Mature VWF circulates at about 10 µg/mL with a half-life of 8 to 12 hours.<sup>36</sup> The clearance rates of both high

and low molecular weight VWF have been explored in the VWF knockout mouse, and are similar to that of VWF with a full multimeric range.<sup>37</sup> This suggests that ADAMTS13 cleavage probably does not affect the VWF:Ag levels. Truncated variants, deleting various regions of VWF, increased clearance with the deletion of the D<sup>1</sup>-D3 portion, and decreased clearance with the elimination of the distal D4-CK domains.<sup>37</sup>

The overall glycosylation profile of VWF is a prominent factor that influences VWF plasma levels.<sup>38</sup> One of the strongest determinants of VWF level is that of ABO blood group status. Type O individuals have 25% lower VWF levels compared to Types A, B and AB, due to accelerated clearance rates.<sup>39,40</sup> Bombay blood type individuals, lacking H antigen, have even lower VWF levels.<sup>41</sup> Reduced sialylation on VWF also leads to decreased VWF levels.<sup>38</sup> The O-linked glycosylation of VWF is clustered mainly around the A1 domain, and negatively impacts platelet interactions.<sup>42</sup> This is mainly sialylated tumor-associated T-antigen.<sup>14</sup> An inverse relationship between amount of O-linked T-antigen glycans and VWF levels has been demonstrated in several different diseases, including liver cirrhosis and type 1 VWD.<sup>38</sup>

Von Willebrand factor mutations have also been linked to increased clearance. Several cysteine mutations, C1130F, C1149R, and C2971Y have accelerated clearance, but no alterations in ADAMTS13 mediated cleavage.<sup>43</sup> The Vicenza mutation R1205H also has a dramatically decreased half life of only 2-4 hours in patients.<sup>44</sup> Additional mutations that accelerate clearance are being identified using the two assays identified below, using Type 1 VWD patient populations.<sup>36,45</sup>

Currently, no definitive information is available describing the cells or receptors involved with VWF clearance. Intravenous injection of VWF into the VWF knockout mouse shows most accumulation in the liver, as well as spleen and kidney.<sup>37</sup> Preliminary results indicate that macrophages in the liver and spleen are the dominant cell type to endocytose VWF.<sup>38</sup> Blockade of phagocytic cells, such as the liver sinusoidal Kupffer cells, will delay clearance of VWF and

FVIII.<sup>46</sup> Genome-wide association studies have also linked VWF levels to the genes *SCARA5*, a scavenger receptor molecule on epithelial cells that initiates immune responses, and *STAB2*, a transmembrane receptor expressed in liver and spleen sinusoidal endothelial cells, that binds and subjects ligands to endocytosis.<sup>47</sup>

#### **1.4.1 Determination of accelerated clearance**

Pathological conditions can arise when VWF clearance rates are accelerated, with multiple Type 1 VWD mutations falling in this category. Different methodologies exist to establish if there is a clearance mechanism with lowered VWF antigen levels.

The first measures the desmopressin (DDAVP; 1-desamino-8-D arginine vasopressin) response. Upon administration of DDAVP, VWF antigen levels increase 2- to 4-fold, but may be much higher.<sup>48, 49</sup> DDAVP-stimulated release of stored VWF is monitored in the patient over a time course, with an initial peak value being determined as well as the half life of the released VWF.<sup>49</sup>

The second method utilizes the VWF propeptide to VWF antigen ratio, determined via ELISA.<sup>36</sup> The VWF propeptide has a circulating concentration of approximately 1 µg/ml (1 U/mL VWFpp) with a half life of 2 to 3 hours, and is released in equimolar concentrations to VWF. Mature VWF circulates at about 10 µg/mL (1 U/mL VWF antigen) with a half-life of 8 to 12 hours.<sup>36</sup> The normal range of VWFpp is 0.55-2.19 U/ml in a normal cohort, and the VWFpp/VWF:Ag ratio is 1.26, with a normal range of 0.54 to 1.98.<sup>36</sup> Type 1 VWD patients with known decreased VWF survival have VWFpp/VWF:Ag ratios that can be in excess of 10.<sup>45, 50</sup>

A third method involves injecting wild type and mutant VWF proteins into the VWF knockout mouse.<sup>37</sup> Initial experiments used radio-labeled human recombinant proteins to determine clearance rates of wild type and R1205H VWF, showing mean residence times of 2.8 hours and 0.3 hours respectively.<sup>37</sup>

## **1.5 Biological activities of VWF**

Although not an enzyme, von Willebrand factor has several key biological functions that involve binding to a variety of ligands involved in the hemostatic process: it serves as a molecular chaperone to factor VIII, binding to subendothelial matrix proteins and platelet receptors to assist in primary hemostasis, as well as binding to other molecules. The multimer structure of VWF is reduced by ADAMTS13 and Thrombospondin 1.

### **1.5.1 Factor VIII**

Factor VIII is a participant in the intrinsic pathway of the coagulation cascade, and a deficiency of FVIII activity results in Hemophilia A.<sup>51</sup> VWF-FVIII binding is critical to extending the circulating half life of the FVIII cofactor. This non-covalent interaction binds with a Kd of 200 to 400 pM, and all multimer sizes of VWF can bind FVIII.<sup>1</sup> Association rates are relatively rapid so exogenously delivered FVIII will bind endogenous VWF in vivo within approximately 2 seconds.<sup>1</sup> This leaves approximately 5% of plasma FVIII to be free in the circulation.

In the absence of VWF, FVIII is prematurely inactivated by activated protein C. FVIII activity drops below 10% of normal, and the normal FVIII half life of 12 hours drops to 2 hours.<sup>51,52</sup> Mutations preventing VWF propeptide cleavage or in the D3 domain, where the FVIII binding site is located will prevent the VWF-FVIII complex from occurring.<sup>20, 53, 54</sup>

### **1.5.2 Subendothelial Matrix**

VWF has the ability to bind collagen, fibronectin, decorin, and heparin-like molecules in the A1 domain.<sup>55</sup> The A3 domain also binds fibrillar type collagens I and III.<sup>56</sup> These matrix proteins are found under the endothelial layer in the cardiovascular system. In the event of denudation of the endothelium due to vessel injury, the VWF present will bind to these proteins,

facilitating the ability for the platelet plug to form. VWF present in fibrillar collagen enhances platelet adhesion to collagen and collagen-induced platelet aggregation.<sup>57</sup>

### 1.5.3 Platelets

The main function of VWF is to mediate adhesive interactions of platelets exposed to rapid blood flow and exposed subendothelial components. There are two platelet receptors for VWF: the glycoprotein Ib $\alpha$  (GPIb $\alpha$ ) in the GP IB-IX-V complex that binds to the VWF A1 domain, and the integrin  $\alpha_{IIb}\beta_3$  (GP IIb-IIIa complex) that binds to the terminal end of the VWF C1 domain.<sup>1, 58</sup>

When VWF is bound to the subendothelial matrix, the GP IB-IX-V complex is the only receptor on resting platelets that has significant affinity. The VWF A1 domain is required to undergo a conformation change from low binding to high binding, normally stimulated by shear stress or collagen binding.<sup>1</sup> This conformation change occurs optimally under high fluid shear stress,<sup>58, 59</sup> or *in vitro* using ristocetin<sup>60</sup> or botrocetin.<sup>61</sup> After initial binding to VWF, platelets will roll across the surface, resulting in more interactions with platelet receptors, resulting in platelet tethering. This then leads to platelet activation and mobilization of the GP IIb-IIIa complex to the platelet surface, as well as release of platelet  $\alpha$ -granules. This will further increase the platelet binding to the site of injury, and recruit more platelets.<sup>1</sup>

### 1.5.4 Thrombospondin-1

Thrombospondin-1 (TSP1) is an extracellular matrix homotrimeric glycoprotein expressed in many cells and tissues.<sup>62</sup> TSP1 is highly expressed in platelet alpha-granules along with VWF.<sup>62</sup> Murine TSP1<sup>(-/-)</sup> platelet studies have revealed that TSP1 is redundant for platelet aggregation, but that it reinforces and stabilizes platelet aggregation and plug formation under shear stress.<sup>62</sup> ADAMTS13 has sequence homology to TSP1 and contains 1 TSR1 and 6 TSR2 repeats. TSP1, locally released by activated platelets with VWF, competes with ADAMTS13

during VWF proteolysis and controls the degree of VWF multimer processing. In addition, TSP1 and VWF both interact with the platelet GPIb/V/IX membrane complex, primarily under flow conditions. These interactions control the recruitment of platelets to (sub)-endothelial VWF and TSP1, exposed to the circulation, as a consequence of vascular inflammation and endothelial injury. TSP1-VWF interactions do not strictly enhance platelet recruitment and secreted TSP1 even weakly competes with the dynamic platelet rolling and adhesion onto VWF. In addition, TSP1 is critical in preventing atherosclerosis, since TSP1 deficiency accelerates plaque formation by preventing normal phagocytosis.<sup>63</sup>

The roles that TSP1 plays in promoting platelet aggregation are complex, but the most important in VWF regulation is TSP1's role in ADAMTS13-mediated VWF multimer processing. This effect is mitigated by TSP1 being able to reduce VWF multimer size by cleaving the disulfide bonds that hold the multimer subunits together.<sup>64</sup> This appears to be an activity present following the activation of platelets, since TSP<sup>(-/-)</sup> mouse platelets upon activation have higher collagen and VWF-mediated aggregation under static and shear conditions.<sup>65</sup>

### **1.5.5 Osteoprotegerin**

Osteoprotegerin (OPG, also referred to as TNFRSF11B) is central to bone turnover via its role as an inhibitor of the receptor activator of nuclear factor  $\kappa$ B Ligand (RANKL).<sup>66</sup> OPG can promote cell survival by inhibiting TNF-related apoptosis-inducing ligand (TRAIL)-induced apoptosis.<sup>66</sup> OPG is co-expressed with VWF in endothelial cells, associates intracellularly with the VWF A1 domain and is stored in Weibel-Palade bodies.<sup>26, 67</sup> This association is retained upon release in the circulation. It has been demonstrated in vitro that the VWF-FVIII complex can inhibit OPG inhibitory activity upon the TRAIL-induced apoptosis by interfering with OPG binding to the protein RANKL.<sup>68</sup> In addition, OPG has binding affinity for a variety of extracellular matrix proteins, including collagen I and IV, vitronectin, fibronectin, laminin, heparin, and thrombospondin 1.<sup>26</sup> This association with thrombospondin could alter

thrombospondin-mediated regulation of VWF. The OPG-TSP1 complex could result in a change in ADAMTS13-mediated cleavage, or by altering the TSP thiol-reductase activity on VWF, with either of these effects affecting VWF multimer size at the sites of platelet activation.<sup>26</sup> However, the effects of VWF-OPG binding in vivo on bone remodeling, cancer development, thrombosis, hemostasis, or vascular pathology has yet to be determined.

### **1.5.6 Additional VWF Interactions**

Heparin binding in the A1 domain has been identified to be located in the same region as GPIb binding.<sup>69,70</sup> This could cause competition, and result in a decrease in platelet binding in patients undergoing heparin therapy.

The A1 domain of VWF also interacts with sulfatides, 3-sulfated galactosyl ceramides that are expressed on oligodendrocytes, renal tubular cells, certain tumor cells, and platelets. The binding site involves residues in the region of 1392-1423, and overlaps platelet GPIb and botrocetin binding sites.<sup>71</sup> This binding can compete with GPIb binding, or serve as a VWF binding site with no A1 domain conformation change under pathological conditions.<sup>71</sup>

VWF-platelet binding can be inhibited by  $\beta_2$ -glycoprotein I ( $\beta_2$  GPI, also known as Apolipoprotein H), which binds to the A1 domain of VWF.<sup>72</sup>  $\beta_2$  GPI interacts with resting VWF at low affinity. In contrast,  $\beta_2$  GPI binds with high affinity to VWF in its GpIb $\alpha$ -binding conformation, or active form. When in complex with  $\beta_2$  GPI, VWF is unable to induce platelet agglutination or to act as an adhesive surface for platelets at physiologic shear rates, suggesting that  $\beta_2$  GPI prevents VWF from binding to GpIb.<sup>72</sup>

## **1.6 VWF Levels and Activity Assays**

VWF plasma protein levels are reported as VWF antigen (VWF:Ag). The mean population VWF antigen level (VWF:Ag) is 1 U/mL, approximately 10  $\mu$ g/ml.<sup>36</sup> The range of

VWF levels is between approximately 0.5 and 2.0 U/mL for 95% of normal individuals. Levels below 0.5-0.3 U/ml are considered pathologic.<sup>73</sup>

There are assays to measure the binding activities of VWF. Ristocetin cofactor activity (VWF:RCO) measures the ability of VWF to bind to GpIb in the presence of ristocetin. Ristocetin induced platelet aggregation (RIPA) measures the ability patient platelet rich plasma to aggregate at varying doses of ristocetin. Aggregation at low doses of 0.5 mg/mL indicates 2B or platelet-type VWD. FVIII binding capacity (VWF:FVIII) will yield reduced values in the case of 2N VWD. VWF collagen binding (VWF:CB) measures collagen binding capacity. Reduced values correlate with reduction in HMW multimers. Multimer profile analysis can indicate reduction in multimerization, high molecular weight multimer loss, enhanced or reduced ADAMTS13 cleavage, enhanced clearance and mutations that replace/introduce cysteine residues, affecting disulfide bonding.<sup>73</sup>

## 1.7 ADAMTS13

ADAMTS13 is the thirteenth member of the A disintegrin-like and metalloprotease with thrombospondin type 1 motif family of proteases. VWF is the only known substrate for ADAMTS13. ADAMTS13 only cleaves VWF between Tyr1605-Met1606, and maintains plasma VWF within a normal molecular weight range by cleaving high molecular weight (HMW) multimers soon after they are secreted into the plasma, preventing spontaneous platelet agglutination. The identification of ADAMTS13 as the VWF-cleaving protease was made in 1998,<sup>74, 75</sup> with rapid progress in the expression of the cDNA sequence in 2001.<sup>3, 4</sup> The human gene, located on chromosome 9q34 close to the ABO blood group locus, spans approximately 37 kb and contains 29 exons. The mRNA transcript encodes a polypeptide with 1,427 amino acid residues, including a 29 amino acid signal peptide, 45 amino acid propeptide that is cleaved by furin, and the 1,353 amino acid mature ADAMTS13.<sup>4</sup> The functional role for the ADAMTS13 propeptide is unclear, since it is not required for folding or secretion, and does not perform the

common function of maintaining enzyme latency, since ADAMTS13 that has been manipulated to retain the propeptide has similar activity to fully processed, mature ADAMTS13.<sup>76</sup> Mature ADAMTS13 is organized into the metalloprotease domain, followed by the disintegrin-like domain, first TSP1 repeat, cysteine-rich domain, spacer domain, TSP1 repeats 2-8, and finally 2 CUB domains (Figure 1.3).<sup>4</sup>



**Figure 1.3 Schematic diagram of ADAMTS13.**

SP indicates signal peptide; pro, propeptide; protease, metalloprotease; dis-like, disintegrin-like domain; cys, cysteine-rich domain; TSP, thrombospondin type-1 motif; CUB, complement C1r/C1s, Uegf, Bmp1 domain.<sup>77</sup>

### 1.7.1 ADAMTS13 Production and Levels

The majority of ADAMTS13 protein is produced in the hepatic stellate cells.<sup>78</sup> Hepatic stellate cells, along with sinusoidal endothelial cells and Kupffer cells form the sinusoids in the hepatic microcirculation. The hepatic stellate cells are located in the space of Disse, adjacent to the sinusoidal endothelial cells, and regulate sinusoidal blood flow by vasoactive substances.<sup>79</sup>

ADAMTS13 mRNA has also been detected in brain, heart, placenta, and testis.<sup>3</sup> Additional, more controversial, studies have detected ADAMTS13 mRNA and activity in platelets,<sup>80</sup> vascular endothelial cells,<sup>81</sup> and kidney podocytes.<sup>82</sup>

In Caucasian donors, the plasma level of ADAMTS13 antigen is approximately 1.03 µg/ml but it is only 0.62 µg/ml in a Chinese cohort.<sup>83</sup> The plasma activity of ADAMTS13 appears to be regulated inversely by VWF concentration, although the exact mechanism is still unknown.<sup>84, 85</sup>

### 1.7.2 ADAMTS13-Mediated Cleavage of VWF

The VWF multimers released from Weibel-Palade bodies are very large, and have been found to be much more adhesive to platelets in comparison to smaller forms.<sup>2</sup> Upon release, the high molecular weight multimers are bound by P-selectin, also stored in the Weibel-Palade bodies, which causes the tethered VWF to undergo shear stress and partially unfold.<sup>86</sup> This action unfolds the A2 domain, and exposes the cryptic Y1605-M1606 cleavage site, which allows ADAMTS13 mediated cleavage to occur.<sup>87</sup>

ADAMTS13 can bind native VWF, without cleaving the protein, most likely in the distal TSP-1 and CUB domains binding to the C-terminal D4-CK region of VWF.<sup>88, 89</sup> Upon undergoing shear forces, the VWF molecule unfolds, increasing ADAMTS13 binding forces three fold.<sup>88</sup> ADAMTS13 has been shown to preferentially bind to the VWF A3 domain under shear stress conditions, with a weaker interaction with the VWF A1 domain.<sup>90</sup>

The shear-induced unfolding occurs in the A domains in a sequential manner under shear forces. Under simulated in vitro conditions using urea, the A2 domain will completely unfold while the A1 domain unfolds to an intermediate state, followed by A3 completely unfolding and finally A1 gradually unfolding completely under increasing urea concentrations.<sup>91</sup> ADAMTS13 cleavage is inhibited by a chloride binding site in the A1 domain of VWF, since it stabilizes the folded conformation of the A1-A2-A3 domains.<sup>92</sup> The A1 domain also undergoes a conformational change upon GP1b $\alpha$  receptor binding, enhancing VWF-ADAMTS13 binding.<sup>93, 94</sup> The conformation change caused by A1 binding the GP1b $\alpha$  receptor eliminates the chloride binding site, and thus allows for a more open conformation to the A domains.<sup>92</sup>

The A2 domain is not stabilized by disulfide bonds within VWF, unlike A1 and A3. In addition, the A2 domain lacks the highly conserved  $\alpha$ 4 helix, which has been replaced with the flexible and dynamic  $\alpha$ 4-less loop.<sup>95</sup> This leads to low resistance to unfolding, giving the A2 domain the function of a shear bolt. A shear bolt breaks above a designed

force threshold, to protect other parts of a machine from accidental damage. Similarly, the A2 domain unfolds when present in VWF multimers that experience high tensile force and is cleaved by ADAMTS13, resulting in down regulation of the hemostatic activity.<sup>96</sup> VWF will only be exposed to peak shear forces intermittently in the arterioles in normal circulation, but when tethered, VWF will undergo longer, higher shear rates, causing the A2 domain to unfold and allowing ADAMTS13 access to the A2 domain's central cleavage site.<sup>95</sup> These shear forces will increase at sites of vascular damage with a growing thrombus that narrows vessel diameter. ADAMTS13 serves to halt the growth of the thrombus to prevent vessel occlusion, as has been demonstrated in vitro.<sup>97</sup>

The minimal substrate for ADAMTS13 cleavage is the A2 domain's D1596-R1668, VWF73.<sup>98</sup> Several exosites in ADAMTS13 interact with the VWF A2 domain to contribute to substrate specificity and enhance cleavage efficiency. First, the first TSP1 spacer domain in ADAMTS13 interacts with VWF residues between Gln1624 and Arg1668, increasing the cleavage rate 300-fold.<sup>99</sup> The exosite binding was further refined to identify three additional exosites, the first involving VWF1596-1623, the second VWF1642-1652, and the third VWF1653-1668, that are exposed when the VWF A2 domain is unfolded.<sup>100</sup>

### **1.7.3 ADAMTS13 Activity Assays**

There is a plethora of ADAMTS13 substrates and assay conditions, from full-length VWF static assays utilizing patient plasma or recombinant protein,<sup>101, 102</sup> full-length VWF shear force assays,<sup>103-105</sup> intermediate A1-A2-A3 domain<sup>93, 105</sup> and complete A2 domain substrates,<sup>106</sup> to the minimal A2 domain VWF73.<sup>98, 107, 108</sup> The choice of optimal pH, ionic concentration, as well as the divalent metal ion used varies from assay to assay. In addition, there are often conflicting results depending upon which assay systems are used to examine VWF mutations. It must be

stressed that no single *in vitro* method will entirely replicate what is occurring in the cardiovascular system under normal hemostatic conditions or in a thrombotic event.

## **1.8 Von Willebrand Disease**

Von Willebrand disease is the most common inherited bleeding disorder, with a prevalence rate of approximately 1 in 1,000.<sup>5</sup> It is divided into three major categories, quantitative losses of VWF being categorized as moderate (type 1) or severe (type 3) or qualitative defects (type 2).

### **1.8.1 Type 1 VWD**

The most common form of VWD is type 1, accounting for approximately 80% of VWD cases. The disease phenotype of type 1 von Willebrand disease (VWD) is a mild to moderate quantitative reduction of supposedly functionally normal VWF, with plasma VWF levels between 5 and 50% of normal.<sup>109</sup> Usually, there is a corresponding, proportionate reduction in FVIII plasma levels. This is caused by dominant or severe recessive mutations that span the entire *VWF* gene. The type 1 VWD phenotype is caused by a wide array of defects including defective RNA or protein synthesis, premature protein degradation before cellular release, ineffective secretion, rapid plasma clearance, or a mutation that results in a null allele.<sup>110</sup> Only 15% of type 1 VWD cases are the result of a null mutation, and between 30-38% of those studied have no *VWF* gene mutation identified.<sup>111, 112</sup>

### **1.8.2 Type 2 VWD**

The qualitative defects in type 2 VWD involve changes that affect all VWF functions. These can also be accompanied by a decrease in VWF levels.<sup>109</sup> The mutations that cause type 2 VWD are dominant missense changes. Type 2A VWD is a loss of multimer size due to either defective biosynthesis (group I) or enhanced cleavage by ADAMTS13 (group II). This selective deficiency of high molecular weight multimers results in decreased VWF-dependent platelet

adhesion. Type 2B VWD is associated with enhanced affinity for the platelet GPIb receptor, resulting in thrombocytopenia, a loss of VWF, and a loss of high molecular weight VWF multimers. Type 2M VWD has decreased VWF-dependent platelet adhesion without the selective deficiency of high molecular weight VWF multimers, and includes mutations that prevent VWF from binding to platelets or to collagen. Type 2N VWD has a marked decrease in binding affinity to FVIII, resulting in a pseudo-hemophilia phenotype.<sup>109</sup>

### **1.8.3 Type 3 VWD**

The definition of type 3 VWD is the absence of detectable levels of circulating VWF. This results in an accompanying severe decrease in FVIII levels. This is a recessive condition, normally consisting of two null alleles in the *VWF* gene.<sup>109</sup>

## **1.9 Thrombotic Thrombocytopenic Purpura**

Thrombotic thrombocytopenic purpura (TTP) is a disorder of blood coagulation characterized by thrombocytopenia (decreased platelets) and microangiopathic hemolytic anemia accompanied by variable-penetrance of neurologic dysfunction, renal failure, and fever.<sup>113, 114</sup> In the microvasculature of TTP patients, systemic platelet thrombi develop, largely as a result of the accumulation of ultra-large VWF multimers (ULVWF). The ULVWF can be the result of an acquired or congenital deficiency in ADAMTS13 activity. The inherited loss of ADAMTS13 activity is also called Upshaw-Schulman syndrome.<sup>114</sup>

## **1.10 Animal models of von Willebrand Factor and ADAMTS13**

There are great difficulties in evaluating mutations in VWF in the human population due to the small number of available subjects, the large amount of heterogeneity in the human population (including the large number of VWF polymorphisms), as well as variability in the normal range in human VWF levels. At least some of these limitations can be overcome by investigating the pathological mechanisms of VWF mutations in inbred strains of mice.<sup>115</sup>

### 1.10.1 VWF knockout mouse and mouse VWF

The VWF knockout mouse, developed by Cecile Denis *et al.*,<sup>116</sup> has a gene insertion into intron 5 of the mouse *Vwf* gene, interrupting the D1 domain in the propeptide. This resulted in aberrant messenger RNA size, along with total loss of expression of both mouse VWF and mouse VWF propeptide. These mice recapitulate type 3 VWD, with a loss of platelet accumulation in a ferric chloride injury model of thrombosis, increased tail bleeding times, and lower FVIII levels of only 15-20% normal activity.

Compared to its human ortholog, the mouse VWF amino acid sequence is highly similar with 83% sequence identity and 90% homology.<sup>117</sup> In addition, all exons with the exception of exon 1 (236 bp in mouse, 228 bp in human) are identical in length with conserved splice sites. Glycosylation sites and cysteine residues are also highly conserved.<sup>117</sup>

Despite this conservation, there are several important changes in VWF function between the human and mouse VWF orthologs. Mouse VWF does not interact well with the human GP1b platelet receptor.<sup>118</sup> Desmopressin also does not work well in the mouse, although it has been used with RIIS/J strain,<sup>119</sup> which have low VWF levels due to a mutation in the glycosyltransferase B4GALNT2 that leads to enhanced clearance.<sup>120</sup> Additional modifiers of mouse VWF level, both within the mouse *Vwf* gene and in other areas of the mouse genome, have been recently described using genetic studies in mice, which may or may not all translate to human VWF.<sup>121</sup>

### 1.10.2 ADAMTS13 knockout mouse and mouse ADAMTS13

Two different ADAMTS13 knockout mice were developed simultaneously. The first, developed by Banno, *et al.*<sup>122</sup> replaced exons 3-6 with a neomycin resistance cassette. The second knockout mouse developed by Motto, *et al.*<sup>123</sup> replaced exons 1-6 of the mouse *Adamts13* gene with a neomycin resistance cassette. Both strains of mice showed a loss of ADAMTS13 cleavage activity and an increase in VWF-mediated platelet-endothelial interactions, but no other

pathology linked to TTP. Challenging the ADAMTS13 knockout mice with shigatoxin<sup>123</sup> or a mixture of collagen and epinephrine<sup>122</sup> results in a TTP-like disease pathology in the animals.

There is a high degree of similarity between the mouse and human ADAMTS13 orthologs. Murine and human ADAMTS-13 have an overall similarity of 69% at the amino acid level.<sup>124</sup> This is higher in regions shown to have binding regions for VWF, with the metalloprotease domain at 77%, disintegrin-like domain 81%, TSP1-1 domain at 88% and cysteine-rich domain at 80% similarity.<sup>124</sup>

There is species-dependent variability of ADAMTS13-mediated proteolysis. Mouse ADAMTS13 has poor activity on the human VWF substrate in both full-length and A2 domain VWF73 assays.<sup>125</sup> This is further exacerbated by the insertion of an intracisternal A-particle (IAP) retrotransposon element in many commonly used mouse strains, including the C57BL/6 mouse. This insertion leads to the premature truncation of ADAMTS13, lacking the C-terminal 2 TSP1 domains and 2 CUB domains.<sup>126</sup> In vivo, the mice with this truncation exhibit the normal range of multimers and there is little change in cleavage under static conditions. However, the truncated enzyme results in increased thrombotic occlusions under shear stress conditions, since it is not fully active in vivo.<sup>127</sup>

### **1.10.3 Hydrodynamic Delivery**

Hydrodynamic delivery of naked plasmid DNA via tail vein injection was first reported by Zhang, et al. in 1999.<sup>128</sup> The method uses a large volume (generally 10% of the animal's mass) of Ringer's solution or saline as the vehicle to physically force the DNA through the plasma membranes of hepatocytes in the liver.<sup>129, 130</sup> Ubiquitous or liver-specific promoters are used, allowing the expression of the gene of interest by the animal for days, weeks, and even months.

An attempt to correct a murine model of VWD was performed via hydrodynamic delivery in 2006.<sup>131</sup> Unfortunately, the animals in the study received mutant mouse VWF cDNA,

with a C799R mutation, that does not produce normal multimers. Very low antigen levels of less than 1 U/ml VWF were achieved with this approach.<sup>132</sup> Further studies using the CMV promoter showed short term expression reaching VWF levels slightly above that of normal mice.<sup>133</sup> Liver specific expression using alpha1-antitrypsin promoter,<sup>134</sup> pLIVE,<sup>135</sup> or the ET promoter<sup>136</sup> provides better longer term expression for weeks to months of sustained expression at or above normal physiologic levels.

#### **1.10.4 Intravital Microscopy Experimental Models of Thrombosis**

There are a multitude of different vascular thrombosis models in use to study the pathophysiology of thrombosis. This includes large and small arterial and venous vessels as well as physical and chemical methods. To study the high shear rate conditions for which the VWF-GPIIb/IIIa interaction is essential to mediate normal platelet adhesion, arterioles in either the mesentery or cremaster are used. Ferric chloride is the chemical injury methodology of choice, since it is specific for injury to the endothelium.<sup>116, 137, 138</sup> By performing these experiments using intravital microscopy with rhodamine-6-G labeled platelets, it allows real-time monitoring of platelet accumulation and thrombus size.

#### **1.11 Thesis Hypotheses**

VWF mutations can negatively or positively influence ADAMTS13 proteolysis of VWF. The hydrodynamic delivery of VWF cDNA in the VWF knockout mouse will provide a means to evaluate alterations VWF clearance, multimer structure, and function in a thrombotic injury model in vivo. This mouse model will show that these mutations that alter ADAMTS13-mediated cleavage have additional effects on VWF structure, levels, and function. In addition, naturally occurring human type 1 VWD mutations have complex pathological effects that can be observed in this mouse model.

## **1.12 Thesis Objectives**

The overall objective of this thesis is to explore sequence changes in von Willebrand Factor that influence VWF function. This includes altering ADAMTS13-mediated cleavage or VWF biosynthesis, secretion, multimeric structure and clearance.

### **1.12.1 ADAMTS13-mediated cleavage of von Willebrand Factor**

Determine the effect of von Willebrand disease mutations as well as naturally occurring polymorphisms in the A domains of VWF on ADAMTS13-mediated cleavage.

### **1.12.2 Mouse models of VWF changes that alter ADAMTS13 mediated cleavage**

Determine the pathologic effects of VWF mutations in the mouse model that significantly alter ADAMTS13-mediated cleavage in vitro.

### **1.12.3 In vitro and in vivo models of the type 1 VWD mutations R1205H and Y1584C**

Perform a panel of experiments to determine the effects on biosynthesis, secretion, clearance, and ADAMTS13-mediated cleavage of two common and recurrent type 1 VWD mutations to further understand their pathogenic mechanisms.

## **Chapter 2**

# **ADAMTS13 cleavage efficiency is altered by mutation and, to a lesser extent, polymorphic sequence changes in the A1 and A2 domains of von Willebrand factor**

### **2.1 Summary**

The multimeric plasma protein von Willebrand factor (VWF) is regulated in size by its protease, ADAMTS13 (a disintegrin and metalloproteinase with thrombospondin type 1 motif, member 13). Y1605-M1606 cleavage site mutations and single nucleotide polymorphisms (SNPs) in the VWF A1 and A2 domains were examined for alteration in ADAMTS13-mediated cleavage of VWF. Recombinant human full-length VWF (rVWF) was digested with recombinant human ADAMTS13 (rADAMTS13) using a dialysis membrane method with 1.5 M urea, and analyzed via multimer migration distance. The glutathione-S-transferase (GST) and histidine-tagged construct, E1554-R1668 of VWF (VWF115) was assayed via enzyme-linked immunosorbent assay: VWF115 was bound to anti-GST coated plates, digested with rADAMTS13, and intact VWF115 detected via horseradish peroxidase-labeled anti-histidine tag antibody. All alterations examined in the Y1605-M1606 cleavage site greatly reduced the cleavability of VWF by ADAMTS13 in the rVWF assay. Greatest cleavage resistance in both assays was observed in Y1605A/M1606A. In contrast, Y1605H and M1606L show a loss of cleavability only in the rVWF assay, suggesting that an aromatic ring at 1605 is critical for ADAMTS13 recognition. Additionally, under our rVWF assay conditions, the G1643S polymorphism showed increased cleavage, suggesting a Type 2A VWD phenotype, while D1472H, Q1571H and P1601T showed slightly decreased ADAMTS13 cleavage. Our two complementary assay conditions show that A-domain changes in VWF alter ADAMTS13-mediated proteolysis.

## 2.2 Introduction

The large plasma glycoprotein von Willebrand factor (VWF) serves as a molecular chaperone for factor VIII and mediates tethering and adhesion of platelets at the site of vascular injury.<sup>2</sup> The protein exists as 540 kDa dimers, which can be linked as multimers ranging from the single 540 kDa dimer to multimers greater than 20,000 kDa.<sup>2</sup> The larger VWF multimers are more biologically active and bind platelets and the subendothelial matrix more efficiently.<sup>2</sup> The multimer size of VWF is regulated by the metalloprotease ADAMTS13 (a disintegrin and metalloproteinase with thrombospondin type 1 motif, member 13). ADAMTS13 cleaves VWF at the Y1605-M1606 bond, in the A2 domain.<sup>102</sup> Elucidating the cleavage mechanisms, critical binding sites and minimal substrates for ADAMTS13-mediated cleavage has resulted in a recent proliferation of assays and substrates.<sup>98, 105, 107, 108, 139</sup> Recent work with VWF A-domain peptides has established both the minimal substrate for ADAMTS13, VWF73, as well as amino acids that are critical for optimal ADAMTS13 cleavage due to their location in the A2 domain.<sup>98, 140</sup>

This study examined mutations at the Y1605-M1606 cleavage site as well as four A-domain single nucleotide polymorphisms. Further work determining the specificity of ADAMTS13 for variant forms of the substrate will offer new biochemical perspective on polymorphisms in VWF that could contribute to pathological processes. Additionally, determination of the specificity of ADAMTS13 for the Y1605-M1606 cleavage site can be explored using both a minimal 115 amino acid substrate and the multimeric protein.

## 2.3 Materials and Methods

### 2.3.1 Plasmid mutagenesis and recombinant protein production

The A1 and A2 domain single nucleotide polymorphisms (SNPs), D/H1472, Q/H1571, P/T1601, and G/S1643 are described as polymorphisms in the International Society on Thrombosis and Haemostasis Scientific and Standardization Committee (ISTH SSC) VWF database (<http://www.vwf.group.shef.ac.uk/>). Y1605N, Y1605H, Y1605F, M1606L, and

Y1605A/M1606A (cleavage site mutations), R1597W (type 2A VWD), D1614A/E1615A/K1617A (cleavage resistant control), along with the SNPs above were made in the full-length and VWF115 substrates (Table 2.1).

Full-length VWF was produced using pCIneoVWF-ESN, based on pCIneoVWFES,<sup>141</sup> with the unique *NruI* site at nucleotide position 4977 in the VWF cDNA. VWF115, a glutathione-S-transferase (GST) and histidine-tagged 115 amino acid fragment of the VWF A2 domain, E1554-R1668, was constructed from pGEX-6P-1 backbone (GE Healthcare Life Sciences, Piscataway, NJ, USA) and pCIneoVWF-ESN.<sup>98</sup> Mutagenesis was performed in both plasmids using the QuikChange II XL Site-Directed Mutagenesis Kit (Stratagene, La Jolla, CA, USA) according to the manufacturer's procedures.

HEK293T cells were transiently transfected using the calcium phosphate method as previously described.<sup>141</sup> VWF was secreted into serum-free OptiMEM containing 100 U/ml penicillin, 100 µg/ml streptomycin, 1X Insulin/Selenium/Transferrin G (Invitrogen, Carlsbad, CA, USA). Medium was harvested after 72 hours and recombinant VWF (rVWF) was concentrated using Amicon Ultra-15 100K MWCO units (Millipore, Billerica, MA, USA). rVWF protein concentration was determined by VWF enzyme-linked immunosorbent assay (ELISA) using polyclonal antibodies (DAKO, Carpinteria, CA, USA) against a standard human plasma pool (CRYOcheck, Precision BioLogic Inc, Dartmouth, NS, Canada).

Human ADAMTS13 in the pcDNA3.1 expression vector (a gift of Dr. F. Scheiflinger, Baxter, Austria) was produced via stable transfection in HEK293T cells similar to the rVWF, using G418 selection.<sup>3</sup> Recombinant ADAMTS13 (rADAMTS13) was concentrated using Amicon Ultra-70 100K MWCO units (Millipore). rADAMTS13 activity was determined using the ADAMTS13

| Full-Length VWF Multimers |                    |                               |         |                  |                     | VWF115                   |                    |                       |         |                  |                     |
|---------------------------|--------------------|-------------------------------|---------|------------------|---------------------|--------------------------|--------------------|-----------------------|---------|------------------|---------------------|
|                           | ADAMTS13<br>(U/ml) | 95%<br>Confidence<br>Interval | P Value | Times<br>Assayed | Normalized<br>Value |                          | ADAMTS13<br>(U/ml) | Standard<br>Deviation | P value | Times<br>Assayed | Normalized<br>Value |
| Wild Type                 | 0.221              | 0.1913 to 0.256               | (-)     | 5                | 1                   | Wild Type                | 0.097              | 0.0541                | (-)     | 13               | 1                   |
| D1472H                    | 0.305              | 0.247 to 0.378                | 0.0024  | 2                | 1.38                | (-)                      | (-)                | (-)                   | (-)     | (-)              | (-)                 |
| Q1571H                    | 0.595              | 0.476 to 0.742                | <0.0001 | 2                | 2.69                | Q1571H                   | 0.107              | 0.0137                | 0.729   | 4                | 1.1                 |
| R1597W                    | 0.146              | 0.0602 to 0.352               | 0.1077  | 1                | 0.659               | R1597W                   | 0.078              | 0.0267                | 0.51    | 4                | 0.8                 |
| P1601T                    | 0.523              | 0.457 to 0.598                | <0.0001 | 2                | 2.37                | P1601T                   | 0.22               | 0.127                 | 0.0068  | 7                | 2.26                |
| Y1605F                    | 3.14               | 0.817 to 14.0                 | <0.0001 | 1                | 14.2                | Y1605F                   | 0.107              | 0.0311                | 0.734   | 4                | 1.1                 |
| Y1605H                    | 2                  | 0.340 to 11.8                 | <0.0001 | 1                | 9.06                | Y1605H                   | 0.172              | 0.0924                | 0.0377  | 6                | 1.78                |
| Y1605N                    | 1.71               | 0.8556 to 3.43                | <0.0001 | 1                | 7.75                | Y1605N                   | 7.721              | 7.17                  | 0.0008  | 5                | 80                  |
| M1606L                    | 2.68               | 0.334 to 13.1                 | <0.0001 | 1                | 12.1                | M1606L                   | 0.072              | 0.0122                | 0.386   | 4                | 0.74                |
| Y1605A/M1606A             | >67                | (-)                           | <0.0001 | 2                | >303.               | Y1605A/M1606A            | 23                 | 17.6                  | 0.0004  | 5                | 237                 |
| D1614A/E1615A/<br>K1617A  | 3.45               | 0.716 to 24.2                 | <0.0001 | 1                | 15.6                | D1614A/E1615A/<br>K1617A | 6.07               | 3.00                  | <0.0001 | 6                | 62.6                |
| G1643S                    | 0.0509             | 0.0360 to 0.0592              | <0.0001 | 2                | 0.23                | G1643S                   | 0.172              | 0.0728                | 0.0174  | 7                | 1.77                |

**Table 2.1 Summarized results of rADAMTS13-mediated digestion.**

ADAMTS13 concentration necessary for 50% loss of multimer migration distance of full-length VWF or 50% digestion of VWF115 substrate is listed. GraphPad Prism calculated values for 95% confidence interval for the multimer graphs and standard deviation for VWF 115 graphs are listed. Number of values refers to the number of replicate assays performed. P values are the results of T tests against the wild type results. ADAMTS13 concentrations are normalized to a value of 1 for cleavage of wild type VWF.

Activity ELISA Kit (Japan Clinical Laboratories, Kyoto, Japan) against a human standard plasma pool (Cryocheck).<sup>107</sup>

The VWF115 protein was produced in BL21-Gold *E. coli* (Stratagene) and grown in 2x YTA medium (16g tryptone, 10g yeast extract, 5 g NaCl/L) via a 3 hour induction with 0.5 mM isopropyl-beta-d-thiogalactopyranoside (IPTG). Cells were pelleted and stored at -20°C. Lysate was prepared using the CelLytic B Plus kit (Sigma, St. Louis, MO, USA) for soluble proteins. The protein was purified using Ni-NTA agarose (Qiagen, Valencia, CA, USA) under native conditions and stored in elution buffer (50 mM NaH<sub>2</sub>PO<sub>4</sub>, 300 mM NaCl, 200 mM Imidazole, 20% glycerol, pH 8.0) at -80°C.

### **2.3.2 Proteolysis of rVWF and VWF115 by rADAMTS13**

Recombinant ADAMTS13 was diluted two-fold in 5 mM Tris, pH 8.0, and activated with 10 mM BaCl<sub>2</sub> final concentration for 5 minutes at 37 °C. A 100 µl aliquot of rADAMTS13 was added to 100 µl rVWF, 1 U/ml in 5 mM Tris, pH 8.0, and dialyzed against 1.5 M urea, 5 mM Tris, pH 8.0, on VSWP02500 filters (Millipore). After five hours, the samples were collected and 25 mM EDTA, final concentration, was added. Samples were stored at -80°C until multimer analysis was performed. The rVWF multimers were analyzed by electrophoresis using a 1.4% separating sodium dodecyl sulfate (SDS) agarose gel and visualized using polyclonal horseradish peroxidase-labeled human VWF antibody (DAKO) as previously described.<sup>142</sup> Lanes were analyzed for migration distance using AlphaEaseFC version 3.1.2 (Alpha Innotech, San Leandro, CA, USA).

The VWF115 rADAMTS13 digestion ELISA assay was modified from the ADAMTS13 Activity ELISA.<sup>107</sup> As a result of the examination of mutations at and near the Y1605 neo-epitope used in the ADAMTS13 Activity ELISA, HIS tag detection was necessary. Reacti-Bind Anti-GST coated plates (Pierce, Rockford, IL, USA) were coated with 1.25 mg/ml VWF115 in phosphate buffered saline (PBS), pH 7.2 for one hour, and washed with PBS/0.05% Tween-20

(PBS/Tween). Twofold dilutions of rADAMTS13 were made in 5 mM acetate, 5mM MgCl<sub>2</sub>, pH 7.5 and added to each well for 4 hours at 37°C, the wells were washed with PBS/Tween, and 1 µg/ml HISProbe (Pierce) in PBS/Tween was added for 1 hour. 1X OPD reagent (Sigma) was used for visualization, the reaction stopped at 10 minutes with 2.5M H<sub>2</sub>SO<sub>4</sub>, and absorbance was read at 492 nm.

All data and statistical analysis was performed using GraphPad Prism 4.03 for Windows, GraphPad Software, San Diego, CA, USA, [www.graphpad.com](http://www.graphpad.com). P values <0.05 were considered significant.

## **2.4 Results**

### **2.4.1 Expression and characterization of VWF and ADAMTS13 protein**

All mutant forms and wild type rVWF showed similar multimer patterns and all exhibited ultra large VWF compared with normal plasma because of the lack of ADAMTS13 exposure in cell culture (Figure 2.1) The rVWF protein probably has a different glycan content to normal VWF, as it is expressed in a non-endothelial cell line.

Human recombinant ADAMTS13 was stably expressed in transfected 293T cells. The control medium had no observed ADAMTS13 activity. Prior to concentration, the rADAMTS13 medium had an activity of 5.85 U/ml, and concentrated rADAMTS13 medium had an activity of 67 U/ml. The rADAMTS13 probably has a different glycosylation pattern compared with plasma ADAMTS13, because of the nature of recombinant protein production.

All purified VWF115 proteins showed a single band at approximately 40.4 kDa via SDS polyacrylamide gel electrophoresis (data not shown). Concentration was determined by absorbance at 280 nm and confirmed via SDS PAGE and ELISA.

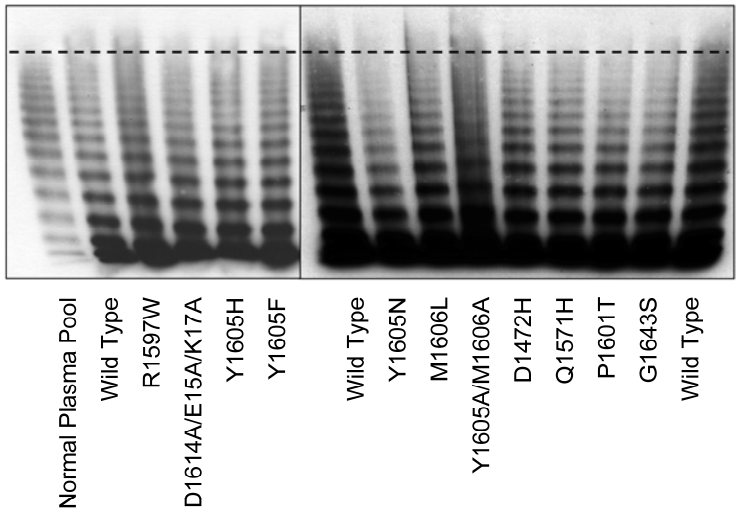


**Figure 2.1 Recombinant VWF has ultra-large (UL) VWF multimers in both wild type and mutant forms.**

Multimer analysis of wild type and mutated forms of VWF shows that all VWF proteins exhibit the same multimeric pattern. Compared to normal human plasma, all recombinant proteins show ultra large VWF multimers (shown above the dashed line).

#### **2.4.2 Proteolysis of full-length rVWF by rADAMTS13**

All experiments were performed in the presence of 1.5 M urea, using a two-fold dilution series of rADAMTS13 on 11 rVWF mutants and rVWF wild type protein. Wild type VWF was assayed five times, D1472H, Q1571H, P1601T, G1643S, and Y1605A/M1606A twice, and all other mutations once. Figure 2.2 shows typical multimer results of wild type rVWF, with additional results in figure 2.4. The multimer-derived curves are shown in Figure 2.3 and results are summarized in Table 2.1. The maximum migration distance was determined by examining different exposures of the multimer films, with the clearest exposure being used for measurement. Higher bands were not apparent even under highly over-exposed conditions. Additionally, repeated digestions yielded highly reproducible results, as seen in Figure 2.3.

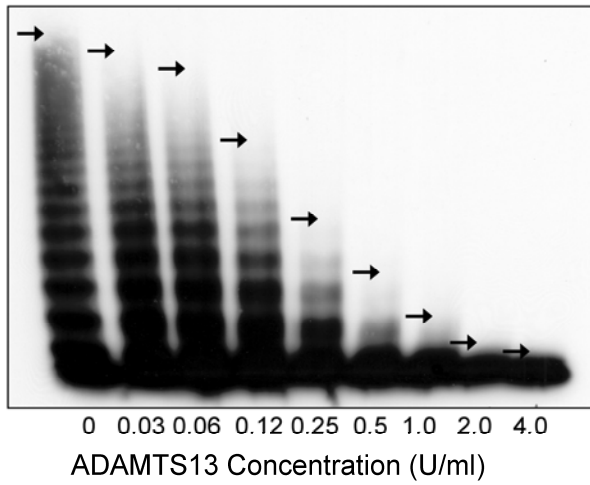


**Figure 2.2 Multimer Analysis of ADAMTS13 Digestion of Full-Length Wild Type VWF.**

Recombinant full-length VWF was digested with ADAMTS13 as outlined under methods. Varying concentrations of ADAMTS13 were incubated with 1 U/ml rVWF for 5 hours with 1.5M Urea. After multimer visualization, the distance migrated was measured, shown as arrows.

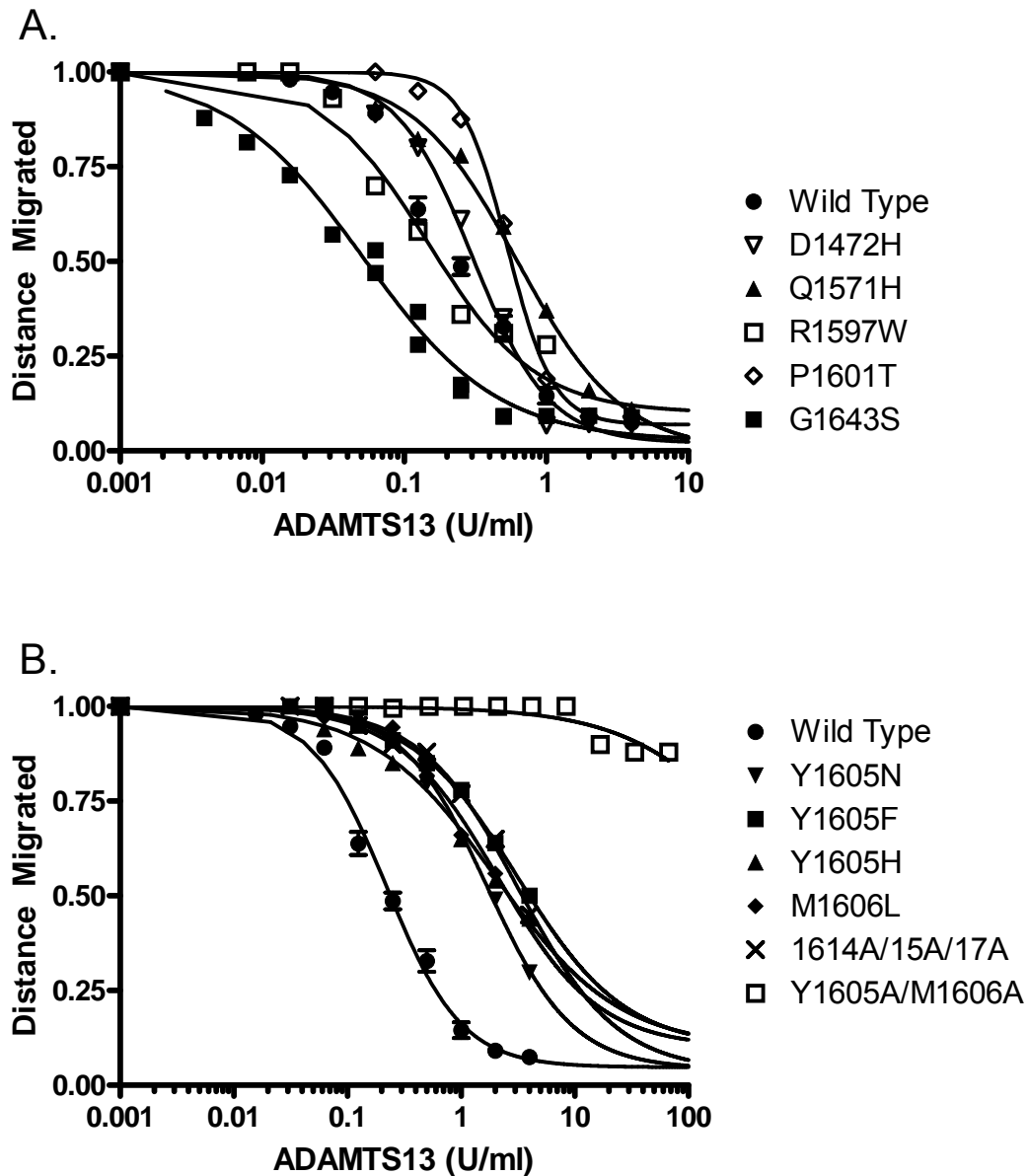


**Figure 2.3 Analysis of ADAMTS13 Digestion of Full-Length VWF.**

Recombinant full-length VWF was digested with ADAMTS13 as outlined under methods. Varying concentrations of ADAMTS13 were incubated with 1 U/ml rVWF for 5 hours with 1.5M Urea. Multimer graphs for Single Nucleotide Polymorphisms (A) and Cleavage Site Mutants (B) Distances were graphed using a four-parameter curve fit. The concentration of ADAMTS13 required to cause a 50% loss of multimer height was determined. Wild Type VWF is represented by mean values and Standard Deviation error bars.

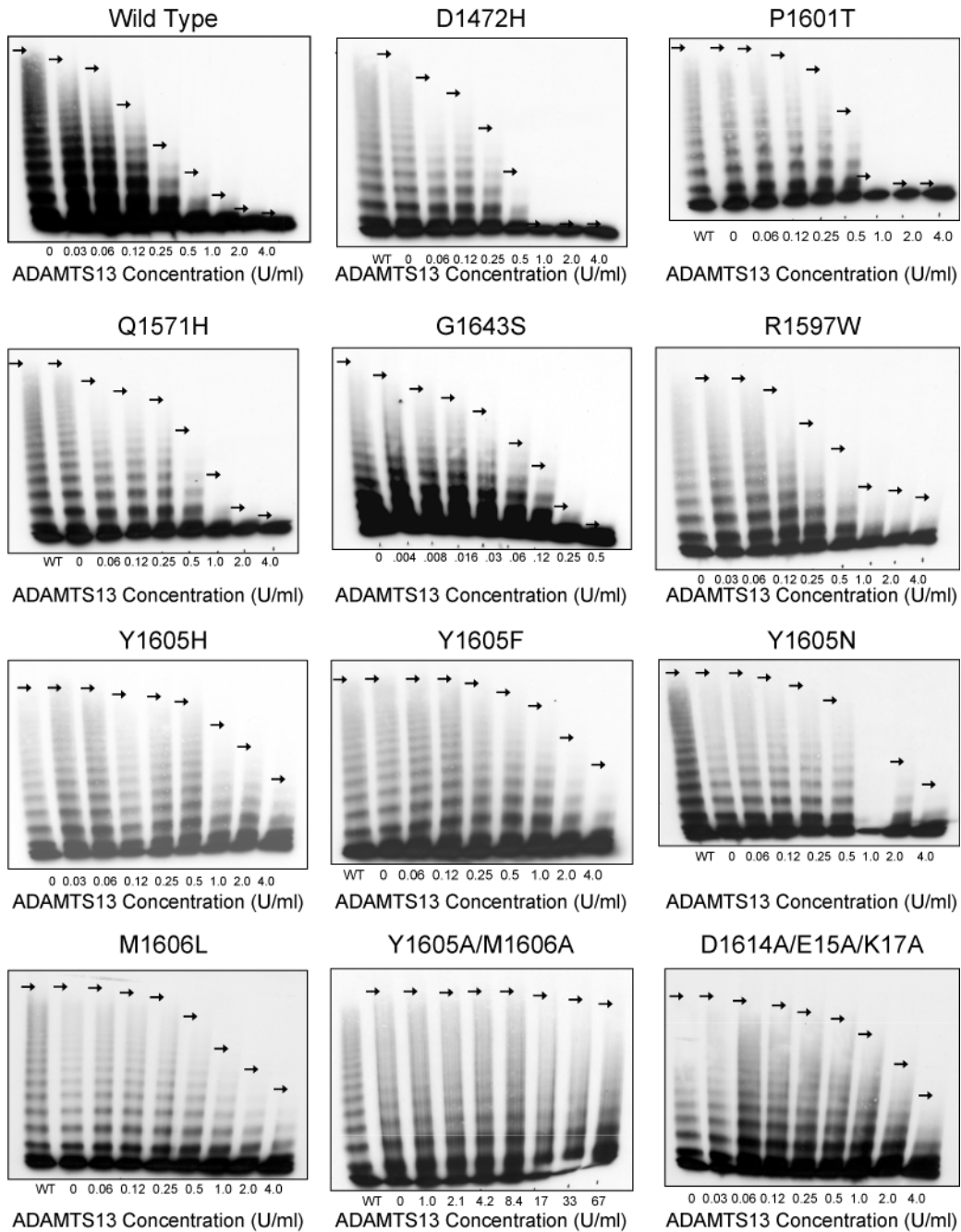


**Figure 2.4 Data for Analysis of ADAMTS13 Digestion of Full-Length VWF.**

Recombinant full-length VWF was digested with ADAMTS13 as outlined under methods. Varying concentrations of ADAMTS13 were incubated with 1 U/ml rVWF for 5 hours with 1.5M Urea. After multimer visualization, the distance migrated was measured, shown as arrows. Graphs generated from this data are shown in Figure 2.3.

### 2.4.3 VWF115 proteolysis by rADAMTS13

All experiments were performed using non-denaturing conditions with a minimum of four replicates using varying concentrations of rADAMTS13. Wild type VWF115 was performed 13 times. The concentration of ADAMTS13 required for a 50% loss of intact VWF115 substrate was determined via a four parameter curve fit (Figure 2.5 and Table 2.1). Representative assays are graphed in Figure 2.6. The wild type VWF115 required an average concentration of 0.097 U/ml ADAMTS13 to achieve 50% substrate cleavage. The D1472H SNP variant was not included in these studies, as it is located outside the VWF115 sequence.

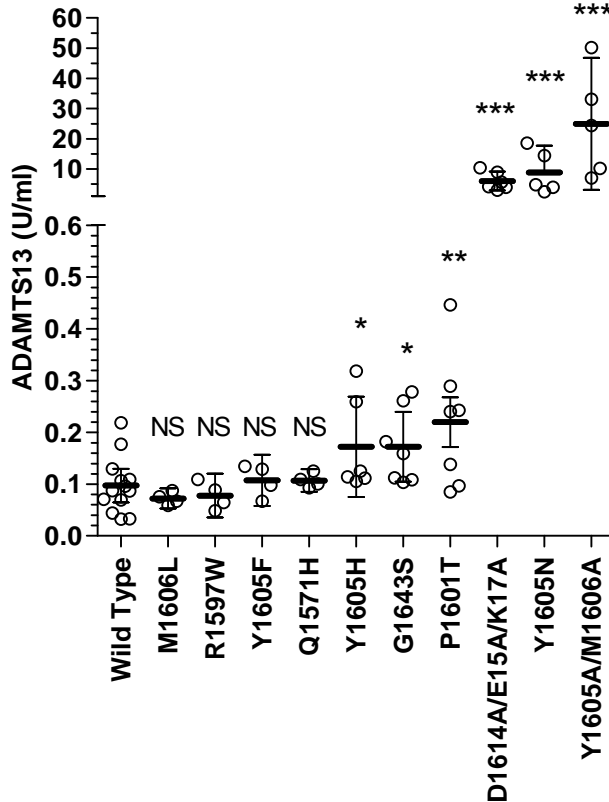


**Figure 2.5 ADAMTS13 concentrations necessary for 50% loss of intact VWF115.**

VWF115 was digested with ADAMTS13 as outlined under methods. Varying concentrations of ADAMTS13 were incubated with VWF115 for 4 hours under non-denaturing conditions. Circles represent results for individual tests. Bars represent the mean, error bars show standard deviation. \*\*\*:  $P < 0.001$ , \*\*:  $0.001 \leq P < 0.01$ , \*:  $0.01 \leq P < 0.05$ . NS:  $P > 0.05$ .

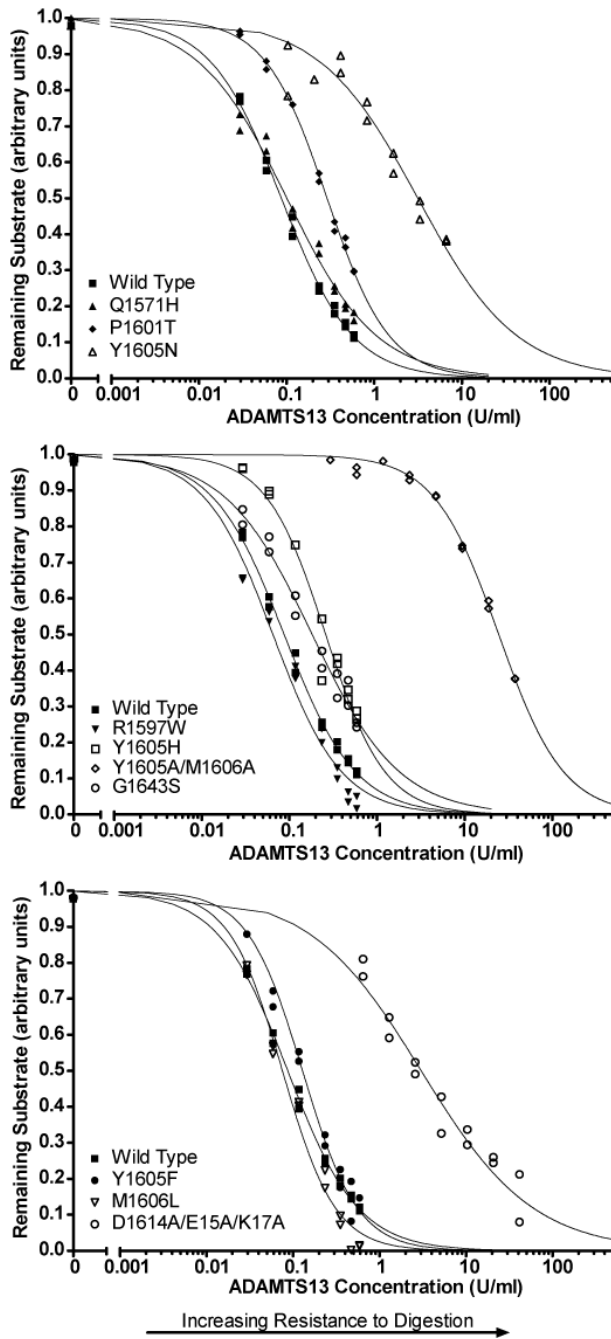


**Figure 2.6 Data for the Analysis of the ADAMTS13 concentrations necessary for 50% loss of intact VWF115.**

VWF115 was digested with ADAMTS13 as outlined under methods. Varying concentrations of ADAMTS13 were incubated with VWF115 for 4 hours under non-denaturing conditions. The amount of intact VWF115 was measured in duplicate and graphed using a four-parameter curve fit. Individual representative assays near the mean of each construct are presented, as seen in Figure 2.5.

#### **2.4.4 Effect of Y1605-M1606 cleavage site mutations on ADAMTS13 cleavage**

All of the cleavage site mutations showed a large decrease in cleavage compared to wild type VWF in the full-length assay. With the full-length substrate, ADAMTS13 is able to discern the loss of the normal Y1605/M1606 site with all the substitutions tested (Table 2.1). The Y1605A/M1606A double mutant had the largest resistance to cleavage (>300-fold.  $p < 0.0001$ ).

In the VWF115 assay, the amount of ADAMTS13 cleavage present ranged from no significant change to a 237-fold decrease depending on the amino acid substitution. M1606L and Y1605F both had statistically insignificant changes in the VWF115 assay, with a 26% decrease ( $p = 0.386$ ) and a 10% increase ( $p = 0.734$ ) respectively in ADAMTS13 concentration. Y1605H showed a slight decrease in cleavage, with 78% more ADAMTS13 being required ( $p = 0.037$ ). Y1605N and Y1605A/M1606A required large increases in ADAMTS13 concentrations of 80-fold ( $p = 0.0008$ ) and 237-fold ( $p < 0.0001$ ) respectively. The Y1605A/M1606A mutant exhibits the greatest loss of cleavage, with the replacement of both R groups with methyl groups. These results show that ADAMTS13 requires the aromatic tyrosine group for VWF cleavage in the small VWF115 substrate.

#### **2.4.5 Effect of VWF Single Nucleotide Polymorphisms on ADAMTS13 Cleavage**

The D/H1472 polymorphism lies in the A1 domain region that binds to the glycoprotein Ib $\alpha$  receptor.<sup>143</sup> In a previous report addressing this polymorphism, analysis of patient plasma samples showed no change in VWF multimer patterns.<sup>144</sup> The 38% increase in ADAMTS13 concentration required for cleavage of the H1472 variant ( $p = 0.0024$ ), suggests that the amino acid change from an acidic to an aromatic basic amino acid alters VWF conformation or VWF-ADAMTS13 interactions.

The Q/H1571 polymorphism is located on an external loop in the A2 domain.<sup>145</sup> Since VWF115 only contains residues E1554-G1668, the interactions of Q1571 with amino acids outside this region were not present, and there was no significant change in cleavage. However, there was a 169% increase in the amount of ADAMTS13 required for cleavage of H1571 in the full-length assay ( $p < 0.0001$ ).

The proline R-group of P1601 projects outward with no hydrogen bonding with other A1 domain amino acids.<sup>145</sup> The 137% increase in ADAMTS13 required for full-length cleavage ( $p < 0.0001$ ) of T1601, and 126% increase in ADAMTS13 for VWF115 cleavage ( $p = 0.0068$ ) implied that this polymorphism inhibited ADAMTS13-mediated cleavage.

The G/S1643 polymorphism had the most dramatic change on ADAMTS13-mediated cleavage of VWF. In the VWF115 assay, the ADAMTS13 concentration required for cleavage was 77% higher than for the wild type ( $p = 0.017$ ). In contrast, in the full-length assay, a 77% lower ADAMTS13 concentration was required ( $p < 0.0001$ ), possibly caused by a conformational change in the VWF115 substrate. Located on the outside of the A2 domain in a loop domain, G1643 does not interact with any other A2 domain amino acids.<sup>145</sup> Both E1638K and L1639P have been reported as Type 2A VWD mutations, and E1638K has been shown experimentally to cause an increase in ADAMTS13-mediated cleavage, showing that this is a critical region for VWF-ADAMTS13 cleavage.<sup>105, 140, 145</sup> However, this variant most likely has a more subtle phenotype physiologically, since it has not been identified as a Type 2A VWD mutation, despite occurring at a 1% frequency in a French population (Lavergne, <http://www.vwf.group.shef.ac.uk/>).

#### **2.4.6 The effect of ADAMTS13 cleavage controls**

The type 2A VWD mutation, R1597W, was selected as a positive digest control based on its high frequency as listed in the ISTH SSC VWF database and previously published data.<sup>105, 140,</sup>

<sup>146</sup> The R1597W Type 2A VWD mutation has been shown to increase susceptibility to ADAMTS13 cleavage in full-length and A1-A2-A3 substrates.<sup>105, 146</sup> In our VWF115 assay, ADAMTS13 cleavage was not greatly increased by R1597W (0.8-fold ADAMTS13 concentration  $p = 0.51$ ), similar to what had been previously reported in a VWF115 assay.<sup>140</sup> In the full-length VWF assay, the results showed an increase in VWF cleavage (0.66-fold ADAMTS13 conc.  $p = 0.026$ ).

The control triple mutant D1614A/E1615A/K1617A had the second largest increase in ADAMTS13 concentration necessary for 50% multimer cleavage (15.6 fold increase.  $p < 0.0001$ ). In the VWF115 assay, D1614A/E1615A/K1617A required a 62.6-fold increase in ADAMTS13 concentration ( $p = 0.0004$ ).

## 2.5 Discussion

ADAMTS13 cleaves the single bond between Y1605 and M1606 in the VWF A2 domain.<sup>2</sup> ADAMTS13 cleavage requires partial unfolding of the globular VWF multimer either by shear stress, VWF binding to its ligands, or by chemical means.<sup>101</sup> However, smaller A2 domain fragments are much more readily cleaved under normal physiological ionic conditions.<sup>98, 140, 147</sup> The use of both the full-length multimerized rVWF and the short VWF115 substrate and rADAMTS13 enabled us to focus on both localized A2 domain-ADAMTS13 and global VWF-ADAMTS13 interactions through two complementary assays.

Most VWF substrates and ADAMTS13 activity assays require access to expensive reagents and equipment. The monoclonal antibody full-length VWF assay requires the use of antibodies that are not commercially available.<sup>148</sup> FRETs-VWF73, although very effective for screening differences in ADAMTS13 cleavage, is an expensive substrate that would require separate synthesis for each VWF mutation.<sup>108</sup> The A2 domain peptide substrates can also be evaluated semi-quantitatively using SDS-PAGE and protein staining or Western blotting to

determine cleavage efficiency. Accurate quantification of the VWF73 cleavage products requires either an antibody that recognizes the cleavage site, the epitope of which can be disrupted by mutations at the site,<sup>107</sup> or the use of mass spectrometry, high performance liquid chromatography, or surface plasmon resonance to quantitatively determine cleavage and VWF-ADAMTS13 interactions.<sup>140</sup> Finally, the recent phage display strategy for screening mutants in the VWF73 substrate while highly efficient, still requires testing of the candidate VWF fusion proteins.<sup>149</sup>

Recent ADAMTS13 activity assays used to evaluate patient plasma samples utilized VWF73 as a substrate for ADAMTS13 cleavage.<sup>107, 108, 140</sup> In light of the wide variation of our VWF115 results, these assays should be considered carefully when evaluating the effects of VWF variability on ADAMTS13 cleavage.

This study examined three types of sequence changes in the ADAMTS13 substrate molecule, VWF. Amino acid substitutions at the 1605-1606 cleavage site consistently resulted in reduced cleavage of the full-length substrate (9 to >300-fold more ADAMTS13 required) but in the 115mer assay, cleavage efficiency was variable and very dependent upon the type of substitution (0.74 to 237-fold ADAMTS13 concentrations). Overall, the VWF115 results suggest that the aromatic tyrosine group is especially critical for ADAMTS13 cleavage efficiency. In contrast to the 1605-1606 mutants, the four VWF SNP substitutions showed only moderate variances in ADAMTS13 cleavage, between 0.23 to 2.69-fold ADAMTS13 concentrations in the full-length assay and between 0.8 and 2.26-fold in the VWF115 assay. For two of the SNPs, Q1571H and P1601T, the effect of the substitution was similar in both assay systems, while for the G1643S polymorphism the results were contrasting. In the full-length assay, G1643S shows the characteristics of a type 2A molecule while in the VWF115 assay there is mild resistance to ADAMTS13 (1.77-fold concentration). The two “control” cleavage molecules used in the study,

the triple mutant D1614A/E1615A/K1617A and R1597W have shown an expected marked increase in resistance to cleavage in the case of the triple mutant and enhanced cleavage for the Type 2A R1597W protein. However, the results for the R1597W mutant were less than expected from the type 2A clinical phenotype and less obvious in the full-length assay than the G1643S polymorphic variant.

This study represents the first time that full-length VWF multimer profiles have been examined quantitatively to evaluate ADAMTS13-mediated proteolysis. Previous work using multimer analysis has relied on reporting plasma VWF multimer profiles without quantification.<sup>105, 144</sup> We have also modified the ADAMTS13 activity ELISA using VWF115 substrates as a complementary test of the effect of VWF substrate variability. We demonstrated that changes to the 1605-1606 VWF cleavage site result in a dramatic loss of cleavage. The examination of the VWF polymorphisms in this study suggests that these previously described SNPs may alter VWF folding and function. The G1643S polymorphism may make VWF more cleavable *in vivo*, and result in a type 2A phenotype with an increased bleeding risk. In contrast, the SNPs D1472H, Q1571H, and P1601T appear to moderately impede ADAMTS13-mediated cleavage, leading to a persistence of larger VWF multimers and possibly contributing to a prothrombotic influence. Further study employing more physiological experimental systems, such as shear flow, will be necessary to determine if this is the case.

## **2.6 Acknowledgements**

We thank Dr. Freidrich Scheiflinger for the kind gift of the rADAMTS13 expression vector, Christine Brown and Patrick Thompson for the production of the recombinant ADAMTS13 and Jeff Sutherland for creation of the VWF A2 domain model. This project was supported by an operating grant from the Canadian Institutes for Health Research (MOP-42467). CMP was supported by an Ontario Graduate Scholarship and a Heart and Stroke Foundation of

Ontario Master's Studentship. DL is the recipient of a Career Investigator Award from the Heart and Stroke Foundation of Ontario and a Canada Research Chair in Molecular Hemostasis.

## Chapter 3

# Evaluation of von Willebrand Factor mutations influencing ADAMTS13-mediated cleavage in a mouse model system: R1597W and Y1605A/M1606A.

### 3.1 Summary

Von Willebrand Factor (VWF) is tightly regulated by the metalloproteinase ADAMTS13, which cleaves VWF to reduce VWF multimer size and binding affinity for collagen and platelets. Two VWF mutations, R1597W (enhanced cleavage), and Y1605A-M1606A (decreased cleavage) were examined in the mouse. In vitro ADAMTS13 digestion of full-length mouse VWF resulted in ADAMTS13 levels being >97-fold higher for Y1605A/M1606A, and R1597W was 68% lower than wild type, similar to human VWF. VWF knockout mice received hydrodynamic injections of mouse *Vwf* cDNA. Both mutations exhibited faster clearance by reduced VWF:Ag levels and increased VWF propeptide/VWF:Ag ratios. R1597W multimers from hydrodynamic mice show a lower molecular weight profile compared to wild type and Y1605A/M1606A mice. When co-injected with *Adamts13* cDNA, Y1605A/M1606A multimers were larger compared to wild type, and R1597W had a single band. R1597W showed reduced thrombus formation and platelet accumulation in a ferric chloride injury model while Y1605A/M1606A had a loss of occlusive thrombi but increased platelet accumulation compared to wild type. This study demonstrates that mutations that alter ADAMTS13 cleavage also can affect clearance, VWF antigen level, multimer structure, and thrombotic potential in the VWF knockout hydrodynamic injection model.

### 3.2 Introduction

The large multimeric glycoprotein von Willebrand Factor (VWF) is critical to normal hemostasis through mediating platelet-subendothelial interactions as well as binding to platelets to mediate their aggregation at the site of endothelial damage.<sup>1</sup> In addition, it serves as a molecular chaperone for FVIII. When activated, endothelial cells release ultra-high molecular weight VWF. This highly adhesive VWF is tightly regulated by the metalloproteinase, ADAMTS13 (the thirteenth member of **A** **d**isintegrin-like **a**nd **m**etalloprotease with **t**hrombospondin type 1 motif family), which cleaves the A2 domain of VWF at Y1605/M1606, thereby reducing VWF multimer size and binding affinity.<sup>3</sup>

In type 2A group II von Willebrand disease (2A VWD) mutations, the largest VWF multimers are absent due to an increased susceptibility for cleavage by ADAMTS13.<sup>105</sup> This lower molecular weight VWF has a decreased binding affinity for collagen and platelets, and results in a bleeding phenotype.<sup>146</sup> In contrast, an uncontrolled increase in ultra-large VWF multimers results in spontaneous platelet binding and thrombus formation in diseases like thrombotic thrombocytopenic purpura and hemolytic uremic syndrome.<sup>114</sup>

The type 2A group II VWD mutation R1597W is one of the most commonly reported forms of this subtype. This mutation is located in the VWF A2 domain, near the ADAMTS13 cleavage site. Patients with the R1597W mutation exhibit a loss of high molecular weight VWF multimers due to increased ADAMTS13-mediated cleavage. This, in turn, results in an increased bleeding time and lower VWF ristocetin-cofactor values.<sup>146</sup> R1597W has been previously demonstrated *in vitro* to have an enhanced susceptibility to ADAMTS13-mediated cleavage,<sup>105, 140, 150</sup> but near normal synthesis compared to wild type recombinant protein.<sup>105, 151</sup>

The cleavage site knockout Y1605A/M1606A has previously been demonstrated to greatly decrease the rate of ADAMTS13-mediated cleavage on both full-length multimerized

recombinant VWF, and an A2 domain VWF substrate.<sup>150</sup> In vivo, this should increase multimer size, and increase the thrombogenic potential of the VWF molecules, similar to an ADAMTS13 deficiency. ADAMTS13 knockout mice produce a prothrombotic phenotype with increased VWF multimer size, but require another pathological challenge to produce TTP-like symptoms.<sup>122, 123</sup>

The VWF knockout mouse can be used to examine different human VWD mutations through the establishment of mouse VWF expression by hydrodynamic delivery of the mouse *Vwf* cDNA. The homogeneous, inbred genotype of the mice, relatively low cost to introduce new mutations, and the ability to evaluate larger study populations than would be available for human subjects makes this a valuable and convenient methodology to examine different VWD mutations. This strategy also enables the evaluation of discrete VWF variants without the potential confounding influence of additional coding region polymorphisms. This experimental approach has already recapitulated the human disease phenotypes for defective binding to collagen and GPIIb/IIIa,<sup>135</sup> and type 2B VWD.<sup>136, 152</sup> Until now, this methodology has not been used to evaluate VWF sequence changes that affect ADAMTS13-mediated cleavage.

This study examines the role of ADAMTS13-mediated cleavage on VWF clearance rate, multimer size, and function in the VWF knockout mouse via both recombinant protein infusions and gene therapy via hydrodynamic tail vein injection.

### **3.3 Materials and Methods**

#### **3.3.1 Plasmid construction and mutagenesis**

The mouse *Vwf* cDNA (courtesy of Peter Lenting) was cloned into the pCIneo plasmid for recombinant full-length mouse VWF protein (mVWF) and into the pSC11 plasmid<sup>153</sup> with the liver-specific enhanced murine transthyretin (ET) promoter (courtesy of Luigi Naldini)<sup>154</sup> for

hydrodynamic delivery. mVWF115, a GST and histidine tagged 115 amino acid fragment of the VWF A2 domain, G1554-T1668, was constructed from the pGEX-6P-1 backbone (GE Healthcare Life Sciences, Piscataway, NJ, USA) and mouse *Vwf* cDNA.<sup>98</sup> Site-directed mutagenesis was performed using the Quikchange XL II kit (Stratagene, La Jolla CA). Both R1597 and Y1605/M1606 are conserved between human and mouse. Mouse ADAMTS13 cDNA (courtesy of Dr. F. Scheiflinger, Baxter, Austria) was cloned into the pSC11 plasmid<sup>153</sup> with the liver-specific ET promoter<sup>154</sup> for hydrodynamic delivery.

### **3.3.2 Recombinant protein production and cell culture**

HEK293T cells were transiently transfected using the calcium phosphate method as previously described.<sup>141, 150</sup> VWF was secreted into serum-free OptiMEM containing 100 U/ml penicillin, 100 µg/ml streptomycin, 1X Insulin/Selenium/Transferrin G (Invitrogen, Carlsbad, CA, USA). Medium was harvested after 72 hours and recombinant VWF was concentrated using Amicon Ultra-15 or Ultra-70 100K MWCO units (Millipore, Billerica, MA, USA).

Mouse ADAMTS13 (mADAMTS13) derived from the pcDNA3.1-mADAMTS13 expression vector (a gift of Dr. F. Scheiflinger, Baxter, Austria) was produced via stable transfection in HEK293T cells similar to the recombinant VWF, using G418 selection.<sup>3</sup> ADAMTS13 activity was determined using the ADAMTS13 Activity ELISA Kit (Japan Clinical Laboratories, Kyoto, Japan).<sup>107</sup>

The mVWF115 proteins were produced in BL21-Gold *E. coli* (Stratagene) and purified via Ni-NTA agarose (Qiagen, Valencia, CA).<sup>150</sup>

### **3.3.3 VWF antigen, propeptide and multimer quantitation**

Mouse VWF protein concentration was determined by VWF enzyme-linked immunosorbent assay (ELISA) using polyclonal human VWF antibodies A0082 and P0226

(DAKO, Carpinteria, CA, USA). Mouse VWF propeptide (VWFpp) concentration was determined using the 349.3 capture antibody, and detected via the horseradish peroxidase-linked 349.2 antibody. Both anti-mouse VWFpp antibodies were provided by Sandra Haberichter. Mouse VWF, mouse VWF propeptide, and mADAMTS13 activity concentrations were determined using a normal C57Bl/6 plasma pool, derived from 25 normal, mixed sex, eight week old C57Bl/6 mice, with the means arbitrarily determined to be 1 U/mL mVWF, mVWFpp, mADAMTS13 respectively.

Mouse VWF multimers were analyzed by electrophoresis using a 1.4% separating sodium dodecyl sulfate (SDS) agarose gel and visualized using the polyclonal HRP-labeled human VWF antibody P0226 (DAKO) as previously described.<sup>142</sup> Lanes were analyzed by 1-D densitometry for multimer distance and band number using AlphaEaseFC version 3.1.2 (Alpha Innotech, San Leandro, CA, USA).<sup>150</sup>

### **3.3.4 In vitro ADAMTS13 digests**

For full length mVWF digestion, recombinant mouse ADAMTS13 (mADAMTS13) was diluted two-fold in 5 mM Tris (tris(hydroxymethyl)aminomethane), pH 8.0 and activated with 10 mM BaCl<sub>2</sub> for 5 minutes at 37°C. 25 µL of mADAMTS13 was added to 25 µL of mVWF (1U/mL in 1.5M urea, 5mM Tris) and incubated for 24 hours at 37°C. EDTA at a final concentration of 50 mM was added to stop the reaction.<sup>124</sup> Samples were frozen at -80°C until multimer analysis. Analysis of the relative multimer migration was analyzed as previously described.<sup>124</sup>

The mVWF115 ADAMTS13 digestion ELISA was modified from the ADAMTS13 Activity ELISA.<sup>107</sup> Reacti-bind Anti-GST coated plates (Pierce, Rockford, IL, USA) were coated with 1.25 mg/ml mVWF115 in PBS, pH 7.2 for one hour, and washed with PBS/0.05% Tween-

20 (PBS/Tween). 2-fold dilutions of ADAMTS13 were made in 5 mM acetate, 5mM MgCl<sub>2</sub>, pH 5.5 and added to each well for 4 hours at 37°C, the wells were washed with PBS/Tween, and 1 µg/ml HISProbe (Pierce) in PBS/Tween was added for 1 hour. 1X OPD reagent (Sigma) was used for visualization, the reaction stopped at 10 minutes with 2.5M H<sub>2</sub>SO<sub>4</sub>, and absorbance was read at 492 nm.

### **3.3.5 von Willebrand Factor Studies in VWF Knockout Mice**

C57Bl/6 wild type mice or VWF knockout mice on a C57Bl/6 background<sup>116</sup> (The Jackson Laboratory, Bar Harbor, ME, USA) aged eight to ten weeks, were used in all experiments. All mouse experiments were reviewed and approved by the Queen's University Animal Care Committee.

### **3.3.6 Hydrodynamic injections**

Plasmid DNA (100 µg pSC11-ET-mVWF) was diluted in a 10% body weight volume of lactated Ringer's solution and injected via tail vein in less than 7 seconds using a 27 gauge needle and 3 ml syringe. VWF and ADAMTS13 co-injections received 50 µg pSC11-ET-mVWF and 20 µg pSC11-ET-mADAMTS13 plasmid. Animals were 8-9 weeks of age at the time of injection.

### **3.3.7 Blood collection**

Blood was collected using a 70 µl untreated glass capillary tube via retroorbital plexus under isoflurane/oxygen anesthetic using 10% buffered citrate as anticoagulant. Blood was centrifuged at 11,000g for 5 minutes to generate platelet poor plasma, and samples stored at -80°C until tested.

### **3.3.8 Recombinant Protein Infusions**

Recombinant mouse VWF was infused into mice at 0.2 U/g weight via tail vein in saline. Each mouse was sampled once for the experiment, with a minimum of 4 animals per time point.

### **3.3.9 Intravital Microscopy for the Ferric Chloride Injury Model of Thrombosis**

Intravital microscopy was performed using a trinocular Wild-Leitz ELR-intravital microscope (Leica Microsystems Canada, Willowdale, ON, Canada), fitted with transmitted (50W halogen) and fluorescence (50W mercury incidence) light accessories. Images of thrombosis formation were captured by a Hamamatsu ORCA ER video camera (Bridgewater, NJ, USA) with fluorescent light. Analysis of the formed thrombi and the accumulated fluorescence intensity was performed using Image ProPlus 6.0 (Media Cybernetics, Bethesda, MD, USA).

Ferric chloride injury was induced as described previously,<sup>137, 138</sup> with slight modifications. Male mice were anaesthetized via intraperitoneal injection of ketamine/xylazine/atropine. The jugular vein was cannulated for injection of rhodamine 6G (40 ng; Sigma-Aldrich, Oakville, ON, Canada) to fluorescently label platelets *in vivo* and the cremaster exteriorized. Throughout the experiment, the muscle was superfused with 37°C saline. Arterioles ranging in size from 7.5 to 18 µm were chosen and after rhodamine 6g infusion, injury was induced through the application of 10% ferric chloride-soaked filter paper (1x1 mm) for 3 minutes. Following injury, the injured area in a single arteriole was observed for 40 minutes. The time to vessel occlusion with thrombus and accumulated fluorescence intensity from images captured at 5 minute intervals were examined. Occlusion times exceeding 40 minutes were recorded as 40 minutes.

### **3.3.10 Graphing and Statistical Analysis**

All data and statistical analysis was performed using GraphPad Prism 4.03 for Windows, GraphPad Software, San Diego, CA, USA, [www.graphpad.com](http://www.graphpad.com). Data are presented as mean values ± standard error of the mean. Statistical analyses were performed using the Student's unpaired t-test, one-way analysis of variance (ANOVA) or two-way ANOVA.

## **3.4 Results**

### **3.4.1 Expression and characterization of recombinant proteins**

The three recombinant mVWF proteins examined in this study have similar multimer patterns and all exhibited ultra large mVWF compared to normal mouse plasma (data not shown). The recombinant mVWF proteins produced in HEK293T cells will presumably have altered glycan content compared to that of normal mouse VWF, and this characteristic could alter mADAMTS13 cleavage rates and protein clearance. Mouse ADAMTS13 was produced in stably transfected HEK293T cells, and activity was compared to normal mouse plasma pool. Conditioned media had mADAMTS13 activity of 1.0 units per ml, while concentrated media had an activity of 32 units per ml using the commercial ADAMTS13 activity assay kit.<sup>107</sup> The purified mVWF115 proteins all resolved as a single 40.4 kDa band via SDS-polyacrylamide gel electrophoresis (data not shown).

### **3.4.2 ADAMTS13 digests of full-length mouse VWF**

Full-length mVWF digests were performed in the presence of 1.5 M urea using a two-fold dilution series of mouse ADAMTS13 (Figure 3.1A). Each assay was performed in duplicate. Multimers were measured for relative migration distance compared to undigested mVWF and plotted using a four parameter curve fit to determine  $EC_{50}$ , the mADAMTS13 enzyme activity to cause a 50% loss of relative multimer migration distance. Wild type mVWF required a mean  $EC_{50}$  value of 0.341 units/ml mADAMTS13. R1597W had an  $EC_{50}$  of 0.109 units/ml, a significant 68% decrease in mADAMTS13 requirement ( $P < 0.0001$ ), while the  $EC_{50}$  of Y1605A/M1606A was greater than 32 units/ml mADAMTS13, the maximum concentration tested ( $P < 0.0001$ ), almost 100-fold that of wild type VWF.

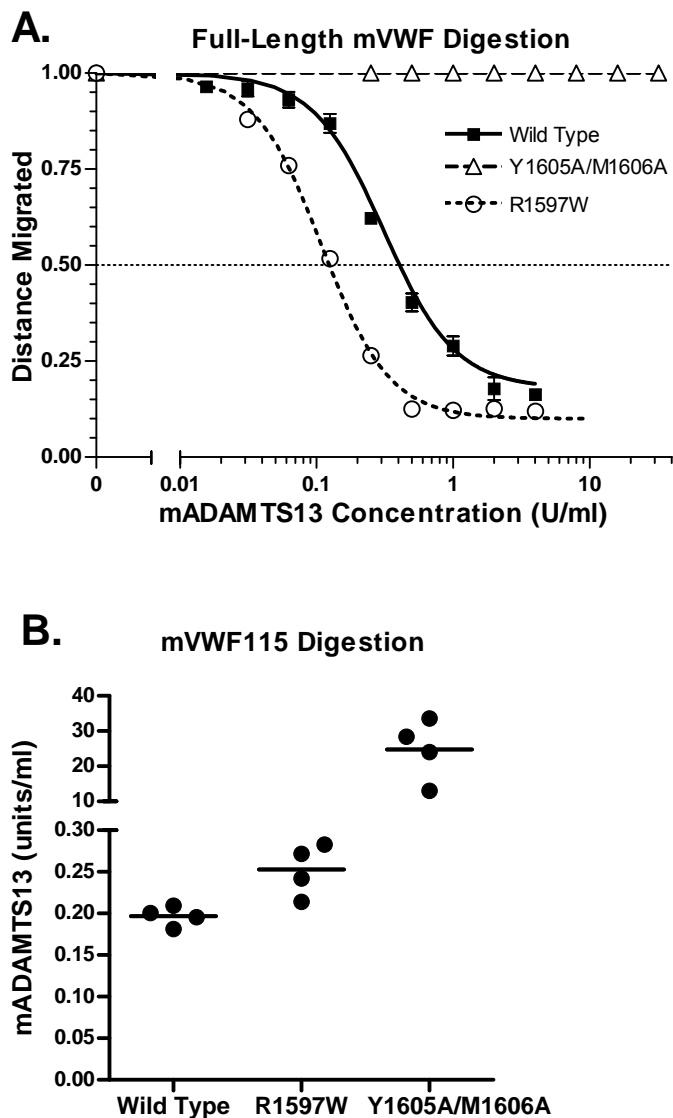


**Figure 3.1 ADAMTS13 Digestion of Full-Length mVWF and mVWF115.**

Recombinant ADAMTS13 digests were performed as outlined under methods. (A) Varying concentrations of ADAMTS13 were incubated with 1 U/ml full-length VWF for 24 hours with 1.5M Urea. Multimer graphs for wild type, R1597W, and Y1605A/M1606A mouse VWF were plotted using a four-parameter curve fit. The concentration of ADAMTS13 required to cause a 50% loss of multimer height was determined. Symbols represent mean values and standard error from two experiments. (B) Comparison of the ADAMTS13 concentrations necessary for 50% loss of intact VWF115. Varying ADAMTS13 concentrations were incubated with VWF115 for 4 hours under non-denaturing conditions. The assay was run 4 times for each construct. Bars represent the mean values.

### **3.4.3 Mouse ADAMTS13 digestion of the mVWF115 substrates.**

Mouse VWF115 digests were performed under non-denaturing conditions with four replicates per mVWF115 substrate. Cleavage was determined indirectly by measuring the loss of the C-terminal histidine tag, since the mutations used in this study alter the epitopes at and around the mADAMTS13 cleavage site in the mVWF115 substrate. The amount of remaining intact mVWF115 was plotted using a four parameter curve fit. Figure 3.1B shows the concentrations of mADAMTS13 required to cleave the mVWF115 by 50%, with bars representing the mean values and circles representing individual assay results. Wild type mVWF115 required a mean of 0.20 U/ml mADAMTS13 for 50% digestion. Fifty percent cleavage of Y1605A/M1606A was achieved with a mADAMTS13 concentration of 23.8 U/ml ( $P = 0.0013$ ), a factor of 119-fold higher, and 50% cleavage of R1597W was achieved with 0.253 U/ml mADAMTS13 ( $P = 0.015$ ), thus requiring 26.5% more mADAMTS13 than the wild type protein.

### **3.4.4 Recombinant protein Infusions**

Mice were infused with recombinant mouse VWF, and a minimum of 4 mice were sampled per time point (Figure 3.2). Data were fit to a one-phase exponential decay with plateau phase. The half-life for wild type protein was 35.1 minutes, R1597W was 27.5 minutes ( $P = 0.025$ ) and Y1605A/M1606A was 18.4 minutes ( $P < 0.001$ ).

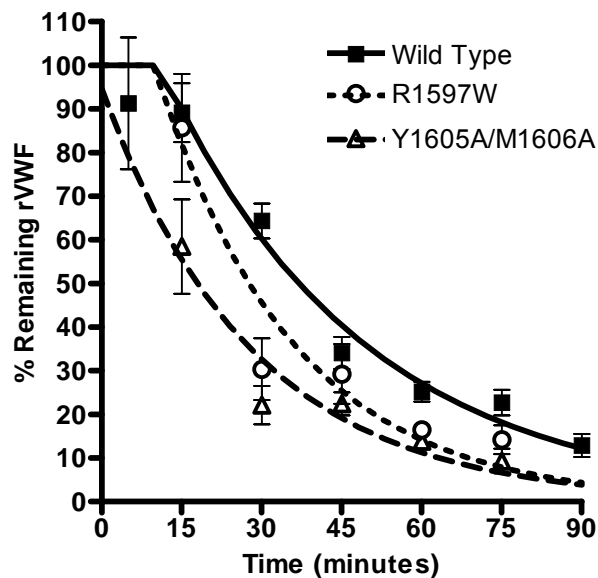


**Figure 3.2 Recombinant Mouse VWF Protein Clearance.**

Recombinant mouse VWF protein (200 U/kg) was injected via tail vein into VWF knockout mice. Mice were sampled once,  $N \geq 4$  per time point. Half-life was determined for each recombinant VWF protein using a one phase decay model with plateau phase.

### 3.4.5 VWF expression via hydrodynamic transgene delivery

VWF knockout mice received plasmid DNA containing the liver specific ET promoter and mouse *Vwf* cDNA. This results in hepatocyte-specific expression of the mouse VWF protein, which presumably has an altered glycan content compared to normal endothelial and platelet-derived mVWF. This method replaces only the plasma component of mVWF in the knockout animals. Complete blood counts were performed with the injection of all *Vwf* cDNAs examined, and only transient thrombocytopenia was observed on day 2, with full recovery following all injections by day 5. The thrombocytopenia is probably a response to the diffuse vascular trauma caused by the injection. No other adverse events or alterations in CBC values were observed (data not shown).

### 3.4.6 VWF antigen levels

VWF knockout mice were sampled post-hydrodynamic injection ( $N \geq 10$ ), and antigen levels determined by VWF:Ag ELISA. The peak levels of VWF:Ag were observed at day 2 (wild type 25.3U/ml), with a rapid decrease between days 5 and 8, and a more slowly decreasing plateau phase from days 14 to 42 (Figure 3.3A). There was no statistical difference for VWF:Ag levels between the three *Vwf* cDNAs injected between days 2 and 42 inclusive. However, both mutant cDNAs demonstrated a lower VWF:Ag level from day 14 onwards compared to the wild

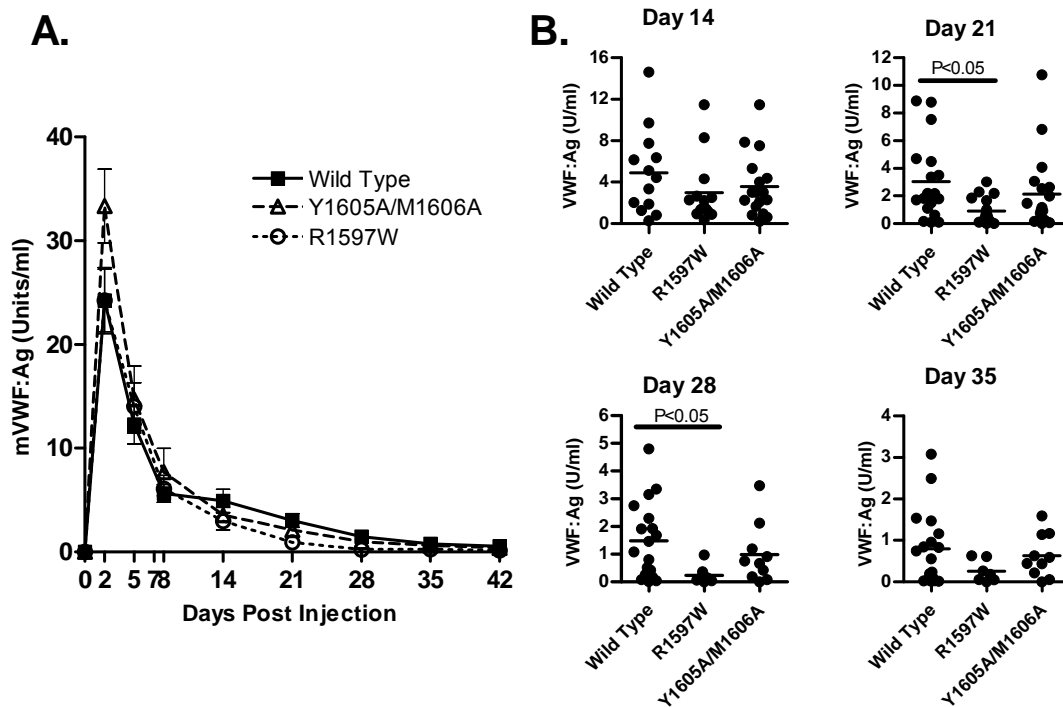


**Figure 3.3 Mouse VWF antigen levels post-hydrodynamic injection.**

VWF knockout mice expressing wild type, R1597W or Y1605A/M1606A mVWF were sampled post-hydrodynamic injection ( $N \geq 10$ ). VWF:Ag levels were determined via ELISA. (A) VWF:Ag levels from day 2 to 42 post hydrodynamic injection. Symbols represent means with SEM error bars. (B) Data by day for days 14, 21, 28, and 35. Each circle represents data from a single mouse. No statistical differences were found with the exceptions of wild type vs. R1597W on days 21 and 28, using one way ANOVA, Tukey's post test.

type cDNA (Figure 3.3B). R1597W was statistically significantly lower than wild type at day 21 (0.981 U/ml versus 3.04 U/ml,  $p < 0.05$ ) and day 28 (0.237 U/ml versus 1.49 U/ml,  $p < 0.05$ ).

Y1605A/M1606A dropped below 1 U/ml by day 28 (0.982 U/ml) and wild type mVWF dropped below 1 U/ml by day 35 (0.798 U/ml).

### 3.4.7 VWFpp/VWF:Ag ratio determination

VWF knockout mice were sampled post-hydrodynamic injection ( $N \geq 10$ ) and VWF:Ag and VWFpp levels were determined via ELISA. Values were normalized to a mean VWFpp/VWF:Ag ratio equal to 1.0 in WT cDNA injected mice, (Figure 3.4) a value that is 6.5 fold lower than that measured in the plasma of normal C57Bl/6 mice (data not shown). The R1597W mutant showed a ratio of 1.81, greater than wild type ( $P < 0.001$ ). The

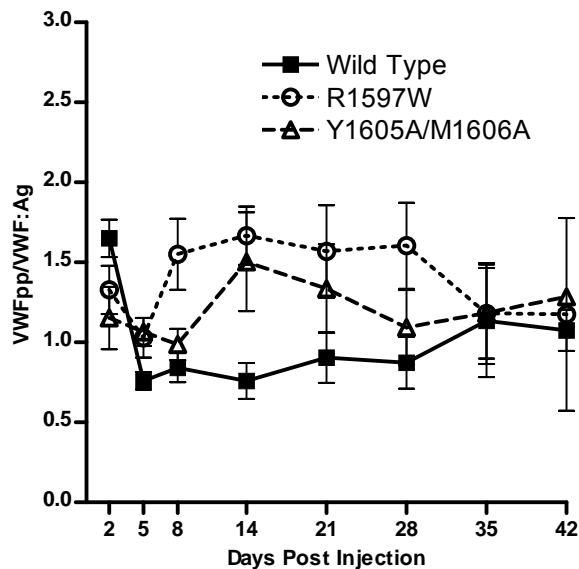


**Figure 3.4 VWFpp/VWF:Ag ratio determination.**

VWF knockout mice expressing wild type, R1597W or Y1605A/M1606A cDNA were sampled post-hydrodynamic injection ( $N \geq 10$ ). VWF:Ag and VWFpp levels were determined via ELISA. Values are normalized to a mean wild type ratio equal to 1.0, which is 6.5 fold lower than that in normal C57BL/6 mouse plasma.

VWFpp/VWF:Ag ratio for the Y1605A/M1606A mutant was 1.629, higher than wild type ( $P < 0.01$ ). Thus, both mutations demonstrate a higher VWFpp/VWF:Ag ratio, which is a surrogate marker for accelerated VWF clearance from plasma.

### 3.4.8 Multimer Analysis

Multimeric profiles of the hydrodynamically-expressed mVWF were examined to determine if the mutations altered the mVWF multimer structure. The mouse VWF produced from the liver post-hydrodynamic injection has an altered multimer appearance compared to that of normal mouse plasma (Figure 3.5A). Plasma was diluted to 1 U/ml VWF:Ag, and samples that had clotted lost most multimer bands, an example can be seen for wild type day 14. Single multimer bands rather than a normal triplet structure were observed, with a slightly lower molecular weight per band. In addition, the multimer profile was skewed toward lower molecular weight multimers compared to normal mouse plasma. Compared to wild type mVWF, R1597W demonstrated a loss of multimer bands, while Y1605A/M1606A had a population of higher molecular weight bands. Multimer band number counts were used to quantify differences in multimeric structure (Figure 3.5B). Wild type cDNA had a peak level of 22.0 bands at day 2 ( $N = 7$ ), and a low of 8.57 bands at day 28, with an average band number of 12.54. Y1605A/M1606A had an average of 12.63 bands, an increase of 0.11 bands compared to wild type ( $P > 0.05$ ,  $N = 5$ ). In contrast, R1597W had an average of 6.05, a decrease of 6.49 bands ( $P < 0.001$ ,  $N = 5$ ).

Animals receiving a co-injection of *Vwf* and *Adamts13* cDNAs had a diminished multimer size (Figure 3.5C). Mouse ADAMTS13 activity in these mice was determined in a static assay using m73 substrate with an antibody that detects intact A2 domain substrate (data not shown). Mouse ADAMTS13 activity levels were increased to an average of 5.2 U/ml on day

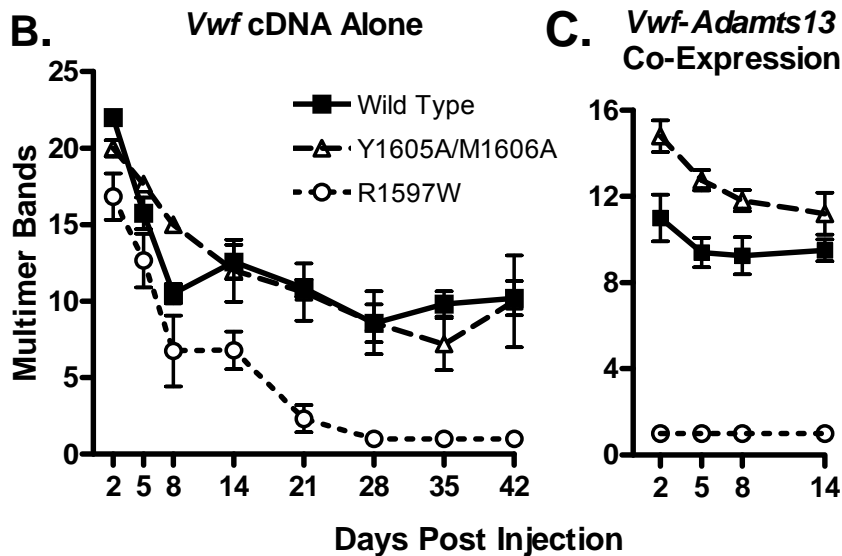
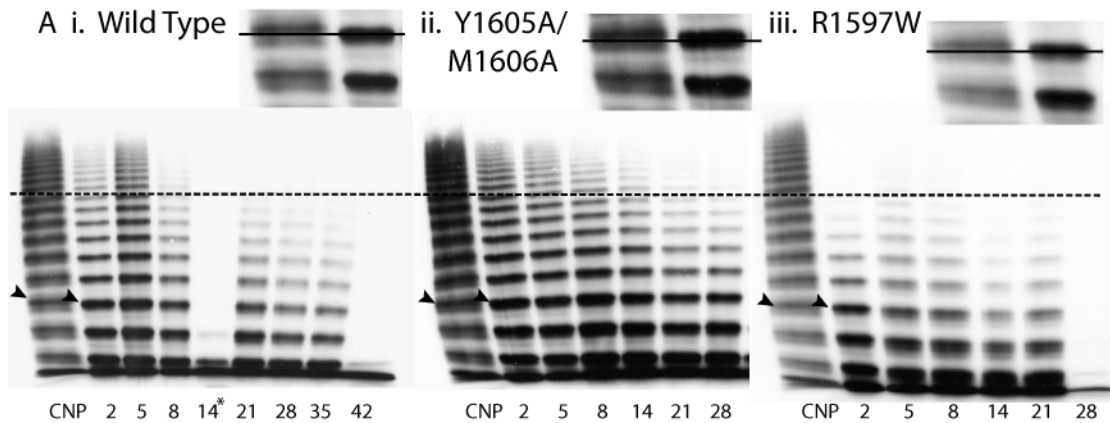


**Figure 3.5 Hydrodynamic VWF Multimer Structure.**

VWF knockout mice expressing wild type, R1597W, and Y1605A/M1606A mouse VWF were sampled post-hydrodynamic injection and evaluated for multimeric structure. Plasma was run on a 1.4% agarose gel at a VWF concentration of 1.0 U/ml. (A) Exemplar multimers are shown for i) wild type, ii) Y1605A/M1606A, and iii) R1597W. The dotted line represents high molecular weight multimers, greater than 10 multimer bands. Arrow heads indicate the top bands in the enlarged inset bands, with a line through the inset figure illustrating the single band of lower molecular weight in the recombinant proteins compared to C57Bl/6 normal plasma pool (CNP) triplet multimer bands. \* denotes a multimer from a clotted sample. (B) Multimer analysis was performed on VWF knockout mice expressing mVWF post-hydrodynamic injection by counting the total number of resolved multimer bands in each lane.  $N \geq 4$ . (C) Multimer analysis on VWF knockout mice expressing mVWF and mADAMTS13 post-hydrodynamic injection.  $N \geq 4$ .

2, 4.7 U/ml on day 5, 2.8 U/ml on day 8 and 2.4 U/mL on day 14. With the co-injected *Adamts13* cDNA, wild type mVWF had an average band number of 9.79 from days 2-14, which was significantly different compared to the two mutations. Y1605A/M1606A had a higher molecular weight multimer structure with 12.64 bands ( $P < 0.01$ ). In marked contrast, after *Adamts13* co-injection, R1597W resolved only a single band for all time points, a decrease of 8.79 bands ( $P < 0.001$ ), demonstrating that the addition of full-length mADAMTS13 to the VWF knockout mouse exaggerates the cleavage profile differences for these two mutant mVWF proteins.

### **3.4.9 Evaluation of in vivo thrombogenesis**

Performance of the ferric chloride injury model of thrombosis on cremaster arterioles demonstrated a difference in mean occlusion times between the two mutations studied and that of wild type mVWF, despite the fact that their plasma levels were not significantly different at the time of study (Figure 3.6). All mice were expressing VWF:Ag levels between 0.5 and 2.5 U/ml mVWF at the time of these studies. Wild type animals ( $n = 8$ ) had a mean occlusion time of 29.9 minutes. R1597W ( $n = 7$ ) was much greater at 37.3 minutes ( $P = 0.006$ ), demonstrating a loss of VWF function. Y1605A/M1606A ( $n = 8$ ) had a similar loss of occlusion with a mean of 37.3 minutes ( $P = .02$ ). Platelet accumulation via fluorescence intensity demonstrated that Y1605A/M1606A had an increased accumulation compared to wild type and R1597W (Figure 3.6 B and C). Total relative platelet accumulation, represented as area under the curve for wild type VWF was 47.11, R1597W 47.4 ( $P = 0.94$ ) and Y1605A/M1606A was significantly higher at 61.8 ( $P = 0.038$ ).



Mouse ADAMTS13 has poor activity on the human VWF substrate in both full-length and A2 domain VWF73 assays.<sup>125</sup> There is 81% sequence identity and 91% homology between the human and mouse VWF amino acid sequences.<sup>117</sup> This could lead to changes in function, despite there being conservation for R1597 and Y1605/M1606 between humans and mice. Therefore, it was necessary to confirm that our mutations of interest behaved similarly in a fully mouse VWF-ADAMTS13 experimental system.

Full-length mouse ADAMTS13 digests appeared similar to that of previously reported *in vitro* human ADAMTS13 data (Figure 3.1). There was a 78% decrease in the mADAMTS13 concentration required to achieve 50% cleavage in R1597W compared with wild type mVWF in the full-length material.<sup>105, 150</sup> In contrast, Y1606A/M1606A did not show any cleavage with the maximum mADAMTS13 concentration tested, 97-fold higher than wild type. The mVWF115 assay also showed a 126-fold higher value in mADAMTS13 concentration with the Y1605A/M1606A cleavage site knockout. However, in contrast to the results with the full-length substrate, R1597W showed a 28% increase in mADAMTS13 concentration compared to the wild type mVWF115. This could be due to the more open structure in mVWF115, a GST and histidine tagged 115 amino acid fragment of the mVWF A2 domain, G1554-T1668. Three amino acids that interact with R1597 are absent in this substrate, thus altering the behaviour of this variant. The crystal structure of the human VWF A2 domain indicates that R1597 is in a short helix in a flexible extended loop and interacts with L1497, D1498, S1534, and S1593.<sup>95</sup> Because three of these four amino acids are absent in the mVWF115, this mutation will not be accurately modeled in this substrate. This is an important caveat to keep in mind when evaluating mutations in the A2 domain with the minimal substrates for ADAMTS13.

Since *in vitro* mouse full-length VWF digestion by mouse ADAMTS13 appears similar to that of the human system, we investigated the multimer structure of the hydrodynamic

injection mice expressing the VWF proteins longer term (Figure 3.5). The multimer structure in Y1605A/M1606A showed a statistically insignificant population of higher molecular weight bands than wild type VWF (average increase of 0.11 bands). R1597W multimer structure was significantly lower, with a loss of half the bands.

In the C57Bl/6 mouse strain, there is a retrotransposon insertion in the mouse *Adamts13* gene that leads to the premature truncation of ADAMTS13, resulting in a protein lacking the C-terminal 2 Tsp1 domains and CUB domains.<sup>126</sup> In vivo, there is little change in cleavage under static conditions, and C57Bl/6 mice exhibit normal VWF multimer patterns. However, the truncated enzyme results in increased thrombotic occlusions under shear stress conditions, since it is not fully active in vivo.<sup>127</sup> This could be a factor in the lack of major differences in the multimer patterns between Y1605A/M1606A and the wild type proteins. To mitigate any artifacts caused by the partially functional ADAMTS13 in our mice, we performed co-injections with a full-length mouse *Adamts13* cDNA to observe any influences on the VWF multimer profile (Figure 3.5C). With the co-injected *Adamts13* cDNA, the Y1605A/M1606A multimer profile was significantly higher than that of wild type VWF (12.64 versus 9.79 bands). In marked contrast, after co-injection of the *Adamts13* cDNA, R1597W resolved only a single band for all time points, a decrease of 8.79 bands ( $P < 0.001$ ), demonstrating that the addition of full-length ADAMTS13 to the VWF knockout mouse exaggerates the cleavage profile differences for these two mutant VWF proteins.

Protein clearance studies were performed to determine if these mutations altered the half-life of the VWF protein. The recombinant proteins were cleared rapidly, with wild type half life being 35.1 minutes, too short for evaluation of thrombosis or hemostasis injury models (Figure 3.2). Both mutants had significantly shorter half-lives, with R1597W showing a 22% decrease and Y1605A/M1606A a 48% decrease. This rapid clearance could be due in part to alterations in

the A2 domain folding of the molecule, that could, in turn, alter VWF interactions with ADAMTS13, other plasma proteins, or clearance receptors.<sup>95</sup> Previous work in the VWF knockout mouse showed no influence of multimer structure on protein clearance.<sup>37</sup>

Longer term expression of VWF was achieved in this study using hydrodynamic tail vein injection of the mouse *Vwf* cDNA. There were minimal differences in the plasma levels of the two mutations compared to wild type, although R1597W was slightly lower in the plateau phase from day 14 onward (Figure 3.3). VWFpp/VWF:Ag ratios were mildly increased for both mutations, suggesting increased clearance of the mutant proteins, and thus supports the results of the recombinant protein infusions (Figure 3.4).

We have also evaluated the pro-coagulant function of the two mutant proteins in an established in vivo thrombosis model in the hydrodynamic-injection mice (Figure 3.6). These studies were carried out at similar plasma levels of the proteins to eliminate the influence of VWF concentration. R1597W exhibited lengthened times to vessel occlusion when expressed at physiologic concentrations between 0.5 and 2.5 U/ml at the time of the experiment. This supports the expectation that the loss of higher molecular weight VWF multimers would lead to a loss of platelet adhesion and thrombus stability. Y1605A/M1606A, however, did not lead to a definite prothrombotic phenotype. Rather, increased platelet accumulation was observed with a lack of vessel occlusion. This suggests that other mechanisms are at work in this system.

Interestingly, even very high plasma levels of the Y1605A/M1606A mutant were not associated with any laboratory evidence for TTP in these mice. Platelet counts were stable, there were no changes in the CBC and no fragmented red cells were seen in the blood smears. This finding supports previous evidence suggesting that a combination of pathologic challenges are required in these mice to trigger the TTP phenotype.<sup>122, 123</sup>

This study demonstrates that changes in the human *VWF* gene that result in alterations in ADAMTS13-mediated cleavage will also affect the mouse VWF molecule. R1597W was more easily cleaved by mADAMTS13 in a full-length digest assay and exhibited a lower multimeric profile compared to wild type VWF protein when expressed in the VWF knockout mouse. In addition, R1597W was less thrombogenic and had a shorter half-life and a slightly increased VWFpp/VWF:Ag ratio, suggesting that this variant protein is cleared from plasma more rapidly. This mechanism likely contributes to the lower VWF:Ag levels observed in days 14-35 post-hydrodynamic injection. Overall, these findings in the mouse model recapitulate the human type 2A disease phenotype.

The Y1605A/M1606A mutant demonstrated a marked decrease in mADAMTS13-mediated cleavage *in vitro*. In the hydrodynamic injection mice, Y1605A/M1606A shows minor multimer profile differences compared to wild type VWF. However, when full-length mADAMTS13 was co-expressed in the mice, the cleavage site mutant mice showed a population of higher molecular weight multimers. In addition, an accelerated clearance phenotype is suggested by the results of the recombinant protein infusion and VWFpp/VWF:Ag ratio studies.

This study establishes that VWF mutations alter ADAMTS13-mediated cleavage in the mouse model. In addition, this leads to significant alterations to the multimer structure of the VWF present in animals receiving co-hydrodynamic injection of full-length normal *Adamts13* cDNA. The pathologic implications of these studies stress the disease phenotypes that are present in both type 2A VWD and congenital TTP patients. The altered VWF structure is only problematic under a secondary stress, such as the ferric-chloride induced injury model used here. This study illustrates the importance of examining potentially pathogenic sequence changes in a whole animal system, rather than relying on individual *in vitro* methodologies to explain a patient's disease phenotype.

## Chapter 4

# Investigating the pathologic mechanisms of the common Type 1 von Willebrand Disease mutations R1205H and Y1584C through in vitro and in vivo mouse models

### 4.1 Summary

Type 1 von Willebrand Disease (VWD) results from mutations that alter VWF synthesis, secretion, and clearance. The mechanisms underlying two common type 1 VWD mutations, the severe R1205H and more moderate Y1584C variant, were examined in this study. In vitro biosynthesis was reduced for both mutations in human and mouse VWF, with the effect being more severe in R1205H. VWF knockout mice received hydrodynamic injections of mouse *Vwf* cDNA for each mutation. Lower mVWF antigen levels were demonstrated in both homozygous and heterozygous forms for both type 1 mutations from days 14-42. Recombinant protein infusions and hydrodynamic-expressed VWF propeptide to antigen ratios demonstrate that R1205H mouse VWF has a moderately increased clearance rate, while Y1584C is normal. Recombinant ADAMTS13 digestions of Y1584C demonstrated enhanced cleavage of both human and mouse VWF115 substrates, and Y1584C multimers from hydrodynamic mice show a lower molecular weight profile compared to wild type and R1205H mice. Y1584C showed reduced thrombus formation in a ferric chloride injury model while R1205H demonstrated similar thrombogenic activity to wild type VWF. This study has elucidated several novel mechanistic details for these two mutations and highlights that type 1 VWD can be recapitulated in the VWF knockout hydrodynamic injection model.

## 4.2 Introduction

The large multimeric glycoprotein von Willebrand Factor (VWF) is critical to normal hemostasis through mediating platelet-subendothelial interactions as well as binding to platelets to support their aggregation at the site of endothelial damage. In addition, VWF serves as a molecular chaperone for FVIII. The disease phenotype of type 1 von Willebrand disease (VWD) is a mild to moderate quantitative reduction of supposedly functionally normal VWF, with plasma VWF levels between 5 and 50% of normal.<sup>73</sup> This autosomal dominant disease can be caused by a wide array of defects including defective RNA or protein synthesis, premature protein degradation before cellular release, ineffective secretion, rapid plasma clearance, or a mutation that results in a null allele.<sup>110</sup>

R1205H, the Vicenza mutation, has a relatively severe type 1 phenotype that appears to be related to accelerated VWF clearance. Often occurring with a second VWF variation, M740I, the Vicenza mutation shows a significant reduction in VWF antigen (VWF:Ag) to ~0.15 U/mL, VWF Ristocetin Cofactor Activity (VWF:RCo) ~0.20 U/mL, and Factor VIII levels <0.30 U/mL, but maintains normal platelet VWF levels and function.<sup>44, 45, 155, 156</sup> Patient bleeding scores, a marker of VWD severity, range between 2-17 (n = 18), with a mean of 8 (bleeding score  $\geq 4$  is positive).<sup>73, 111, 157, 158</sup> Accelerated clearance of the mutant protein has been demonstrated via desmopressin (DDAVP) studies<sup>44</sup> and human recombinant protein infusion in the VWF knockout mouse,<sup>37</sup> as well as through high VWFpp/VWF:Ag ratios, with observed ratios of 10 or greater for this indirect measurement of VWF clearance from the plasma.<sup>45</sup> R1205H VWF also often displays an increase in high molecular weight multimers along with occasional alteration in the typical multimer triplet band pattern, but this is not consistent in all patients.<sup>44, 45, 155, 159</sup> The increase in high molecular weight material observed in some R1205H patients has been attributed to the rapid clearance of the protein and thus reduced opportunity for proteolytic remodeling.<sup>160</sup>

Patients with the R1205H mutation also have a normal or enhanced DDAVP response since there is normal Weibel-Palade body storage and release.<sup>161, 162</sup>

The commonly occurring Y1584C mutation has a mild type 1 VWD phenotype. This mutation was first identified in 14% of index cases during the Canadian Type 1 VWD study with an associated founder polymorphic haplotype.<sup>112, 141</sup> Heterozygous patients have a mean VWF:Ag of 0.40 U/ml, and possess predominately group “O” blood type.<sup>141</sup> The Y1584C mutation was also found in 8% of index cases in the European MCMDM-1VWD study, with VWF:Ag levels ranging from 0.21-0.80 U/mL.<sup>111</sup> Patient bleeding scores range between 0-20 (n = 23) with a mean of 4, showing a highly variable but generally mild phenotype.<sup>73, 111, 158</sup> In vitro studies show that Y/C1584 and C/C1584 patient plasma has enhanced ADAMTS13-mediated proteolysis, although this susceptibility is much lower than that of type 2A group II VWD mutations.<sup>163, 164</sup> In addition, in vitro expression studies in COS-7 cells have shown 38% reduction in VWF synthesis and 47% increase in intracellular retention for the homozygous C1584 protein.<sup>141</sup>

The VWF knockout mouse has been used recently to examine several different human VWD mutations through the establishment of mouse VWF expression by hydrodynamic delivery of the mouse VWF cDNA. The homogeneous, inbred genotype of the mice, relatively low cost to introduce new mutations, and the ability to evaluate larger study populations than would be available for human subjects makes this a valuable and convenient methodology to examine different VWD mutations. This approach also allows single amino acid substitutions to be examined on the background of a consistent (non-polymorphic) cDNA sequence. This experimental strategy has already recapitulated the human disease phenotypes for defective binding to collagen and GPIIbIIIa,<sup>135</sup> and type 2B VWD.<sup>136, 152</sup> However, until now, quantitative von Willebrand disease phenotypes have not been explored using this methodology.

Both R1205H and Y1584C have been well described in type 1 VWD patient populations. However, neither mutation has been examined for longer-term expression in an animal model system to evaluate the associated pathogenic mechanisms. This study examines through both in vitro and in vivo strategies the impact of the severe R1205H and mild Y1584C type 1 VWD mutations in mouse models of the phenotype.

## **4.3 Materials and Methods**

### **4.3.1 Plasmid construction and mutagenesis**

Full-length human VWF was produced using pCIneoVWF-ESN.<sup>150</sup> The mouse *Vwf* cDNA (courtesy of Peter Lenting) was cloned into the pCIneo plasmid for recombinant protein and into the pSC11 plasmid<sup>153</sup> with the liver-specific Enhanced murine Transthyretin (ET) promoter (courtesy of Luigi Naldini)<sup>154</sup> for hydrodynamic delivery. hVWF115, a GST and histidine tagged 115 amino acid fragment of the VWF A2 domain, E1554-R1668, was constructed from the pGEX-6P-1 backbone (GE Healthcare Life Sciences, Piscataway, NJ, USA) and pCIneoVWF-ESN, with mVWF115 being produced in a similar manner.<sup>98</sup> Site-directed mutagenesis was performed using the Quikchange XL II kit (Stratagene, La Jolla CA). Both R1205 and Y1584 are conserved between human and mouse. Mouse *Adamts13* cDNA (courtesy of Dr. F. Scheiflinger, Baxter, Austria) was cloned into the pSC11 plasmid<sup>153</sup> with the liver-specific ET promoter<sup>154</sup> for hydrodynamic delivery.

### **4.3.2 Recombinant protein production and cell culture**

HEK293T cells were transiently transfected using the calcium phosphate method as previously described.<sup>141, 150</sup> A total of 10 µg of *VWF* cDNA plasmid was transfected per 10 cm dish, consisting of wild type, R1205H, Y1584C, or co-transfections of 5 µg of wild type and mutant cDNA. VWF was secreted into serum-free OptiMEM containing 100 U/ml penicillin,

100 µg/ml streptomycin, 1X Insulin/Selenium/Transferrin G (Invitrogen, Carlsbad, CA, USA). Medium was harvested after 72 hours and recombinant VWF was concentrated using Amicon Ultra-15 or Ultra-70 100K MWCO units (Millipore, Billerica, MA, USA). Medium and cellular lysates from individual 10 cm dishes were evaluated for VWF protein levels.

Human and mouse ADAMTS13 derived from the pcDNA3.1-hADAMTS13 and pcDNA3.1-mADAMTS13 expression vectors (gifts of Dr. F. Scheiflinger, Baxter, Austria) were produced via stable transfection in HEK293T cells similar to the recombinant VWF, using G418 selection.<sup>3</sup> ADAMTS13 activity was determined using the ADAMTS13 activity ELISA Kit (Japan Clinical Laboratories, Kyoto, Japan).<sup>107</sup>

The VWF115 proteins were produced in BL21-Gold *E. coli* (Stratagene) and purified via Ni-NTA agarose (Qiagen, Valencia, CA).<sup>150</sup>

#### **4.3.3 VWF antigen, propeptide and multimer quantitation**

VWF protein concentration was determined by VWF enzyme-linked immunosorbent assay (ELISA) using polyclonal human VWF antibodies A0082 and P0226 (DAKO, Carpinteria, CA, USA). Human VWF concentration was assayed against a standard human plasma pool (CRYOcheck, Precision Biologic, Dartmouth, NS, CA). Mouse VWF propeptide concentration was determined using the 349.3 capture antibody, and detected via the horseradish peroxidase-linked 349.2 antibody, both anti-mouse VWF propeptide antibodies were provided by Sandra Haberichter. Mouse VWF, VWF propeptide, and ADAMTS13 activity concentrations were determined using a normal C57Bl/6 mouse plasma pool, comprising plasma derived from 25 normal, eight week old, mixed gender, C57Bl/6 mice, with the means arbitrarily determined to be 1 U/mL mVWF, mVWFpp, and mADAMTS13.

VWF multimers were analyzed by electrophoresis using a 1.4% separating sodium dodecyl sulfate (SDS) agarose gel and visualized using the polyclonal HRP-labeled human VWF

antibody P0226 (DAKO) as previously described.<sup>142</sup> Lanes were analyzed by 1-D densitometry for multimer distance and band number using AlphaEaseFC version 3.1.2 (Alpha Innotech, San Leandro, CA, USA).<sup>150</sup>

#### **4.3.4 In vitro ADAMTS13 digests of recombinant VWF**

For full-length hVWF digestion, recombinant human ADAMTS13 (hADAMTS13) was diluted two-fold in 5 mM Tris (tris(hydroxymethyl)aminomethane), pH 8.0, and activated with 10 mM BaCl<sub>2</sub> final concentration for 5 minutes at 37 °C. A 100 µl aliquot of hADAMTS13 was added to 100 µl rVWF, 1 U/ml in 5 mM Tris, pH 8.0, and dialyzed against 1.5 M urea, 5 mM Tris, pH 8.0, on VSWP02500 filters (Millipore). After five hours, the samples were collected and 25 mM EDTA (ethylenediaminetetraacetic acid), final concentration, was added.

For full-length mVWF digestion, recombinant mouse ADAMTS13 (mADAMTS13) was diluted two-fold in 5 mM Tris, pH 8.0 and activated with 10 mM BaCl<sub>2</sub> for 5 minutes at 37°C. 25 µL of mADAMTS13 was added to 25 µL of rVWF (1U/mL in 1.5M urea, 5mM Tris) and incubated for 24 hours at 37°C. EDTA at a final concentration of 50 mM was added to stop the reaction.<sup>124</sup> Samples were frozen at -80°C until multimer analysis. Analysis of the relative multimer migration for full-length digests was analyzed as previously described, using a four-parameter curve fit to determine EC<sub>50</sub>, or ADAMTS13 concentration to cause 50% loss of relative multimer distance.<sup>124</sup> Curve fit F-tests for logEC<sub>50</sub> were performed to determine statistical significance.

The hVWF115 and mVWF115 ADAMTS13 digestion ELISA assays were modified from the ADAMTS13 activity ELISA.<sup>107</sup> Reacti-Bind Anti-GST plates (Pierce, Rockford, IL, USA) were coated with 1.25 mg/ml VWF115 in PBS, pH 7.2 for one hour, and washed with PBS/0.05% Tween-20 (PBS/Tween). 2-fold dilutions of ADAMTS13 were made in 5 mM acetate, 5 mM MgCl<sub>2</sub>, pH 5.5 and added to each well for 4 hours at 37°C, the wells were washed with

PBS/Tween, and 1 µg/ml HISProbe (Pierce) in PBS/Tween was added for 1 hour. 1X OPD reagent (Sigma) was used for visualization, the reaction stopped at 10 minutes with 2.5M H<sub>2</sub>SO<sub>4</sub>, and absorbance was read at 492 nm. EC<sub>50</sub>, the ADAMTS13 concentration to digest half the VWF115 substrate, was determined via four-parameter curve fit. T-tests of the mean EC<sub>50</sub> values were performed to determine statistical significance.

#### **4.3.5 Von Willebrand Factor studies in VWF Knockout Mice**

C57Bl/6 wild type mice or VWF knock out mice on a C57Bl/6 background<sup>116</sup> (The Jackson Laboratory, Bar Harbor, ME, USA) aged eight to ten weeks, were used in all experiments. All mouse experiments were reviewed and approved by the Queen's University Animal Care Committee.

#### **4.3.6 Hydrodynamic injections**

Plasmid DNA was diluted in a 10% body weight volume of lactated Ringer's solution and injected via tail vein in less than 7 seconds using a 27-gauge needle and 3 ml syringe. Animals were 8-9 weeks of age at the time of injection. Wild type, R1205H, and Y1584C mice received 100 µg of *Vwf* cDNA plasmid, pSC11-ET-mVWF. Wild type/R1205H and wild type/Y1584C mice received 50 µg of wild type and 50 µg mutant plasmid in co-injection studies. VWF and ADAMTS13 co-injections received 50 µg *Vwf* cDNA and 20 µg *Adamts13* cDNA.

#### **4.3.7 Blood collection**

Blood was collected using a 70 µl untreated glass capillary tube via retroorbital plexus under isoflurane/oxygen anesthetic using 10% buffered citrate as anticoagulant. Blood was centrifuged at 11,000g for 5 minutes to generate platelet poor plasma, and samples stored at -80°C until tested.

#### **4.3.8 Recombinant mVWF Protein Infusions**

Recombinant mouse VWF was infused into mice at 0.2 U/g weight via tail vein in saline. Each mouse was sampled once, with a minimum of 3 animals per time point. Data was fit to a one-phase exponential decay with plateau phase and curve fit F-test for half-life used to determine statistical significance.

#### **4.3.9 Intravital Microscopy for the Ferric Chloride Injury Model of Thrombosis**

Intravital microscopy was performed using a trinocular Wild-Leitz ELR-intravital microscope (Leica Microsystems Canada, Willowdale, ON, Canada), fitted with transmitted (50W halogen) and fluorescence (50W mercury incidence) light accessories. Images of thrombus formation were captured by a Hamamatsu ORCA ER video camera (Bridgewater, NJ, USA) with fluorescent light. Analysis of the formed thrombi and the accumulated fluorescence intensity was performed using Image ProPlus 6.0 (Media Cybernetics, Bethesda, MD, USA).

Ferric chloride injury was induced as described previously,<sup>137, 138</sup> with slight modifications. Male mice were anesthetized via intraperitoneal injection of ketamine/xylazine/atropine. The jugular vein was cannulated for injection of rhodamine 6G (40 ng; Sigma-Aldrich, Oakville, ON, Canada) to fluorescently label platelets *in vivo* and the cremaster exteriorized. Throughout the experiment, the muscle was superfused with 37°C saline. Arterioles ranging in size from 7.5 to 18 µm were chosen and after rhodamine 6G infusion, injury was induced through the application of 10% ferric chloride-soaked filter paper (1x1 mm) for 3 minutes. Following injury, the injured area in a single arteriole was observed for 40 minutes. The time to vessel occlusion with thrombus and accumulated fluorescence intensity from images captured at 5 minute intervals were examined. Occlusion times exceeding 40 minutes were recorded as 40 minutes.

#### **4.3.10 Graphing and Statistical Analysis**

All data and statistical analysis was performed using GraphPad Prism 4.03 for Windows, GraphPad Software, San Diego, CA, USA, [www.graphpad.com](http://www.graphpad.com). Data are presented as mean values  $\pm$  standard error of the mean. Statistical analyses were performed using the Student's unpaired t-test, one-way analysis of variance (ANOVA) with Tukey's post-tests or two-way ANOVA with Bonferroni post-tests, as appropriate. P values less than 0.05 were considered statistically significant.

### **4.4 Results**

#### **4.4.1 Expression and characterization of recombinant proteins**

Recombinant human VWF was produced via transient transfection in HEK293T cells (Figure 4.1A). All values were normalized to total wild type VWF antigen equal to 100%. Human VWF produced via transient transfection showed a decrease in total protein production for both Y1584C (69.6% of wild type,  $P < 0.001$ ) and R1205H (64.0% of wild type,  $P < 0.001$ ). These reductions are less severe in co-transfections of wild type cDNA with each mutation (modeling the heterozygous state for each mutation). Compared to wild type VWF protein expression, wild type/Y1584C had levels of 79.8% ( $P < 0.05$ ), and wild type/R1205H had levels of 69.8% ( $P < 0.001$ ). Although R1205H does show more cellular retention than the wild type VWF (15.8% compared to 11.4%), this difference is not statistically significant.

Mouse VWF exhibited higher cellular retention rates compared to that of human VWF, with wild type mouse VWF having 22.9% cellular retention compared to 11.4% in human VWF (Figure 4.1). There were no significant differences in cellular retention between wild type mVWF compared to the mouse mutant proteins (Figure 4.1B). However, secreted mouse VWF levels were different. Wild type mVWF (77.0%) was not different from that of Y1584C (85.5%),

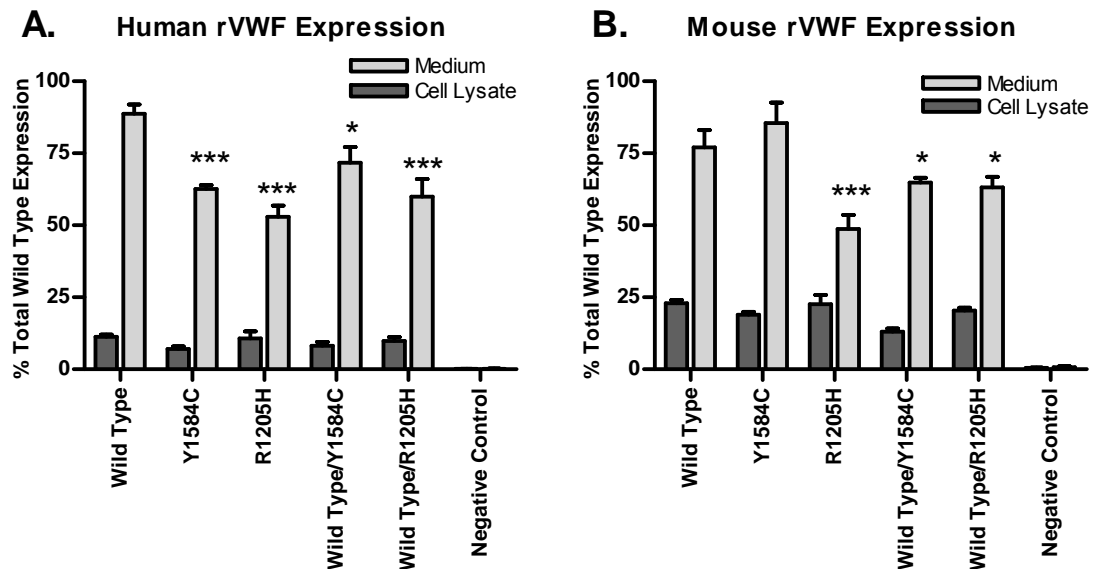


**Figure 4.1 Expression of human and mouse recombinant VWF.**

Transient transfections of VWF cDNAs were performed in HEK293T cells, and expressed in serum-free medium. Total medium and cellular lysate per 10 cm dish was measured via VWF:Ag ELISA, and results normalized to total wild type VWF equal to 100 for both human (A) and mouse (B). \*  $P < 0.05$ . \*\*\*  $P < 0.001$ .

$P > 0.05$ ). In contrast, mouse VWF proteins, R1205H (48.7%,  $P < 0.001$ ), wild type/Y1584C (64.8%,  $P < 0.05$ ), and wild type/R1205H (63.2%,  $P < 0.05$ ) all demonstrated significantly lower secretion rates than wild type mVWF, with R1205H being the most severely reduced in mouse VWF.

The recombinant human and mouse VWF proteins examined in this study have similar multimer patterns and all exhibited ultra large VWF compared to normal human pooled plasma and normal mouse plasma (data not shown). The recombinant VWF proteins produced in HEK293T cells will presumably have altered glycan content compared to that of normal plasma VWF, and this characteristic could alter ADAMT13 cleavage rates and protein clearance.

#### 4.4.2 In vitro ADAMTS13 digests of recombinant VWF

Full-length VWF digests were performed in the presence of 1.5 M urea using a two-fold dilution series of ADAMTS13 (figure 4.2A). Each assay was performed in duplicate. Human full-length VWF digests showed no significant difference between wild type (1.71 U/mL hADAMTS13), Y1584C (1.67 U/ml,  $P = 0.85$ ), or R1205H (2.10 U/mL hADAMTS13,  $P = 0.12$ ). Mouse full-length VWF digests also resulted in no significant difference in EC50 values between wild type (0.341 U/mL mADAMTS13), R1205H (0.371 U/mL mADAMTS13,  $P = 0.34$ ) and Y1584C (0.423 U/mL mADAMTS13,  $P = 0.30$ ).

VWF115 digests of wild type and Y1584C protein were performed under non-denaturing conditions (Figure 4.2B). R1205H was excluded from these studies, since this change is outside the region in VWF115. The hADAMTS13 had cleaved 50% of wild type hVWF115 at 0.0865 U/mL hADAMTS13, and Y1584C required 40% lower hADAMTS13 levels at 0.0521 U/mL ( $P = 0.013$ ). Mouse ADAMTS13 had cleaved 50% of wild type mVWF115 at 0.197 U/mL mADAMTS13, while Y1584C required 21% lower mADAMTS13 levels at 0.157 U/mL ( $P = 0.014$ ).

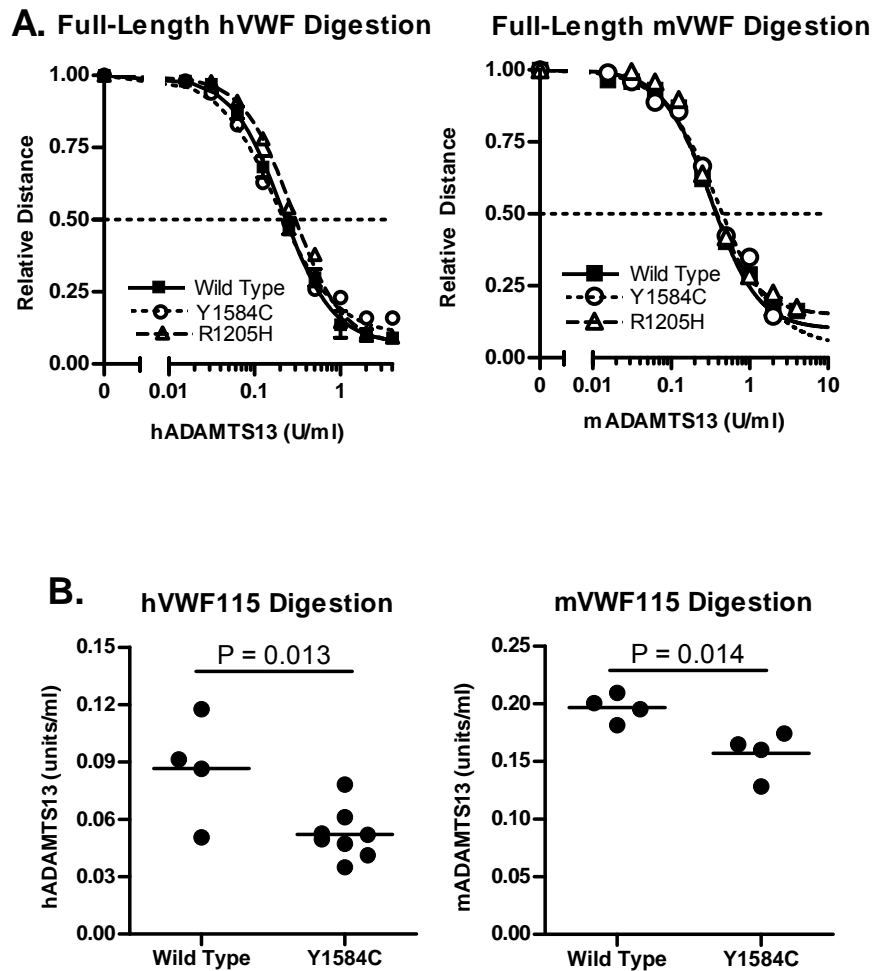


**Figure 4.2 Analysis of ADAMTS13 Digestion of Full-Length mVWF and mVWF115.**

Recombinant ADAMTS13 digests were performed as outlined under methods. (A) Varying concentrations of ADAMTS13 were incubated with 1 U/ml full-length VWF for 24 hours with 1.5M Urea. Multimer graphs for wild type, Y1584C, and R1205H VWF were plotted using a four-parameter curve fit. The concentration of ADAMTS13 required to cause a 50% loss of multimer height was determined. Symbols represent mean values and standard error from two experiments. (B) Comparison of the ADAMTS13 concentrations necessary for 50% loss of intact human and mouse VWF115. Varying ADAMTS13 concentrations were incubated with VWF115 for 4 hours under non-denaturing conditions. Bars represent the mean values, and each circle represents a separate assay.

#### 4.4.3 Recombinant Mouse VWF Protein Infusions

Mice were infused with recombinant mouse VWF (0.2 U/gm body weight), and a minimum of 3 mice were sampled per time point. Data was fit to a one-phase exponential decay with plateau phase, the best fitting model for the data (Figure 4.3). The half-life for wild type protein was 35.1 minutes, Y1584C was 40.8 minutes ( $P = 0.64$ ) and R1205H was 21.9 minutes ( $P < 0.0001$ ). These relatively short half-lives may not represent the circulation time for normal mouse plasma VWF (most likely due to glycosylation differences in HEK293T cell-derived VWF), but the evaluation of the three recombinant molecules using the same experimental protocol provides a valid approach to comparing their half-lives.

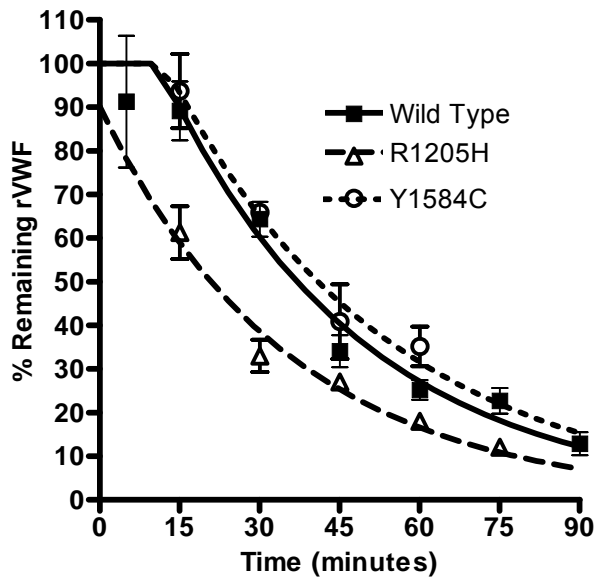


**Figure 4.3 Recombinant Mouse Protein Clearance.**

Recombinant mouse VWF protein (0.20 U/g) was injected via tail vein into VWF knockout mice. Mice were sampled once,  $N \geq 3$  mice per time point. Data is reported as % remaining recombinant mouse VWF. Half-life was determined for each recombinant VWF protein.

#### 4.4.4 Hydrodynamic Injections

VWF knockout mice received plasmid DNA containing the liver-specific ET promoter and mouse VWF cDNA. This results in hepatocyte-specific expression of the mouse VWF protein, which presumably has an altered glycan content compared to normal endothelial and platelet-derived VWF. This transgene delivery method replaces only the plasma component of VWF content in the knockout animals. Complete blood counts were performed with all VWF cDNA combinations tested. A transient thrombocytopenia was observed on day 2 after transgene administration, with full recovery following all injections by day 5. The thrombocytopenia is probably a response to the physical vascular trauma caused by the injection. No other adverse events or alterations in CBC values were observed (data not shown).

#### 4.4.5 VWF Antigen Levels

VWF:Ag levels reached maximum levels two days post-hydrodynamic injection (Figure 4.4A). Wild type VWF:Ag reached a level of 25.0 U/mL, while R1205H was 35% lower at 16.3 U/mL ( $P < 0.001$ ). Both Y1584C and wild type/R1205H “heterozygotes” were not significantly different from wild type VWF:Ag levels (27.2 U/mL and 25.7 U/mL, respectively,  $P > 0.05$ ). The level in wild type/Y1584C “heterozygotes” was significantly higher at 39.9 U/mL ( $P < 0.001$ ). The initial peak VWF:Ag levels declined to a more stable plateau phase by day 14, at which point, mice that had received the wild type VWF cDNA had the highest VWF:Ag expression levels through days 14 to 42 (Figure 4.4B and C). From day 14 onwards, the two type 1 VWD mutations, either alone or co-expressed with wild type VWF (representative of the heterozygous state), demonstrated lower VWF:Ag levels. R1205H VWF:Ag levels were an average 34% of wild type VWF ( $p < 0.001$ ) from days 14 to 42, and wild type/R1205H were 27% ( $p < 0.001$ ). Y1584C VWF:Ag levels were 29% of wild type ( $p < 0.001$ ), while wild type/Y1584C levels were 51% ( $p < 0.001$ ). Results from days 21 and 28 (Figure 4.4C) show the

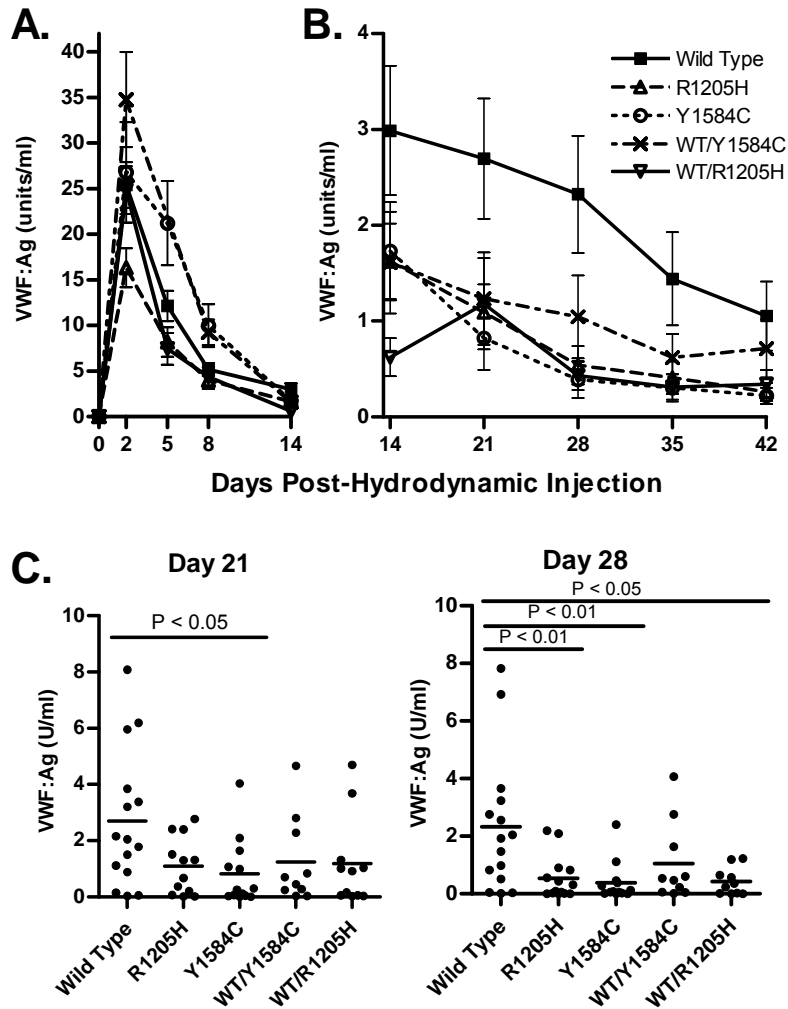


**Figure 4.4 Mouse VWF antigen levels post-hydrodynamic injection.**

VWF knockout mice expressing wild type, R1205H, Y1584C, or wild type and mutant mVWF were sampled post-hydrodynamic injection ( $N \geq 10$ ). VWF:Ag levels were determined via ELISA. (A) VWF:Ag levels from day 2 to 14 post hydrodynamic injection. (B) VWF:Ag levels from days 14 to 42 post hydrodynamic injection. Symbols represent means with SEM error bars. (C) VWF:Ag levels for days 21 and 28. Each circle represents data from a single mouse, bars represent the mean VWF:Ag value.

variability between the individual animals in the study, compared to the mean values.

Statistically significant differences are observed for R1205H and Y1584C VWF:Ag levels compared to wild type VWF:Ag.

#### 4.4.6 VWF propeptide to VWF Antigen Ratios

VWF propeptide levels were measured, and followed a similar expression profile to that of VWF:Ag, with maximum levels on day 2, and a plateau phase from day 14 onwards (data not shown). VWFpp/VWF:Ag ratio was determined, with a mean value of 1 being equal to the mean of wild type VWFpp/VWF:Ag ratios (Figure 4.5). This value was 6.5-fold lower than that of the observed VWFpp/VWF:Ag ratio documented in the plasma of normal C57Bl/6 mice. This finding suggests an alteration in clearance for either VWF:Ag and/or VWFpp proteins in the mice

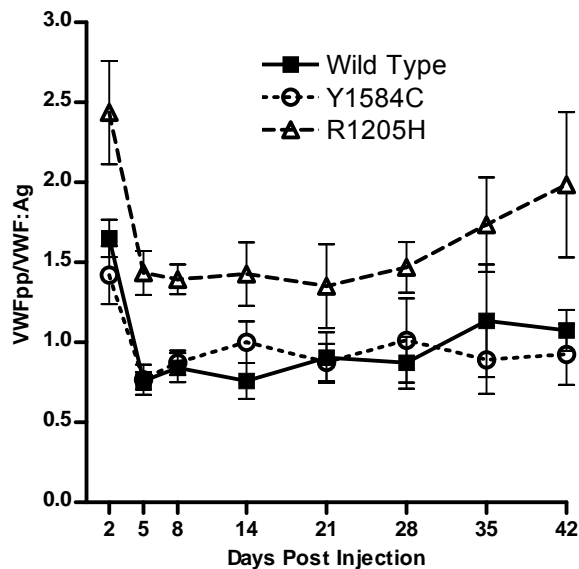


**Figure 4.5 VWFpp/VWF:Ag ratios for hydrodynamic mVWF**

VWF knockout mice expressing wild type, R1205H or Y1584C cDNA were sampled post-hydrodynamic injection ( $N \geq 10$ ). VWF:Ag and VWFpp levels were determined via ELISA. Values are normalized to a mean wild type ratio equal to 1.0, which is 6.5 fold lower than that of normal C57BL/6J mice.

expressing VWF from the liver. The VWFpp/VWF:Ag ratio for Y1584C was not significantly different from that of wild type VWF, with mean ratio values of 0.97 versus 1.00 ( $P > 0.05$ ). R1205H, however, did demonstrate an increased mean VWFpp/VWF:Ag ratio of 1.65 ( $P < 0.001$ ), which is a surrogate marker for accelerated VWF clearance from plasma.

#### **4.4.7 Multimeric structure**

Multimeric profiles of the liver-expressed mVWF were examined to determine if the mutations altered the VWF multimer structure. The mouse VWF produced from the liver, post-hydrodynamic injection, has an altered multimer appearance compared to that of normal mouse plasma (Figure 4.6A). Single multimer bands rather than a normal triplet structure were observed, with a slightly lower molecular weight for each band. In addition, the multimer profile was skewed toward lower molecular weight multimers compared to normal mouse plasma.

Compared to wild type VWF, Y1584C demonstrated a loss of multimer bands, while R1205H had no change in multimer band number. Multimer band number counts were used to quantify differences in multimeric structure (Figure 4.6B). Wild type VWF had a peak level of 22 bands at day 2, and a low of 8.57 bands at day 28, with an average band number of 12.54. R1205H had an average of 11.69 bands, a decrease of 0.85 bands compared to wild type ( $P > 0.05$ ). In contrast, Y1584C had an average of 8.31 multimer bands, a decrease of 4.23 bands ( $P < 0.001$ ).

Animals receiving co-injected VWF and ADAMTS13 cDNAs via hydrodynamic delivery (to compensate for the truncated and functionally defective ADAMTS13 in C57Bl/6 mice) had a diminished multimer size (Figure 4.6C). ADAMTS13 activity in these mice was determined using m73 substrate with an antibody that detects intact A2 domain substrate, in a static activity assay. Mouse ADAMTS13 levels were found to be an average of 5.92 U/ml on day 5, 4.14 U/ml on day 8 and 5.14 U/ml on day 14 (data not shown). With the co-injected ADAMTS13 cDNA,

wild type VWF had an average band number of 9.38 from days 5-14. R1205H had a slightly higher molecular weight multimer structure with 10.2 bands ( $P > 0.05$ ). In contrast, Y1584C

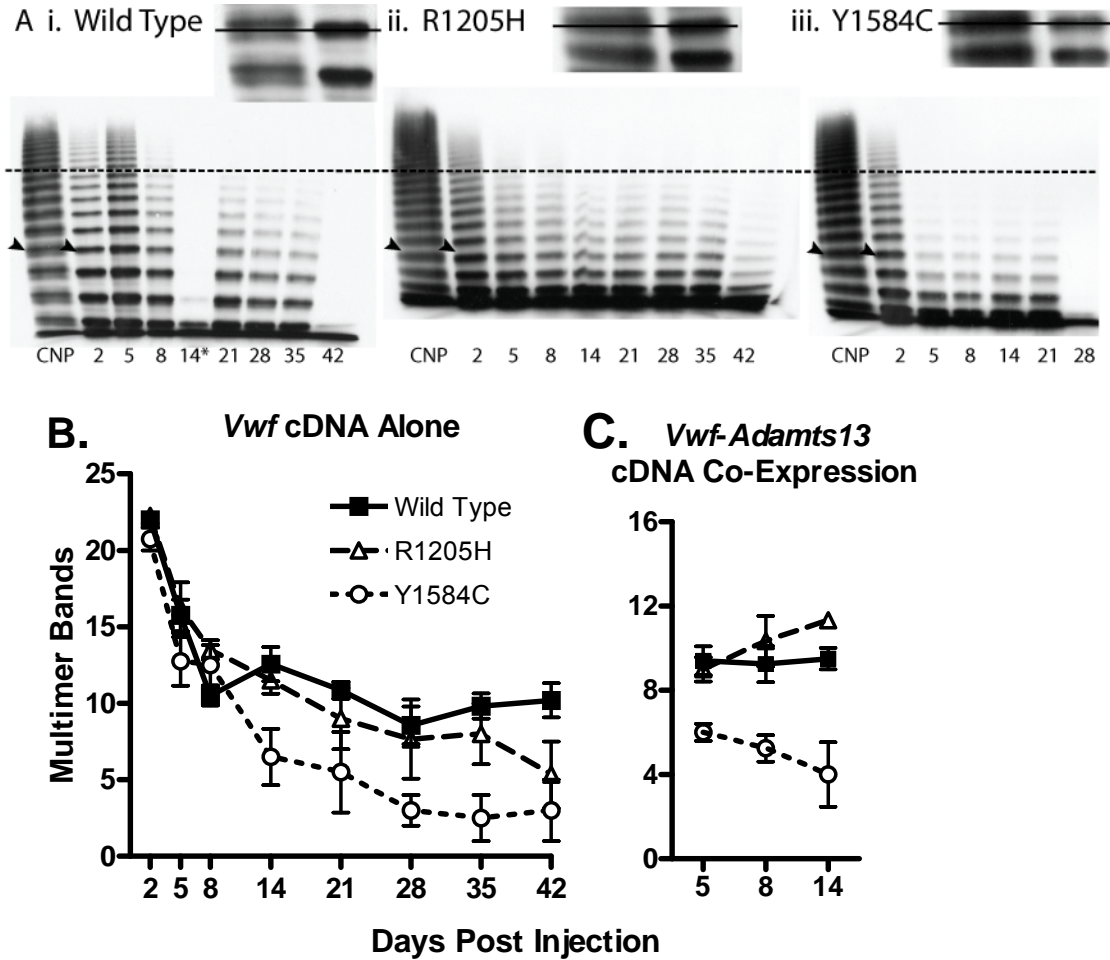


**Figure 4.6 Hydrodynamic mVWF Multimer Structure.**

VWF knockout mice expressing wild type, R1205H, or Y1584C mouse VWF were sampled post-hydrodynamic injection and evaluated for multimeric structure. Plasma was run on a 1.4% agarose gel at an mVWF concentration of 1.0 U/ml. (A) Exemplar multimers are shown for i) wild type, ii) R1205H, and iii) Y1584C. The dotted line represents high molecular weight multimers, greater than 10 multimer bands. Arrow heads indicate the top bands in the enlarged inset bands, with a line through the inset figure illustrating the single band of lower molecular weight in the recombinant proteins compared to C57Bl/6 normal plasma pool (CNP) triplet multimer bands. \* denotes a multimer from a clotted sample. Wild type day 14 and Y1584C day 28 samples were less than 1 U/ml. (B) Multimer analysis was performed on VWF knockout mice expressing mVWF post-hydrodynamic injection by counting the total number of resolved multimer bands in each lane.  $N \geq 4$ . (C) Multimer analysis on VWF knockout mice expressing mVWF and mADAMTS13 post-hydrodynamic injection.  $N \geq 4$ .

showed a decrease to 5.08 bands ( $P < 0.01$ ), demonstrating that the addition of full-length ADAMTS13 to the VWF knockout mouse exaggerates the abnormal multimer structure for Y1584C.

#### 4.4.8 Evaluation of in vivo thrombogenesis

Performance of the ferric chloride injury model of thrombosis on cremaster arterioles demonstrated a marked difference in mean occlusion times between the two type 1 VWD mutations studied, despite the fact that their plasma levels were not significantly different at the time of study (Figure 4.7). All mice were expressing VWF:Ag levels between 0.5 and 2.4 U/ml mVWF at the time of thrombogenesis testing. The Y1584C VWF mice had a much longer time to occlusion compared to wild type (38.7 versus 29.9 minutes,  $P = 0.001$ ). In contrast, studies with the R1205H mutant showed quite variable occlusion times but a mean value similar to that

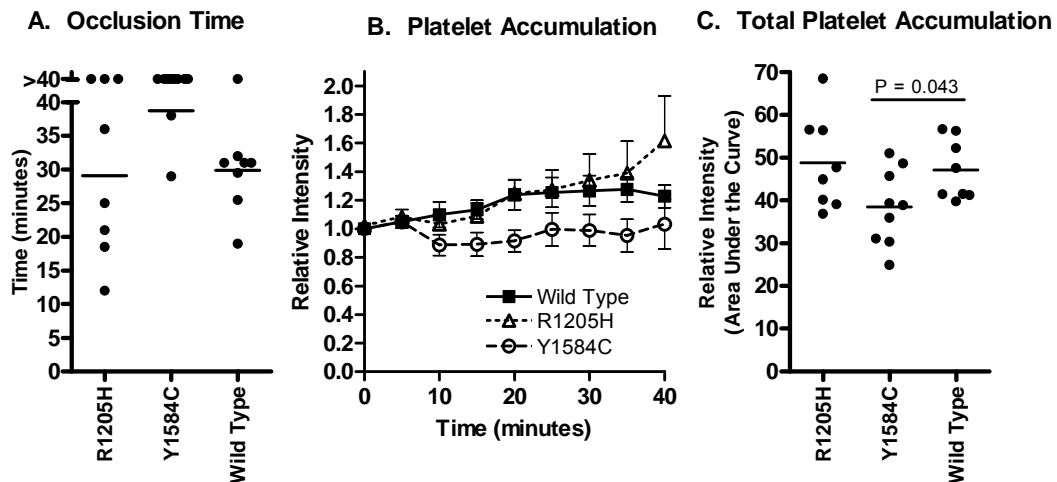


**Figure 4.7 Thrombogenesis in response to ferric chloride injury.**

VWF knockout mice expressing VWF cDNA post-hydrodynamic injection with VWF:Ag levels between 0.5 and 2.5 U/mL were evaluated using 10% ferric chloride injury to the cremaster. A. Time to a stable occlusive thrombus. The experiment was stopped at 40 minutes, mice that failed to occlude were recorded as 40 minutes. B. Platelet accumulation via mean relative fluorescence intensity. Mean with SEM was graphed for each data set. C. Total platelet accumulation. Area under the curve was determined. Each circle represents a single mouse, bars indicate mean.

seen in wild type mice (29.1 minutes versus 29.9 minutes,  $P > 0.05$ ). Total relative platelet accumulation was also lower for Y1584C compared to wild type (38.5 versus 47.1,  $P = 0.043$ ) R1205H was similar to wild type (48.8,  $P = 0.72$ )

## 4.5 Discussion

We selected two recurrent and contrasting type 1 VWD mutations for this study to carry out a comprehensive pathogenic characterization of the mechanisms responsible for their phenotypes. R1205H, a highly penetrant dominant mutation with a severe type 1 phenotype, was selected since it has previously been demonstrated to show an enhanced clearance mechanism. In contrast, the frequent and incompletely penetrant Y1584C mutation has a mild phenotype, and has shown some *in vitro* evidence to support a biosynthetic defect and enhanced ADAMTS13 proteolysis. Both R1205 and Y1584 are conserved between human and mouse VWF proteins, allowing the R1205H and Y1584C mutations to be examined in the mouse model. This study has now determined the relative pathogenic contributions of defective biosynthesis and release, ADAMTS13-mediated proteolysis, and clearance mediated by these two type 1 VWD mutations through both *in vitro* studies and in a mouse model. We have also evaluated the influence of the two mutant proteins in an *in vivo* thrombosis model to determine if their contributions to this process are similar when plasma VWF levels are equivalent.

The defining characteristic of type 1 VWD is a proportionate decrease in both VWF:Ag and VWF:RCo levels, between 0.05 and 0.5 U/ml. It is implied from this proportionate reduction in both measurements that the low level of VWF has a normal hemostatic function. Before initiating these studies, we did not know if the hydrodynamic injection model of VWF expression would reflect the reductions in plasma VWF:Ag levels seen in patients with these two mutations. However, despite our initial concerns, these studies have shown that in the long term plateau

phase of VWF expression from day 14 onwards, VWF:Ag levels are significantly decreased in both Y1584C and R1205H with substantially lower levels in the R1205H mice, thus recapitulating the difference in human phenotypes. Importantly, these low VWF:Ag levels are also observed in mice that were co-injected with mutant and wild type cDNAs, modeling the heterozygous state observed in most type 1 VWD patients.

Defective biosynthesis and secretion has been described for many VWD mutations. The Y1584C mutant had been previously demonstrated to show decreased protein synthesis and increased cellular retention *in vitro* using COS 7 cells.<sup>141</sup> In contrast, the R1205H mutation has been reported not to alter synthesis.<sup>160</sup> In this study, our *in vitro* experiments demonstrate that both Y1584C and R1205H do adversely affect synthesis of VWF in both the homozygous and heterozygous states. The quantitative biosynthetic defects are replicated with both the human and the mouse VWF constructs, but neither type 1 mutation appears to influence the generation of normal multimer structure. We also suspect that a biosynthetic defect is likely contributing to the decreased VWF:Ag levels observed in the mice expressing VWF after hydrodynamic injection. These mice show normal VWFpp/VWF:Ag ratios for the Y1584C mutant, and only 1.65-fold higher ratios in the mice expressing R1205H, suggesting that accelerated clearance of the proteins is not a major influence in this system.

The effects of ADAMTS13-mediated digestion were examined by *in vitro* digestion of full-length and VWF115 substrates as well as by examining the multimer profiles of hydrodynamic-injection mice. The mouse VWF protein amino acid sequence has 83% identity and 91% homology to that of human VWF, with similar changes in the ADAMTS13 sequences.<sup>117, 124</sup> Although the orthologs are very similar, species differences do exist. Mouse ADAMTS13 has poor activity on the human VWF substrate in both full-length and A2 domain VWF73 assays.<sup>125</sup> This is further exacerbated by a retrotransposon insertion in C57Bl/6 mice that

leads to the premature truncation of ADAMTS13, resulting in a protein lacking the C-terminal 2 Tsp1 domains and CUB domains.<sup>126</sup> In vivo, there is little change in cleavage under static conditions and C57Bl/6 mice exhibit normal VWF multimer patterns. However, the truncated enzyme results in increased thrombotic occlusions under shear stress conditions, since it is not fully active in vivo.<sup>127</sup> To mitigate any artifacts caused by these differences, we digested both human and mouse substrates with their respective species-specific ADAMTS13. In addition, we performed co-injections of full-length mouse ADAMTS13 cDNA with the VWF cDNAs to observe any influences on the VWF multimer profile.

The R1205H mutant protein showed no alteration in the full-length VWF ADAMTS13 digestions and multimer profiles in the hydrodynamically-injected mice were also normal for R1205H. Thus, ADAMTS13-mediated digestion and multimer structure for the R1205H mutant were not altered in any of the in vitro or in vivo assays, indicating that this mutation does not influence the cleavage by ADAMTS13.

In contrast, Y1584C displays a mild type 2A group II VWD phenotype in our study. Although the full-length digests did not show a difference in cleavage rates, the in vitro VWF115 assays did show an enhanced cleavage profile for Y1584C and Y1584C expressing mice had reduced multimer band numbers which was exacerbated by co-injection of the mADAMTS13 cDNA. These results support patient plasma studies that have shown that the Y1584C protein is more susceptible to ADAMTS13-mediated proteolysis.<sup>163, 164</sup> This enhanced cleavage could explain the higher bleeding scores reported in some Y1584C individuals, since this mutation results in VWF:Ag levels in the moderate range.<sup>73</sup>

Increased protein clearance is another pathogenic mechanism that contributes to the type 1 VWD phenotype. R1205H has consistently been shown to have a greatly shortened half-life in patients. This finding has been complemented through the premature clearance of radio-labeled

R1205H human VWF protein in the VWF knockout mouse.<sup>37</sup> Our study examined recombinant mVWF protein clearance rates as well as VWFpp/VWF:Ag ratios, an indirect measure of VWF clearance. The infused recombinant R1205H had a significantly shorter half-life compared to wild type recombinant protein, with a 27% decrease. This is not as dramatic as that observed using radio-labeled human R1205H VWF, which had a 90% decrease in mean residence time compared to wild type human VWF.<sup>37</sup> This more discrepant result could be due to inherent species differences in the VWF molecules. Infused Y1584C protein did not show a significant change in half-life from wild type VWF. VWFpp/VWF:Ag ratios for Y1584C were also similar to the results of wild type VWF in the hydrodynamic-injection mice. R1205H showed an elevated VWFpp/VWF:Ag ratio of 1.65, but this was much lower than the ratios seen in R1205H patients, that are often greater than 10.<sup>45</sup> This difference appears to be due, in part, to the system used to express the plasma VWF in these mice, which also results in a 6-fold decrease in the VWFpp/VWF:Ag ratio for wild type VWF compared to the ratio in normal C57Bl/6 mouse plasma.

We have also evaluated the procoagulant function of the two mutant proteins in an established *in vivo* thrombosis model in the hydrodynamically-injected mice. These studies were carried out at similar plasma levels of the proteins to eliminate the influence of VWF concentration. In these studies, R1205H showed a similar mean occlusion time and platelet accumulation compared to wild type VWF, although there was high variability between mice. In contrast, the Y1584C protein was associated with a significant delay in thrombus formation and loss of platelet accumulation compared to both R1205H and wild type VWF. This may well be due to the loss of higher molecular weight multimer structure secondary to increased ADAMTS13 cleavage of the Y1584C mutant. This mechanism could be a contributing factor to relatively higher bleeding scores for some patients carrying this mutation, despite having milder

reductions of VWF:Ag levels. Furthermore, this increased bleeding tendency could also contribute to an enrichment of this mild quantitative variant in populations of type 1 VWD.

Significantly, our study demonstrates that type 1 VWD phenotypes can be modeled through a comprehensive series of *in vitro* and *in vivo* evaluations. In the study of these two type 1 VWD mutants we documented evidence of decreased VWF biosynthesis, increased ADAMTS13 cleavage, enhanced clearance, and a differential contribution to *in vivo* thrombogenesis. These findings extend current pathophysiologic knowledge for type 1 VWD mutations and provide a practical approach to furthering our understanding of the mechanisms underlying this quantitative trait.

In this study, the Y1584C mutant demonstrated decreased biosynthesis *in vitro*, enhanced proteolysis by ADAMTS13 *in vitro* and *in vivo*, and decreased VWF expression *in vivo*. The increase in ADAMTS13-mediated cleavage produced a mild type 2A VWD multimer profile that probably contributed to the delay in forming occlusive thrombi in our ferric chloride injury model. In contrast, the R1205H mutant demonstrated decreased biosynthesis, moderately increased protein clearance, but no alteration in ADAMTS13-mediated cleavage. Moreover, the protein when expressed at normal physiologic levels demonstrated similar occlusion times to that of wild type VWF in the ferric chloride model, showing that at normal concentrations the R1205H VWF protein behaves normally in thrombogenesis.

These studies demonstrate that multiple approaches are necessary to determine the complex pathogenic mechanisms underlying type 1 VWD. Here, both *in vitro* and *in vivo* methodologies have been used to explore the disease phenotypes in two type 1 VWD mutations. This study establishes that the VWF knockout hydrodynamic delivery approach provides a practical means to evaluate defects in VWF clearance rates, decreased biosynthesis, and

ADAMTS13-mediated cleavage, combined defects of which may contribute to the generation of the type 1 VWD phenotype.

## Chapter 5 Thesis Discussion

### 5.1 Summary

The role of ADAMTS13-mediated cleavage is central to maintaining proper VWF multimer size for normal function. This thesis has examined the sensitivity of ADAMTS13 cleavage to mutagenesis of the VWF substrate. The ADAMTS13 cleavage site at Y1605-M1606 was subjected mutagenesis. The greatest loss of cleavage was observed in the double alanine substitution Y1605A/M1606A. In addition, 4 A-domain single nucleotide polymorphisms were examined, with D1472H, Q1571H, P1601T all showing increased resistance to ADAMTS13-mediated cleavage. In contrast, G1643S has enhanced cleavage in the full-length VWF substrate but is resistant to cleavage in the VWF115 substrate. R1597W, a type 2A VWD mutation, has enhanced cleavage, while a slight increase is observed in Y1584C, but no change in cleavage is seen with R1205H. These variations in cleavage can be explained at least partially by examining the VWF A2 domain crystal structure. Two mutations that severely impact ADAMTS13 cleavage, R1597W (enhanced cleavage) and Y1605A/M1606A (cleavage resistant), were further examined to determine how they affect other aspects of VWF function, synthesis, and clearance. Two type 1 VWD mutations, R1205H (severe phenotype, with increased clearance) and Y1584C (mild phenotype, with increased cleavage) were also examined to evaluate mechanisms responsible for their disease phenotypes. All four mutations showed different and unique mechanisms that altered various aspects of the proteins' expression, clearance, and multimeric structure. These results prove the validity of the VWF knockout mouse hydrodynamic transgene delivery approach for evaluating the mechanistic characterization of putative VWF mutations.

## 5.2 ADAMTS13-mediated cleavage is altered by VWF Variants

ADAMTS13-mediated cleavage of VWF is critical for controlling and maintaining normal hemostasis in the blood. This is a multiple step process, requiring the globular VWF A domains to undergo several different steps in unfolding under shear forces until the central A2 domain cleavage site at Y1605-M1606 is exposed to ADAMTS13.

Since our publication of the human cleavage studies (chapter 2), the subsequent reporting of the VWF A2 domain crystal structure,<sup>95</sup> shear-induced unfolding models,<sup>96, 165</sup> as well as the identification of VWF-ADAMTS13 binding regions<sup>88, 99, 100</sup> have now provided a clearer picture of the mechanisms at play in both the full-length and VWF115 substrate assays.

The A1 and A2 domains undergo simultaneous unfolding to intermediate states that both increase platelet GP1b binding to A1 and enhance ADAMTS13 cleavage in A2.<sup>91</sup> Amino acids critical for maintaining the A domains in tight globular forms are highly conserved. When these amino acids are mutated, there are changes in VWF function. Thus, the type 2A group II VWD changes are clustered in the A2 domain and each of these mutations leads to excessive cleavage by ADAMTS13.<sup>105, 140</sup> This is also observed with the type 2B VWD mutations, located in the bottom face of A1 domain. These mutations both increase platelet GP1B binding as well as enhance ADAMTS13-mediated cleavage.<sup>139</sup> An examination of the A1 domain type 2M mutations has shown increased ADAMTS13-mediated cleavage under static conditions.<sup>139</sup> However, a lack of GP1b binding would reduce the amount of shear stress and subsequent proteolysis in vivo. A3 domain collagen binding mutations have yet to be examined for ADAMTS13-mediated cleavage discrepancies.

The A2 domain exists as a force-sensing shear bolt, and undergoes multiple transition points between the densely packed folded form and the open form.<sup>95, 165</sup> The A2 domain crystal structure (Protein Database ID code 3GXB, [www.pdb.org](http://www.pdb.org)<sup>95, 166</sup>) is comprised of the amino acids

V1492-S1671.<sup>95</sup> A shear-sensing bolt, it is organized with the ADAMTS13 cleavage site at Y1605-M1606 in the center of the  $\beta$ 4-strand, buried deep in the A2 hydrophobic core of  $\beta$ -sheets (figures 5.1 and 5.2). The side chains of Y1605 and M1606 both exhibit multiple conformations, suggesting irregular packing. The structure of the domain allows for unfolding to initiate only from the C-terminus, since the N-terminus is buttressed by  $\beta$ -strands on either side in the domain core (figure 5.1).

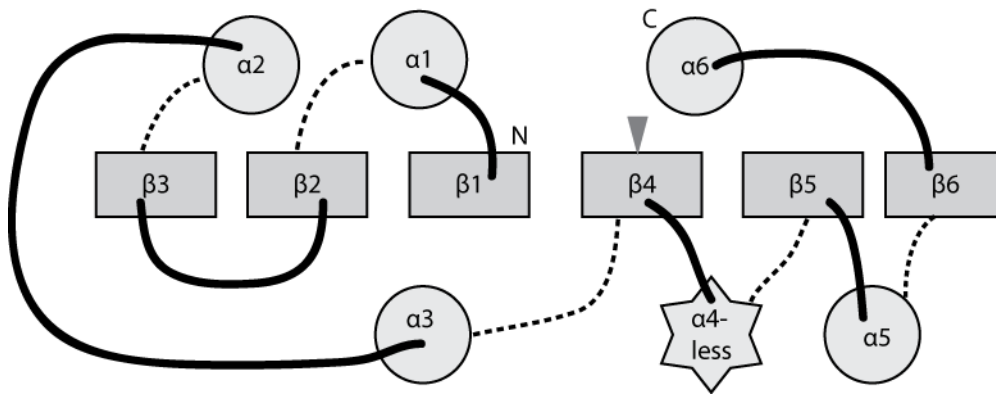


**Figure 5.1 Sketch of the A2 domain illustrates the secondary structural organization.**

The VWF A2 domain adopts a Rossman fold with a central 6-stranded  $\beta$ -sheet surrounded by 5  $\alpha$ -helices and an open  $\alpha$ 4-less loop structure. The N-terminus forms a knot structure that is resistant to shear, while the C-terminus is more susceptible to unfolding. Circles represent  $\alpha$  helices, the star represents the  $\alpha$ 4-less loop, and rectangles represent  $\beta$ -sheets. Solid lines represent connecting loops above the helices and sheets, dashed lines represent connecting loops below. The gray arrow head in the  $\beta$ 4 sheet marks the location of Y1605-M1606, the ADAMTS13 cleavage site. Adapted from Baldauf, et al.<sup>165</sup>

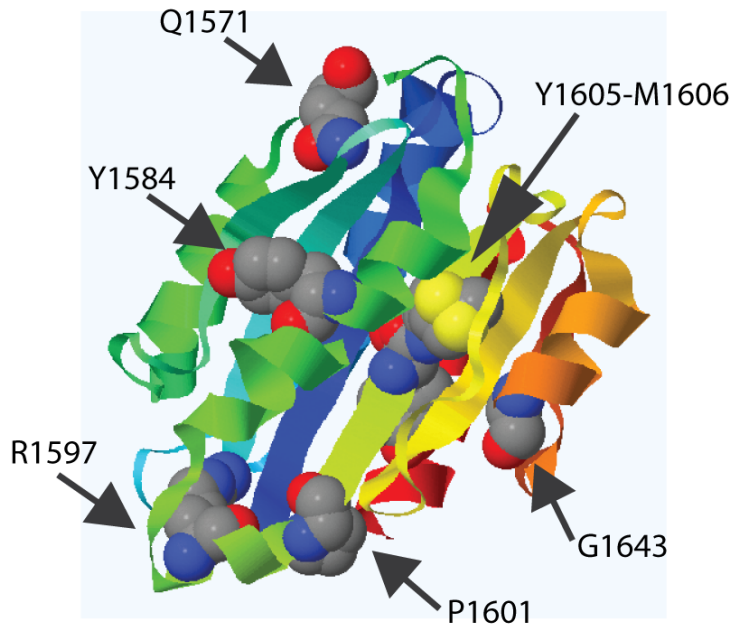


**Figure 5.2 Crystal structure of the A2 domain showing amino acids of interest.**

A molecular model of the VWF A2 domain is shown with the wild type VWF amino acids in cartoon format. The Y1605-M1606 amino acids are shown in the lime green  $\beta$ 4-sheet, in the center of the A2 domain. The other amino acids are in outer regions of the A2 domain. The residues selected for mutagenesis are shown as space filling models. The rest of the A2 domain is represented as a ribbon diagram colored from blue to red, N terminus to C terminus. All atoms are shown depicted by standard coloring (carbon is gray, oxygen red, sulfur yellow, nitrogen blue). Protein Database ID 3GXB<sup>95,166</sup> was manipulated in Proteopedia<sup>167</sup> which uses Jmol: an open-source Java viewer for chemical structures in 3D. <http://www.jmol.org/>.

The hVWF115 substrate, a GST and histidine tagged 115 amino acid fragment of the VWF A2 domain, E1554-R1668, is only a partial fragment of the A2 domain. VWF115 does not have the first 3  $\beta$  sheets and the first  $\alpha$  helix, and truncates the  $\alpha$ 6 helix by three residues (see figure 5.1). The minimal substrate, VWF73, D1596-R1668, removes an additional 2  $\alpha$  helices, illustrating that the C-terminal region of the A2 domain is not necessary for ADAMTS13 binding and does not need to unfold for cleavage to take place in a full-length VWF molecule.<sup>98</sup> This is further illustrated by the recent crystal structure of the non-catalytic domains of ADAMTS13, which has multiple discontinuous exosites for the VWF73 substrate (Figure 5.3).<sup>100</sup> These sites

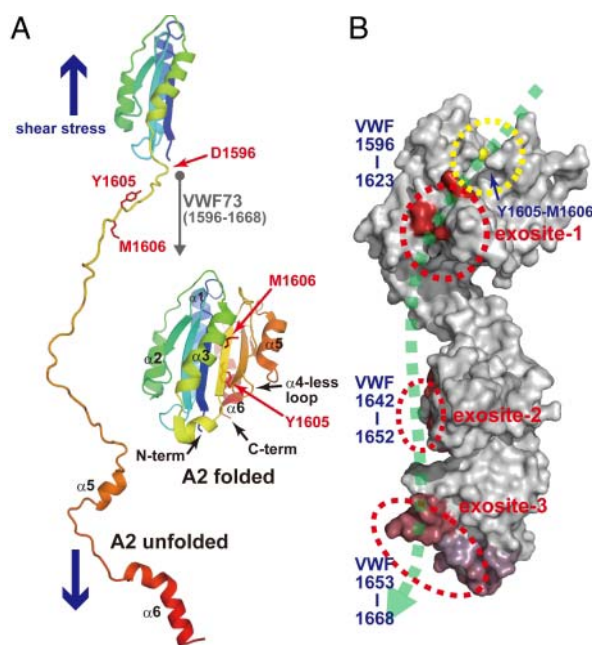


**Figure 5.3 ADAMTS13-VWF interactions.**

(A) Folded and unfolded structures of the VWF A2 domain. The VWF A2 domain adopts a Rossman fold with a central 6-stranded  $\beta$ -sheet surrounded by 5  $\alpha$ -helices (shown as “A2 folded”)<sup>95</sup>. The scissile peptide bond (Y1605-M1606) is buried within the protein core under static conditions. The C-terminal region (residues 1,596–1,668, corresponding to VWF73)<sup>98</sup> of the A2 domain must be unfolded to expose the scissile bond and the exosite-binding regions under shear-stress conditions (shown as A2 unfolded). (B) ADAMTS13-MDTCS-VWF binding model. The molecular surface of the ADAMTS13-MDTCS model is shown in gray and the bound zinc ion is shown in yellow. Residues that mediate VWF binding are depicted by colors indicating ADAMTS13 activity loss via mutagenesis (Red indicates high activity loss, purple moderate loss, blue unaffected), and the exosites and the catalytic cleft are indicated by red and yellow dotted ellipsoids, respectively. The dotted green line represents a VWF molecule (residues 1,596–1,668) bound to ADAMTS-MDTCS. (From Akiyama, et al.<sup>100</sup>)

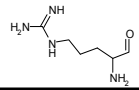
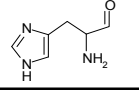
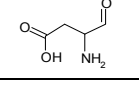
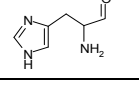
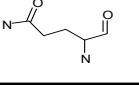
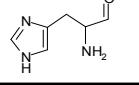
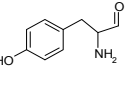
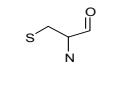
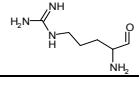
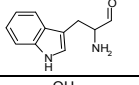
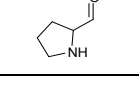
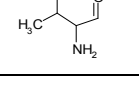
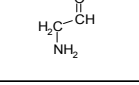
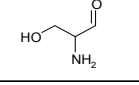
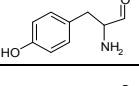
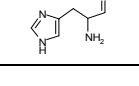
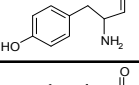
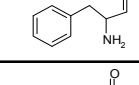
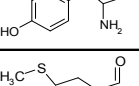
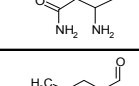
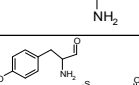
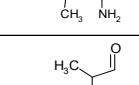
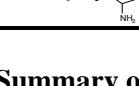
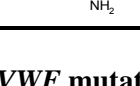
are highly susceptible to amino acid changes that cause a loss of activity, and in the wild type protein they serve to bind VWF in preparation for cleavage.<sup>100</sup>

The full-length digestion assay should mimic the complete molecular interactions of VWF with ADAMTS13. The chemical denaturation with 1.5 M urea is used to simulate mechanical shear forces to make full-length VWF accessible to ADAMTS13 digestion. This

approach could introduce assay-dependent artefacts to the digestion result, but is highly reproducible. In contrast, the shorter A2 domain VWF115 and VWF73 substrates model VWF interactions with the multiple exosites in the ADAMTS13-DTCS structures (figure 5.3), as well as any structural changes in this limited structure.<sup>100</sup> However, these are relatively flexible molecules that can adopt multiple configurations. This is unlike that of a full-length A2 domain in an intact VWF multimer, which under shear forces would be stretched in a linear fashion.<sup>96</sup> Depending on the location of a mutation, either of these assays could be irrelevant to what occurs physiologically. So, one must first determine where the amino acid substitution is located in the VWF molecule, and more specifically where in the A2 domain the change occurs.

The mutations and polymorphisms in this thesis have been selected because of their location in the VWF molecule, and because they are associated with known disease phenotypes and are prevalent in VWD populations. Polymorphisms and cleavage site mutations in the A1 and A2 domains of VWF were selected to determine what effects, if any, they had on ADAMTS13-mediated proteolysis of full-length VWF and the A2 domain VWF115. These data are summarized in table 5.1. The Y1605-M1606 ADAMTS13 cleavage site was highly sensitive to mutagenesis in both assays, depending on the amino acids substituted. The polymorphisms D1472H, Q1571H, and P1601T demonstrated a resistance to cleavage. In contrast, G1643S had increased cleavage in the full-length substrate assay. Known VWD mutations R1597W, Y1584C, and R1205H were also examined for their ADAMTS13 cleavage sensitivity, with R1597W having enhanced cleavage of the full-length substrate, Y1584C enhanced cleavage of only the VWF115 substrate, and R1205H demonstrating normal proteolytic susceptibility. These three mutations, along with Y1605A/M1606A, were examined in the VWF knockout mouse using hydrodynamic injection of VWF transgenes for *in vivo* characterization. The locations of all of these changes in the VWF molecule, and more specifically the site of the substitutions in

the A2 domain if applicable, were examined to determine an explanation for these ADAMTS13 digest results.

| Amino Acid        | Normal/<br>Common SNP   | Mutation/<br>Minor SNP  | Domain | Sublocation                 | Full-length      |         | VWF115           |         |
|-------------------|---|---|--------|-----------------------------|------------------|---------|------------------|---------|
|                   |   |   |        |                             | Normalized Value | P Value | Normalized Value | P value |
| R1205H            |    |    | D3     | (-)                         | 1.23             | 0.12    | (-)              | (-)     |
| D/H1472           |    |    | A1     | outside crystal structure   | 1.38             | 0.0024  | (-)              | (-)     |
| Q/H1571           |    |    | A2     | $\alpha$ 2- $\alpha$ 3 loop | 2.69             | <0.0001 | 1.1              | 0.729   |
| Y1584C            |    |    | A2     | $\alpha$ 3                  | 0.98             | 0.85    | 0.602            | 0.013   |
| R1597W            |    |    | A2     | $\alpha$ 3- $\beta$ 4 loop  | 0.659            | 0.108   | 0.8              | 0.51    |
| P/T1601           |   |   | A2     | $\beta$ 4                   | 2.37             | <0.0001 | 2.26             | 0.0068  |
| G/S1643           |  |  | A2     | $\alpha$ 5                  | 0.23             | <0.0001 | 1.77             | 0.0174  |
| Y1605H            |  |  | A2     | $\beta$ 4                   | 9.06             | <0.0001 | 1.78             | 0.0377  |
| Y1605F            |  |  | A2     | $\beta$ 4                   | 14.2             | <0.0001 | 1.1              | 0.734   |
| Y1605N            |  |  | A2     | $\beta$ 4                   | 7.75             | <0.0001 | 80               | 0.0008  |
| M1606L            |  |  | A2     | $\beta$ 4                   | 12.1             | <0.0001 | 0.74             | 0.386   |
| Y1605A/<br>M1606A |  |  | A2     | $\beta$ 4                   | >303.            | <0.0001 | 237              | 0.0004  |

**Table 5.1 Summary of VWF mutations and polymorphisms examined in the thesis.**

Amino acids are depicted with side chains for reference. Domain location, including sublocation in the A2 domain crystal structure are listed. Relative levels of ADAMTS13 required for 50% substrate cleavage are reported, with wild type VWF assigned a value of 1. Levels above 1 have resistance to ADAMTS13 cleavage, and below 1, are more easily cleaved. P values <0.05 are considered significant. More digest assay details are found in chapter 2.

### 5.2.1 VWF Polymorphisms

D1472H, located in the C-terminal region of the A1 domain, is not described in a crystal structure, but has been shown to alter VWF function. D1472H has been proven to be highly prevalent in the African American population with 63% of subjects possessing the alternative histidine residue at this site.<sup>168</sup> These individuals have a reduced VWF:RCo/VWF:Ag ratio. However, assays measuring VWF-platelet GPIb interaction, independent of ristocetin, are normal. This suggests that this polymorphism causes an A1 domain conformation change that significantly inhibits ristocetin binding to the A1 loop with a subsequent inhibition of VWF-platelet interaction.<sup>168</sup> This change from an acidic to aromatic amino acid in the A1 domain could also be, in part, why the full-length VWF digestion was 38% more resistant to cleavage compared to wild type VWF (table 5.1). D1472H could prevent the A1 domain from adopting a conformation necessary to facilitate opening the A2 domain.

The Q1571H polymorphism is in the loop connecting the  $\alpha 2$  and  $\alpha 3$  helices in the A2 domain. The histidine substitution increases the ADAMTS13 concentration requirement by 2.69-fold for the full-length substrate, suggesting that this change stabilizes the A2 domain structure. These stabilizing interactions are absent in the shorter VWF115 substrate, which could be why the Q1571H digestion results were not different from the wild type substrate in this assay.

The P1601T polymorphic variant showed ADAMTS13 cleavage inhibition with both substrates, with increased ADAMTS13 requirements of 2.37-fold for full-length VWF and 2.26-fold for VWF115. Located in the A2 domain at the end of the  $\beta 4$ -sheet that contains the cleavage site (Figure 5.2), the P1601 amino acid forms one less hydrogen bond than is present in the corresponding serine in the A1 and A3 domains.<sup>95</sup> The change to a flexible threonine residue could replace this hydrogen bond and stabilize the A2 domain, and also possibly prevent proper ADAMTS13 exosite binding (Figure 5.3).

The G1641S polymorphism is located at the end of the  $\alpha$ 5 helix in the A2 domain (table 5.1 and figure 5.2). This small amino acid allows the tight loop before the  $\beta$ 6 sheet. When serine is substituted at this site, this would create strain and destabilize the molecule and promote unfolding. This result was confirmed with a 77% decrease in ADAMTS13 concentration in the full-length substrate assay. This effect was reversed in the VWF115 substrate (77% higher ADAMTS13), which already has a more open conformation. The serine substitution could prevent optimal substrate binding, since G1641 is next to the region recognized by the second ADAMTS13 exosite (Figure 5.3). These two opposing effects could be sufficient to maintain relatively normal VWF multimer sizes by cancelling each other out, and thus explain why this polymorphism has not been identified in type 2A VWD patients.

### **5.2.2 ADAMTS13 cleavage site mutations**

The ADAMTS13 cleavage site at Y1605-M1606 is in the middle of the  $\beta$ 4-strand, deeply buried in the A2 hydrophobic core (figure 5.1 and 5.2). The A2 domain structure shows Y1605 interacting with the  $\alpha$ 6-helix V1665 and the  $\beta$ 4-strand L1603, which adopts two different conformations. M1606 locates to the opposite side of the  $\beta$ 4-sheet, underneath the  $\alpha$ 4-less loop. Like L1603, M1606 exhibits two rotamer conformations of the side chain, showing the poor packing on both sides of the  $\beta$ -sheet.

This study determined that in the full-length substrate assay, the Y1605-M1606 cleavage site was highly sensitive to mutagenesis, with the strongest loss of cleavage occurring with the double alanine substitution (table 5.1). All of the cleavage site mutations showed a large decrease in cleavage efficiency compared to wild type VWF in the full-length assay. With the full-length substrate, ADAMTS13 is able to discern the loss of the normal Y1605/M1606 site with all the substitutions tested: Y1605N (7.75-fold increased ADAMTS13 concentration), Y1605H (9.06-fold), M1606L (12.1-fold), and Y1605F (14.22-fold) all showed a large reduction in

ADAMTS13-mediated cleavage. The Y1605A/M1606A double mutant showed the largest resistance to cleavage (>300-fold ADAMTS13 concentration) with the removal of the tyrosine aromatic ring and methionine sulfur-containing side chain.

In the VWF115 assay, the amount of ADAMTS13 cleavage present ranged from no significant change, to a 237-fold decrease depending on the amino acid substitution. This wide range of effect appears to be the result of a loss of enzyme selectivity on the much smaller VWF115 substrate that has a large part of the A2 domain removed. Only those changes that are chemically very different are sufficient to decrease the amount of ADAMTS13 cleavage in the 115mer assay (Table 5.1). M1606L and Y1605F both had statistically insignificant changes in the VWF115 assay, with a 26% decrease in ADAMTS13 concentration and a 10% increase respectively. Y1605H showed a slight decrease in cleavage, with 78% more ADAMTS13 being required. In contrast, Y1605N and Y1605A/M1606A required large increases in ADAMTS13 concentrations of 80-fold and 237-fold respectively. The charge changes in most of these substituted molecules explain the minimal cleavage shifts. M1606L removes a polar group and adds a methyl group in this location. Y1605F removes the polar hydroxyl group on the aromatic ring, which was interacting with other residues. Y1605H remains aromatic as well, going from the polar hydroxyl group to the positively charged imidazole ring. All of these substituted molecules remain very similar in size, while the charge changes are also small. In contrast, Y1605N loses the aromatic structure and adds a polar amine group. This loss of the aromatic ring appears to be critical for ADAMTS13 cleavage site recognition (figure 5.3), and would alter the interactions with A2 domain amino acids. The Y1605A/M1606A mutant exhibits the greatest loss of cleavage, with the replacement of both R groups with methyl groups.

### 5.2.3 Known von Willebrand Disease Mutations

Three VWD mutations were also examined for changes in ADAMTS13-mediated cleavage. The type 2A group II mutation, R1597W, has previously been demonstrated to have enhanced ADAMTS13 cleavage through destabilizing the A2 domain structure.<sup>95, 105, 140</sup> Y1584C has also been demonstrated to possess enhanced ADAMTS13 cleavage in patient plasma.<sup>163, 164</sup> R1205H has not previously been examined for its effect on ADAMTS13 cleavage efficiency, although no binding with ADAMTS13 in this region of the protein has been demonstrated.

The 2A VWD mutant, R1597W, showed a 34% reduction in ADAMTS13 requirement in the full-length substrate assay since the amino acid substitution disrupts the stabilization of the A2 domain. R1597, in a short  $\alpha$  helical loop between  $\alpha 3$  and  $\beta 4$ , binds to S1534 before  $\beta 2$ , L1497 and D1498 in  $\beta 1$ , and S1593, and stacks with H1536, in the second  $\beta$  sheet (figure 5.2).<sup>95</sup> When R1597 is replaced by the large tryptophan residue, this dense packing is disrupted, opening the A2 domain into a less stable conformation and increasing susceptibility to shear forces and subsequent ADAMTS13-mediated cleavage (table 5.1). However, when using the VWF115 minimal substrate, this effect is lost, since most of these interacting amino acids are not present. Therefore, there is no significant difference in ADAMTS13-mediated cleavage between the wild type and R1597W 115mer substrates. In vivo modelling of this change also demonstrated enhanced cleavage through loss of high molecular weight multimers, a phenomenon which was further enhanced by the reintroduction of full-length murine ADAMTS13 into the mice.

The Y1584C type 1 VWD mutation has been demonstrated to enhance ADAMTS13 cleavage in patient plasma. However, this effect is 38-fold lower than demonstrated with strong type 2A VWD mutants.<sup>163, 164</sup> Y1584C is located in the external  $\alpha 3$  loop of the A2 domain, but does stack with H1588 and has interactions with amino acids V1548, V1546, and L1540 in the  $\beta 2$ -sheet as well as several water molecules. There was no alteration in cleavage for either mouse

or human full-length substrates. The hVWF115 substrate required 40% less ADAMTS13 compared to wild type, and the mVWF115 substrate required 20% less ADAMTS13. It is possible that the mutation's effect is assay dependent, and no change was observed in the full-length molecule due to the use of urea or some other unknown factor.

The D3 domain mutation R1205H often displays an increase in high molecular weight VWF multimers along with the occasional alteration in the typical multimer triplet band pattern, but this is not consistent in all patients.<sup>44, 45, 155, 159</sup> Recent computer modeling suggests that the increase in high molecular weight material observed in some R1205H patients can be attributed only to the decrease in half life of the protein, but that a slight lengthening of the half life will eliminate the phenomenon.<sup>160</sup> No ADAMTS13 cleavage studies had been performed with this mutant to confirm that there is no ADAMTS13-associated component to the multimer anomaly. In this study, R1205H had no alteration in ADAMTS13 cleavage in our full-length substrate assay (Table 5.1). This suggests that this mutation is not involved in ADAMTS13 interactions with the VWF molecule.

#### **5.2.4 In vitro mouse ADAMTS13 studies**

Since we had confirmed that mutations to the cleavage site greatly inhibit ADAMTS13 cleavage, we next studied the effect of these changes in vitro using mouse VWF substrates before going on to perform in vivo experiments. Although the human and mouse VWF proteins have a high degree of homology, there are significant inter-species differences.<sup>117</sup> Mouse ADAMTS13 does not cleave the human VWF substrate well,<sup>125</sup> and mouse platelets do not bind well with human VWF.<sup>118</sup> Because of these issues, we first needed to confirm that the mutations we had studied in the human VWF substrate still produced the same ADAMTS13 cleavage phenotype in a mouse exclusive (murine VWF and ADAMTS13) in vitro system before moving into the in vivo studies. Human and mouse wild type sequences were conserved for all four mutations. All

four VWF mutations examined in this mouse system had similar trends to what we had described for human VWF (Table 5.2). For the remainder of the work we maintained a mouse exclusive experimental system of investigation to avoid cross-species interactions affecting our results.

| Full-Length mVWF |                  |         | mVWF115       |                  |         |
|------------------|------------------|---------|---------------|------------------|---------|
|                  | Normalized Value | P Value |               | Normalized Value | P value |
| R1205H           | 1.09             | 0.316   | (-)           | (-)              | (-)     |
| Y1584C           | 1.24             | 0.245   | Y1584C        | 0.798            | 0.0136  |
| R1597W           | 0.321            | <0.0001 | R1597W        | 1.28             | 0.0148  |
| Y1605A/M1606A    | >100             | <0.0001 | Y1605A/M1606A | 126              | 0.0013  |

**Table 5.2 Summary of mouse ADAMTS13 digest results.**

The ADAMTS13 digest results of the four mutations examined in vivo are summarized here. Relative levels of ADAMTS13 required for 50% substrate cleavage are reported, with wild type VWF assigned a value of 1. Levels above 1 have resistance to ADAMTS13 cleavage, and below 1, are more easily cleaved. P values <0.05 are considered significant. Full experimental details are in chapters 3 and 4.

### 5.3 In Vivo Mouse Studies

ADAMTS13-mediated interactions could also alter other aspects of VWF expression and function. To that end, we investigated these mutations with several experimental strategies. Von Willebrand factor knockout mice received either recombinant mouse VWF infusion, or hydrodynamic tail vein injection of ET promoter-expressed mouse *Vwf* cDNA for stable expression studies. VWF antigen levels and multimer analysis were determined to see if the changes altered synthesis and secretion of the proteins or affected the multimer structure. The ADAMTS13-dependent effect on multimer structure was further studied by performing co-hydrodynamic injections with full-length *Adamts13* cDNA. Clearance mechanisms were

investigated via recombinant protein infusions as well as VWF propeptide/VWF antigen ratios. VWF thrombogenic function was measured using a ferric chloride injury of the cremaster arterioles with mean time to vessel occlusion being determined.

R1597W was more easily cleaved by mADAMTS13 in a full-length digest assay and exhibited a lower multimeric profile compared to wild type VWF protein when expressed in the VWF KO mouse. In addition, R1597W was much less thrombogenic and had a shorter half-life and a slightly increased VWFpp/VWF:Ag ratio, suggesting that this variant protein is cleared from plasma more rapidly. This mechanism likely contributes to the lower VWF:Ag levels observed during days 14-35 post-hydrodynamic injection. Overall, these findings in the mouse model recapitulate the human type 2A disease phenotype and suggest that this model system could be used to evaluate other substitutions that increase susceptibility to ADAMTS13 proteolysis.

The Y1605A/M1606A mutant demonstrated a marked decrease in mADAMTS13-mediated cleavage in vitro. In the hydrodynamically injected mice, Y1605A/M1606A shows a minor increase in high molecular weight forms of multimers compared to wild type VWF. Furthermore, when full-length mADAMTS13 was co-expressed in the mice, the cleavage site mutant mice showed a more distinct population of ultra-high molecular weight multimers. In addition, an accelerated clearance phenotype is suggested by the results of the recombinant protein infusions and VWFpp/VWF:Ag ratio studies. The thrombosis injury model demonstrates increased platelet accumulation with a loss of occlusive thrombi. This shows a defect in thrombogenesis. Despite having larger multimers and decreased ADAMTS13-mediated cleavage, these mice showed no symptoms or signs of a pro-thrombotic state. This lack of a thrombotic phenotype is reminiscent of the ADAMTS13 knockout mice that require a second

challenge, such as the perturbation of the endothelium with shigatoxin, to develop a TTP-like state.<sup>123</sup> This appears also to be the case with the Y1605A/M1606A mutant.

In this study, the Y1584C mutant demonstrated decreased biosynthesis *in vitro*, enhanced proteolysis by ADAMTS13 *in vitro* and *in vivo*, and decreased VWF expression *in vivo*. The multimer size decrease was more moderate than documented for R1597W, but was still highly significant. The increase in ADAMTS13-mediated cleavage produced a mild type 2A VWD multimer profile that very likely contributed to the delay in forming occlusive thrombi in our ferric chloride injury model.

Shear stress is required for the A2 domain to unfold and allow ADAMTS13 cleavage to occur. The cysteines in VWF are highly conserved, and most are involved in disulfide bonds.<sup>117</sup> The A2 domain normally only has a single disulfide bond at two adjacent residues near the C-terminal end of the domain. The addition of the Y1584C mutation could cause aberrant folding within the domain and be the cause for the decreased synthesis and secretion of VWF and result in a reduction of thrombogenic potential. It is possible that in the human patient setting, the enhanced ADAMTS13 cleavage only occurs at the sites of endothelial injury in high shear conditions. Both a theoretical model<sup>96</sup> and *in vitro* thrombus studies<sup>97</sup> demonstrate that ADAMTS13 cleavage activity will increase under increasing shear forces, such as that of narrowing arteries at the site of a growing thrombus. This mechanism is tightly regulated by the shear bolt mechanism of the A2 domain. With Y1584C having a “weakened” shear bolt, the additional cleavage at lower shear forces could prevent normal platelet accumulation in the event of trauma and increase the length and severity of bleeding. In contrast, this mechanism could also prove to be protective in areas like stenotic coronary arteries in patients with atherosclerosis, by preventing the development of occlusive thrombi.

R1205H, the Vicenza mutation, has a relatively severe type 1 phenotype with accelerated VWF clearance. In humans, R1205H heterozygotes show a large decrease in VWF antigen (VWF:Ag) to ~0.15 U/mL, VWF Ristocetin Cofactor Activity (VWF:RCO) ~0.20 U/mL, and Factor VIII levels <0.30 U/mL, but maintain normal platelet VWF levels and function.<sup>44, 45, 155, 156</sup> Accelerated clearance of the mutant protein has been demonstrated via desmopressin (DDAVP) studies,<sup>44</sup> human recombinant protein infusion in the VWF knockout mouse,<sup>37</sup> as well as high VWFpp/VWF:Ag ratios,<sup>45</sup> with observed ratios of 10 or greater for this measurement. Platelet studies with R1205H patients demonstrated equal or enhanced binding of patient platelets to collagen substrates compared to that of normal individuals.<sup>156</sup> As a result of the normal levels of platelet VWF, some of these patients have lower bleeding tendencies than would be expected.<sup>156</sup> Bleeding scores show a mean of 8, but range from 2-17 (n = 18, 6 families), with any score greater or equal to 4 being considered positive.<sup>73, 111, 157, 158</sup> These patients also have a normal or enhanced DDAVP response since there is normal Weibel-Palade body storage and release.<sup>161, 162</sup>

In vitro analysis has shown a doubling for the binding constant of R1205H to the VWF propeptide in the acidic pH of 5.2 and 5.8 found in the trans-Golgi network as well as the Weibel-Palade body storage granules.<sup>37</sup> This loss of association could have biologic implications since the propeptide has been shown to be required for efficient packing to create the helix structure observed in the Weibel-Palade bodies.<sup>23</sup>

This inability to properly condense within the storage organelles could preferentially lead to multimers containing a larger number of mutant subunits being constitutively secreted. Multimers consisting of predominantly wild type subunits would then be preferentially stored. Since the mutant protein is prematurely cleared, this would lead to an even lower level of VWF than would be expected. However, when an injury occurs, or when desmopressin is administered,

the majority of the freshly released VWF would function normally, preventing a major bleeding episode.

The work presented here illustrates that R1205H has a biosynthetic defect, probably due to the loss of VWF propeptide association. In addition, our in vitro ADAMTS13 digestion studies show no difference from the wild type protein, confirming that the ultra-large VWF multimers seen in some R1205H patients is not due to a reduction in ADAMTS13-mediated cleavage. Most noteworthy is the fact that the R1205H protein, when expressed at normal physiologic levels, had a similar mean time to vessel occlusion as the wild type protein in a thrombosis injury model. This illustrates that the mutant protein functions normally, but that the biosynthetic defect combined with enhanced clearance are the dominant contributing factors to the bleeding disease phenotype.

#### **5.4 Future applications and Conclusions**

This study demonstrates that changes in the human *VWF* gene that result in alterations in ADAMTS13-mediated cleavage will also affect the mouse VWF molecule. Synthesis, multimeric size, and time to thrombotic occlusion were all affected by at least one of the mutations studied in this model system. This research demonstrates that this methodology can be used to evaluate other potentially pathogenic sequence variants from the human patient population. In addition, alternative testing methodologies could be investigated using these mutations as control molecules. These could include additional bleeding or thrombosis models, or combining these changes with additional mutations to better understand the mechanisms at work. For example, the Y1605A/M1606A change could be combined with type 2A or 2B mutations to remove the ADAMTS13 cleavage influence from the type 2 disease phenotype.

In conclusion, this study demonstrates that common VWF polymorphisms and mutations introduced at the ADAMTS13 cleavage site alter ADAMTS13-mediated cleavage. Human VWD

mutations that affect ADAMTS13 cleavage also have a similar effect in the mouse. The mouse model has been validated as a method of understanding the mechanisms associated with the mutations in type 1 VWD, and adds valuable information to the understanding of how this disease affects patients.

## References

1. Sadler JE. Biochemistry and genetics of von Willebrand factor. *Annu Rev Biochem.* 1998;67:395-424.
2. Furlan M. Von Willebrand factor: molecular size and functional activity. *Ann Hematol.* 1996;72:341-348.
3. Plaimauer B, Zimmermann K, Volkel D, et al. Cloning, expression, and functional characterization of the von Willebrand factor-cleaving protease (ADAMTS13). *Blood.* 2002;100:3626-3632.
4. Zheng X, Chung D, Takayama TK, Majerus EM, Sadler JE, Fujikawa K. Structure of von Willebrand factor-cleaving protease (ADAMTS13), a metalloprotease involved in thrombotic thrombocytopenic purpura. *J Biol Chem.* 2001;276:41059-41063.
5. Bowman M, Hopman WM, Rapson D, Lillicrap D, James P. The prevalence of symptomatic von Willebrand disease in primary care practice. *J Thromb Haemost.* 2010;8:213-216.
6. Mancuso DJ, Tuley EA, Westfield LA, et al. Human von Willebrand factor gene and pseudogene: structural analysis and differentiation by polymerase chain reaction. *Biochemistry.* 1991;30:253-269.
7. Verweij CL, Diergaarde PJ, Hart M, Pannekoek H. Full-length von Willebrand factor (vWF) cDNA encodes a highly repetitive protein considerably larger than the mature vWF subunit. *EMBO J.* 1986;5:1839-1847.
8. Mancuso DJ, Tuley EA, Westfield LA, et al. Structure of the gene for human von Willebrand factor. *J Biol Chem.* 1989;264:19514-19527.

9. de Wit TR and van Mourik JA. Biosynthesis, processing and secretion of von Willebrand factor: biological implications. *Best Pract Res Clin Haematol.* 2001;14:241-255.
10. Matsui T, Titani K, Mizuochi T. Structures of the asparagine-linked oligosaccharide chains of human von Willebrand factor. Occurrence of blood group A, B, and H(O) structures. *J Biol Chem.* 1992;267:8723-8731.
11. Wagner DD, Mayadas T, Marder VJ. Initial glycosylation and acidic pH in the Golgi apparatus are required for multimerization of von Willebrand factor. *J Cell Biol.* 1986;102:1320-1324.
12. Marti T, Rosselet SJ, Titani K, Walsh KA. Identification of disulfide-bridged substructures within human von Willebrand factor. *Biochemistry.* 1987;26:8099-8109.
13. Voorberg J, Fontijn R, Calafat J, Janssen H, van Mourik JA, Pannekoek H. Assembly and routing of von Willebrand factor variants: the requirements for disulfide-linked dimerization reside within the carboxy-terminal 151 amino acids. *J Cell Biol.* 1991;113:195-205.
14. Samor B, Michalski JC, Mazurier C, et al. Primary structure of the major O-glycosidically linked carbohydrate unit of human von Willebrand factor. *Glycoconj J.* 1989;6:263-270.
15. Rosenberg JB, Haberichter SL, Jozwiak MA, et al. The role of the D1 domain of the von Willebrand factor propeptide in multimerization of VWF. *Blood.* 2002;100:1699-1706.
16. Purvis AR and Sadler JE. A covalent oxidoreductase intermediate in propeptide-dependent von Willebrand factor multimerization. *J Biol Chem.* 2004;279:49982-49988.
17. Wise RJ, Barr PJ, Wong PA, Kiefer MC, Brake AJ, Kaufman RJ. Expression of a human proprotein processing enzyme: correct cleavage of the von Willebrand factor precursor at a paired basic amino acid site. *Proc Natl Acad Sci U S A.* 1990;87:9378-9382.

18. Creemers JW, Groot Kormelink PJ, Roebroek AJ, Nakayama K, Van de Ven WJ. Proprotein processing activity and cleavage site selectivity of the Kex2-like endoprotease PACE4. *FEBS Lett.* 1993;336:65-69.
19. Rehemtulla A and Kaufman RJ. Preferred sequence requirements for cleavage of pro-von Willebrand factor by propeptide-processing enzymes. *Blood.* 1992;79:2349-2355.
20. Allen S, Abuzenadah AM, Blagg JL, et al. Two novel type 2N von Willebrand disease-causing mutations that result in defective factor VIII binding, multimerization, and secretion of von Willebrand factor. *Blood.* 2000;95:2000-2007.
21. Turecek PL, Varadi K, Schlokot U, Pichler L, Dorner F, Schwarz HP. In vivo and in vitro processing of recombinant pro-von Willebrand factor. *Histochem Cell Biol.* 2002;117:123-129.
22. van Mourik JA, Romani de Wit T, Voorberg J. Biogenesis and exocytosis of Weibel-Palade bodies. *Histochem Cell Biol.* 2002;117:113-122.
23. Huang RH, Wang Y, Roth R, et al. Assembly of Weibel-Palade body-like tubules from N-terminal domains of von Willebrand factor. *Proc Natl Acad Sci U S A.* 2008;105:482-487.
24. Haberichter SL, Jozwiak MA, Rosenberg JB, Christopherson PA, Montgomery RR. The von Willebrand factor propeptide (VWFpp) traffics an unrelated protein to storage. *Arterioscler Thromb Vasc Biol.* 2002;22:921-926.
25. Haberichter SL, Jacobi P, Montgomery RR. Critical independent regions in the VWF propeptide and mature VWF that enable normal VWF storage. *Blood.* 2003;101:1384-1391.
26. Zannettino AC, Holding CA, Diamond P, et al. Osteoprotegerin (OPG) is localized to the Weibel-Palade bodies of human vascular endothelial cells and is physically associated with von Willebrand factor. *J Cell Physiol.* 2005;204:714-723.

27. Fiedler U, Scharpfenecker M, Koidl S, et al. The Tie-2 ligand angiopoietin-2 is stored in and rapidly released upon stimulation from endothelial cell Weibel-Palade bodies. *Blood*. 2004;103:4150-4156.
28. Galbusera M, Zoja C, Donadelli R, et al. Fluid shear stress modulates von Willebrand factor release from human vascular endothelium. *Blood*. 1997;90:1558-1564.
29. Sun RJ, Muller S, Wang X, Zhuang FY, Stoltz JF. Regulation of von willebrand factor of human endothelial cells exposed to laminar flows: an in vitro study. *Clin Hemorheol Microcirc*. 2000;23:1-11.
30. Vischer UM, Jornot L, Wollheim CB, Theler JM. Reactive oxygen intermediates induce regulated secretion of von Willebrand factor from cultured human vascular endothelial cells. *Blood*. 1995;85:3164-3172.
31. Rondaij MG, Sellink E, Gijzen KA, et al. Small GTP-binding protein Ral is involved in cAMP-mediated release of von Willebrand factor from endothelial cells. *Arterioscler Thromb Vasc Biol*. 2004;24:1315-1320.
32. Matsushita K, Morrell CN, Lowenstein CJ. Sphingosine 1-phosphate activates Weibel-Palade body exocytosis. *Proc Natl Acad Sci U S A*. 2004;101:11483-11487.
33. Bhatia R, Matsushita K, Yamakuchi M, Morrell CN, Cao W, Lowenstein CJ. Ceramide triggers Weibel-Palade body exocytosis. *Circ Res*. 2004;95:319-324.
34. Matsushita K, Yamakuchi M, Morrell CN, et al. Vascular endothelial growth factor regulation of Weibel-Palade-body exocytosis. *Blood*. 2005;105:207-214.
35. Bonnefoy A and Legrand C. Proteolysis of subendothelial adhesive glycoproteins (fibronectin, thrombospondin, and von Willebrand factor) by plasmin, leukocyte cathepsin G, and elastase. *Thromb Res*. 2000;98:323-332.

36. Haberichter SL, Balistreri M, Christopherson P, et al. Assay of the von Willebrand factor (VWF) propeptide to identify patients with type 1 von Willebrand disease with decreased VWF survival. *Blood*. 2006;108:3344-3351.
37. Lenting PJ, Westein E, Terraube V, et al. An experimental model to study the in vivo survival of von Willebrand factor. Basic aspects and application to the R1205H mutation. *J Biol Chem*. 2004;279:12102-12109.
38. Denis CV, Christophe OD, Oortwijn BD, Lenting PJ. Clearance of von Willebrand factor. *Thromb Haemost*. 2008;99:271-278.
39. O'Donnell J, Boulton FE, Manning RA, Laffan MA. Amount of H antigen expressed on circulating von Willebrand factor is modified by ABO blood group genotype and is a major determinant of plasma von Willebrand factor antigen levels. *Arterioscler Thromb Vasc Biol*. 2002;22:335-341.
40. Gallinaro L, Cattini MG, Sztukowska M, et al. A shorter von Willebrand factor survival in O blood group subjects explains how ABO determinants influence plasma von Willebrand factor. *Blood*. 2008;111:3540-3545.
41. O'Donnell JS, McKinnon TA, Crawley JT, Lane DA, Laffan MA. Bombay phenotype is associated with reduced plasma-VWF levels and an increased susceptibility to ADAMTS13 proteolysis. *Blood*. 2005;106:1988-1991.
42. Schulte am Esch J, 2nd, Robson SC, Knoefel WT, Eisenberger CF, Peiper M, Rogiers X. Impact of O-linked glycosylation of the VWF-A1-domain flanking regions on platelet interaction. *Br J Haematol*. 2005;128:82-90.
43. Schooten CJ, Tjernberg P, Westein E, et al. Cysteine-mutations in von Willebrand factor associated with increased clearance. *J Thromb Haemost*. 2005;3:2228-2237.

44. Casonato A, Pontara E, Sartorello F, et al. Reduced von Willebrand factor survival in type Vicenza von Willebrand disease. *Blood*. 2002;99:180-184.
45. Haberichter SL, Castaman G, Budde U, et al. Identification of type 1 von Willebrand disease patients with reduced von Willebrand factor survival by assay of the VWF propeptide in the European study: molecular and clinical markers for the diagnosis and management of type 1 VWD (MCMDM-1VWD). *Blood*. 2008;111:4979-4985.
46. Sodetz JM, Pizzo SV, McKee PA. Relationship of sialic acid to function and in vivo survival of human factor VIII/von Willebrand factor protein. *J Biol Chem*. 1977;252:5538-5546.
47. Smith NL, Chen MH, Dehghan A, et al. Novel associations of multiple genetic loci with plasma levels of factor VII, factor VIII, and von Willebrand factor: The CHARGE (Cohorts for Heart and Aging Research in Genome Epidemiology) Consortium. *Circulation*. 2010;121:1382-1392.
48. Kaufmann JE and Vischer UM. Cellular mechanisms of the hemostatic effects of desmopressin (DDAVP). *J Thromb Haemost*. 2003;1:682-689.
49. Michiels JJ, van de Velde A, van Vliet HH, van der Planken M, Schroyens W, Berneman Z. Response of von Willebrand factor parameters to desmopressin in patients with type 1 and type 2 congenital von Willebrand disease: diagnostic and therapeutic implications. *Semin Thromb Hemost*. 2002;28:111-132.
50. Sztukowska M, Gallinaro L, Cattini MG, et al. Von Willebrand factor propeptide makes it easy to identify the shorter Von Willebrand factor survival in patients with type 1 and type Vicenza von Willebrand disease. *Br J Haematol*. 2008;143:107-114.
51. Graw J, Brackmann HH, Oldenburg J, Schneppenheim R, Spannagl M, Schwaab R. Haemophilia A: from mutation analysis to new therapies. *Nat Rev Genet*. 2005;6:488-501.

52. Nogami K, Shima M, Nishiya K, et al. A novel mechanism of factor VIII protection by von Willebrand factor from activated protein C-catalyzed inactivation. *Blood*. 2002;99:3993-3998.
53. Hilbert L, Jorieux S, Fontenay-Roupie M, et al. Expression of two type 2N von Willebrand disease mutations identified in exon 18 of von Willebrand factor gene. *Br J Haematol*. 2004;127:184-189.
54. Casonato A, Sartorello F, Cattini MG, et al. An Arg760Cys mutation in the consensus sequence of the von Willebrand factor propeptide cleavage site is responsible for a new von Willebrand disease variant. *Blood*. 2003;101:151-156.
55. Guidetti GF, Bartolini B, Bernardi B, et al. Binding of von Willebrand factor to the small proteoglycan decorin. *FEBS Lett*. 2004;574:95-100.
56. Romijn RA, Westein E, Bouma B, et al. Mapping the collagen-binding site in the von Willebrand factor-A3 domain. *J Biol Chem*. 2003;278:15035-15039.
57. Bernardo A, Bergeron AL, Sun CW, et al. Von Willebrand factor present in fibrillar collagen enhances platelet adhesion to collagen and collagen-induced platelet aggregation. *J Thromb Haemost*. 2004;2:660-669.
58. Ruggeri ZM. Von Willebrand factor, platelets and endothelial cell interactions. *J Thromb Haemost*. 2003;1:1335-1342.
59. Moroi M, Jung SM, Nomura S, Sekiguchi S, Ordinas A, Diaz-Ricart M. Analysis of the involvement of the von Willebrand factor-glycoprotein Ib interaction in platelet adhesion to a collagen-coated surface under flow conditions. *Blood*. 1997;90:4413-4424.
60. Dong JF, Berndt MC, Schade A, McIntire LV, Andrews RK, Lopez JA. Ristocetin-dependent, but not botrocetin-dependent, binding of von Willebrand factor to the platelet glycoprotein Ib-IX-V complex correlates with shear-dependent interactions. *Blood*. 2001;97:162-168.

61. Liu J, Pestina TI, Berndt MC, Jackson CW, Gartner TK. Botrocetin/VWF-induced signaling through GPIb-IX-V produces TxA<sub>2</sub> in an alphaIIb beta3- and aggregation-independent manner. *Blood*. 2005;106:2750-2756.
62. Bonnefoy A, Moura R, Hoylaerts MF. The evolving role of thrombospondin-1 in hemostasis and vascular biology. *Cell Mol Life Sci*. 2008;65:713-727.
63. Moura R, Tjwa M, Vandervoort P, Van Kerckhoven S, Holvoet P, Hoylaerts MF. Thrombospondin-1 deficiency accelerates atherosclerotic plaque maturation in ApoE<sup>-/-</sup> mice. *Circ Res*. 2008;103:1181-1189.
64. Pimanda JE, Annis DS, Raftery M, Mosher DF, Chesterman CN, Hogg PJ. The von Willebrand factor-reducing activity of thrombospondin-1 is located in the calcium-binding/C-terminal sequence and requires a free thiol at position 974. *Blood*. 2002;100:2832-2838.
65. Pimanda JE, Ganderton T, Maekawa A, et al. Role of thrombospondin-1 in control of von Willebrand factor multimer size in mice. *J Biol Chem*. 2004;279:21439-21448.
66. Reid P and Holen I. Pathophysiological roles of osteoprotegerin (OPG). *Eur J Cell Biol*. 2009;88:1-17.
67. Shahbazi S, Lenting PJ, Fribourg C, Terraube V, Denis CV, Christophe OD. Characterization of the interaction between von Willebrand factor and osteoprotegerin. *J Thromb Haemost*. 2007;5:1956-1962.
68. Baud'huin M, Duplomb L, Teletchea S, et al. Factor VIII-von Willebrand factor complex inhibits osteoclastogenesis and controls cell survival. *J Biol Chem*. 2009;284:31704-31713.
69. Adachi T, Matsushita T, Dong Z, et al. Identification of amino acid residues essential for heparin binding by the A1 domain of human von Willebrand factor. *Biochem Biophys Res Commun*. 2006;339:1178-1183.

70. Fujimura Y, Titani K, Holland LZ, et al. A heparin-binding domain of human von Willebrand factor. Characterization and localization to a tryptic fragment extending from amino acid residue Val-449 to Lys-728. *J Biol Chem.* 1987;262:1734-1739.
71. Nakayama T, Matsushita T, Yamamoto K, et al. Identification of amino acid residues responsible for von Willebrand factor binding to sulfatide by charged-to-alanine-scanning mutagenesis. *Int J Hematol.* 2008;87:363-370.
72. Hulstein JJ, Lenting PJ, de Laat B, Derksen RH, Fijnheer R, de Groot PG. beta2-Glycoprotein I inhibits von Willebrand factor dependent platelet adhesion and aggregation. *Blood.* 2007;110:1483-1491.
73. Goodeve AC. The genetic basis of von Willebrand disease. *Blood Rev.* 2010;24:123-134.
74. Fujikawa K, Suzuki H, McMullen B, Chung D. Purification of human von Willebrand factor-cleaving protease and its identification as a new member of the metalloproteinase family. *Blood.* 2001;98:1662-1666.
75. Gerritsen HE, Robles R, Lammler B, Furlan M. Partial amino acid sequence of purified von Willebrand factor-cleaving protease. *Blood.* 2001;98:1654-1661.
76. Majerus EM, Zheng X, Tuley EA, Sadler JE. Cleavage of the ADAMTS13 propeptide is not required for protease activity. *J Biol Chem.* 2003;278:46643-46648.
77. Levy GG, Motto DG, Ginsburg D. ADAMTS13 turns 3. *Blood.* 2005;106:11-17.
78. Zhou W, Inada M, Lee TP, et al. ADAMTS13 is expressed in hepatic stellate cells. *Lab Invest.* 2005;85:780-788.
79. Uemura M, Fujimura Y, Ko S, Matsumoto M, Nakajima Y, Fukui H. Pivotal role of ADAMTS13 function in liver diseases. *Int J Hematol.* 2010;91:20-29.

80. Suzuki M, Murata M, Matsubara Y, et al. Detection of von Willebrand factor-cleaving protease (ADAMTS-13) in human platelets. *Biochem Biophys Res Commun.* 2004;313:212-216.
81. Turner N, Nolasco L, Tao Z, Dong JF, Moake J. Human endothelial cells synthesize and release ADAMTS-13. *J Thromb Haemost.* 2006;4:1396-1404.
82. Manea M, Kristoffersson A, Schneppenheim R, et al. Podocytes express ADAMTS13 in normal renal cortex and in patients with thrombotic thrombocytopenic purpura. *Br J Haematol.* 2007;138:651-662.
83. Feys HB, Liu F, Dong N, et al. ADAMTS-13 plasma level determination uncovers antigen absence in acquired thrombotic thrombocytopenic purpura and ethnic differences. *J Thromb Haemost.* 2006;4:955-962.
84. Mannucci PM, Capoferri C, Canciani MT. Plasma levels of von Willebrand factor regulate ADAMTS-13, its major cleaving protease. *Br J Haematol.* 2004;126:213-218.
85. Reiter RA, Knobl P, Varadi K, Turecek PL. Changes in von Willebrand factor-cleaving protease (ADAMTS13) activity after infusion of desmopressin. *Blood.* 2003;101:946-948.
86. Padilla A, Moake JL, Bernardo A, et al. P-selectin anchors newly released ultralarge von Willebrand factor multimers to the endothelial cell surface. *Blood.* 2004;103:2150-2156.
87. Dong JF, Moake JL, Nolasco L, et al. ADAMTS-13 rapidly cleaves newly secreted ultralarge von Willebrand factor multimers on the endothelial surface under flowing conditions. *Blood.* 2002;100:4033-4039.
88. Feys HB, Anderson PJ, Vanhoorelbeke K, Majerus EM, Sadler JE. Multi-step binding of ADAMTS-13 to von Willebrand factor. *J Thromb Haemost.* 2009;7:2088-2095.
89. Zanardelli S, Chion AC, Groot E, et al. A novel binding site for ADAMTS13 constitutively exposed on the surface of globular VWF. *Blood.* 2009;114:2819-2828.

90. Dong JF, Moake JL, Bernardo A, et al. ADAMTS-13 metalloprotease interacts with the endothelial cell-derived ultra-large von Willebrand factor. *J Biol Chem.* 2003;278:29633-29639.
91. Auton M, Cruz MA, Moake J. Conformational stability and domain unfolding of the Von Willebrand factor A domains. *J Mol Biol.* 2007;366:986-1000.
92. De Cristofaro R, Peyvandi F, Baronciani L, et al. Molecular mapping of the chloride-binding site in von Willebrand factor (VWF): energetics and conformational effects on the VWF/ADAMTS-13 interaction. *J Biol Chem.* 2006;281:30400-30411.
93. Nishio K, Anderson PJ, Zheng XL, Sadler JE. Binding of platelet glycoprotein Ibalpha to von Willebrand factor domain A1 stimulates the cleavage of the adjacent domain A2 by ADAMTS13. *Proc Natl Acad Sci U S A.* 2004;101:10578-10583.
94. Shim K, Anderson PJ, Tuley EA, Wiswall E, Sadler JE. Platelet-VWF complexes are preferred substrates of ADAMTS13 under fluid shear stress. *Blood.* 2008;111:651-657.
95. Zhang Q, Zhou YF, Zhang CZ, Zhang X, Lu C, Springer TA. Structural specializations of A2, a force-sensing domain in the ultralarge vascular protein von Willebrand factor. *Proc Natl Acad Sci U S A.* 2009;106:9226-9231.
96. Zhang X, Halvorsen K, Zhang CZ, Wong WP, Springer TA. Mechanoenzymatic cleavage of the ultralarge vascular protein von Willebrand factor. *Science.* 2009;324:1330-1334.
97. Shida Y, Nishio K, Sugimoto M, et al. Functional imaging of shear-dependent activity of ADAMTS13 in regulating mural thrombus growth under whole blood flow conditions. *Blood.* 2008;111:1295-1298.
98. Kokame K, Matsumoto M, Fujimura Y, Miyata T. VWF73, a region from D1596 to R1668 of von Willebrand factor, provides a minimal substrate for ADAMTS-13. *Blood.* 2004;103:607-612.

99. Gao W, Anderson PJ, Sadler JE. Extensive contacts between ADAMTS13 exosites and von Willebrand factor domain A2 contribute to substrate specificity. *Blood*. 2008;112:1713-1719.
100. Akiyama M, Takeda S, Kokame K, Takagi J, Miyata T. Crystal structures of the noncatalytic domains of ADAMTS13 reveal multiple discontinuous exosites for von Willebrand factor. *Proc Natl Acad Sci U S A*. 2009;106:19274-19279.
101. Tsai HM. Physiologic cleavage of von Willebrand factor by a plasma protease is dependent on its conformation and requires calcium ion. *Blood*. 1996;87:4235-4244.
102. Furlan M, Robles R, Lamie B. Partial purification and characterization of a protease from human plasma cleaving von Willebrand factor to fragments produced by in vivo proteolysis. *Blood*. 1996;87:4223-4234.
103. Zhang P, Pan W, Rux AH, Sachais BS, Zheng XL. The cooperative activity between the carboxyl-terminal TSP1 repeats and the CUB domains of ADAMTS13 is crucial for recognition of von Willebrand factor under flow. *Blood*. 2007;110:1887-1894.
104. Donadelli R, Orje JN, Capoferri C, Remuzzi G, Ruggeri ZM. Size regulation of von Willebrand factor-mediated platelet thrombi by ADAMTS-13 in flowing blood. *Blood*. 2005.
105. Hassenpflug WA, Budde U, Obser T, et al. Impact of mutations in the von Willebrand factor A2 domain on ADAMTS13-dependent proteolysis. *Blood*. 2006;107:2339-2345.
106. Cruz MA, Whitelock J, Dong JF. Evaluation of ADAMTS-13 activity in plasma using recombinant von Willebrand Factor A2 domain polypeptide as substrate. *Thromb Haemost*. 2003;90:1204-1209.

107. Kato S, Matsumoto M, Matsuyama T, Isonishi A, Hiura H, Fujimura Y. Novel monoclonal antibody-based enzyme immunoassay for determining plasma levels of ADAMTS13 activity. *Transfusion*. 2006;46:1444-1452.
108. Kokame K, Nobe Y, Kokubo Y, Okayama A, Miyata T. FRETs-VWF73, a first fluorogenic substrate for ADAMTS13 assay. *Br J Haematol*. 2005;129:93-100.
109. Sadler JE, Budde U, Eikenboom JC, et al. Update on the pathophysiology and classification of von Willebrand disease: a report of the Subcommittee on von Willebrand Factor. *J Thromb Haemost*. 2006;4:2103-2114.
110. Lillicrap D. Genotype/phenotype association in von Willebrand disease: is the glass half full or empty? *J Thromb Haemost*. 2009;7 Suppl 1:65-70.
111. Goodeve A, Eikenboom J, Castaman G, et al. Phenotype and genotype of a cohort of families historically diagnosed with type 1 von Willebrand disease in the European study, Molecular and Clinical Markers for the Diagnosis and Management of Type 1 von Willebrand Disease (MCMDM-1VWD). *Blood*. 2007;109:112-121.
112. James PD, Notley C, Hegadorn C, et al. The mutational spectrum of type 1 von Willebrand disease: Results from a Canadian cohort study. *Blood*. 2007;109:145-154.
113. Desch KC and Motto DG. Thrombotic thrombocytopenic purpura in humans and mice. *Arterioscler Thromb Vasc Biol*. 2007;27:1901-1908.
114. Moake JL. von Willebrand factor, ADAMTS-13, and thrombotic thrombocytopenic purpura. *Semin Hematol*. 2004;41:4-14.
115. Pendu R, Christophe OD, Denis CV. Mouse models of von Willebrand disease. *J Thromb Haemost*. 2009;7 Suppl 1:61-64.
116. Denis C, Methia N, Frenette PS, et al. A mouse model of severe von Willebrand disease: defects in hemostasis and thrombosis. *Proc Natl Acad Sci U S A*. 1998;95:9524-9529.

117. Chitta MS, Duhe RJ, Kermode JC. Cloning of the cDNA for murine von Willebrand factor and identification of orthologous genes reveals the extent of conservation among diverse species. *Platelets*. 2007;18:182-198.
118. Ware J, Russell S, Ruggeri ZM. Cloning of the Murine Platelet Glycoprotein Ib-alpha Gene Highlighting Species-Specific Platelet Adhesion. *Blood Cells, Molecules, and Diseases*. 1997;23:292-301.
119. Qin F, Impeduglia T, Schaffer P, Dardik H. Overexpression of von Willebrand factor is an independent risk factor for pathogenesis of intimal hyperplasia: preliminary studies. *J Vasc Surg*. 2003;37:433-439.
120. Mohlke KL, Purkayastha AA, Westrick RJ, et al. Mvwf, a dominant modifier of murine von Willebrand factor, results from altered lineage-specific expression of a glycosyltransferase. *Cell*. 1999;96:111-120.
121. Shavit JA, Manichaikul A, Lemmerhirt HL, Broman KW, Ginsburg D. Modifiers of von Willebrand factor identified by natural variation in inbred strains of mice. *Blood*. 2009;114:5368-5374.
122. Banno F, Kokame K, Okuda T, et al. Complete deficiency in ADAMTS13 is prothrombotic, but it alone is not sufficient to cause thrombotic thrombocytopenic purpura. *Blood*. 2006;107:3161-3166.
123. Motto DG, Chauhan AK, Zhu G, et al. Shigatoxin triggers thrombotic thrombocytopenic purpura in genetically susceptible ADAMTS13-deficient mice. *J Clin Invest*. 2005;115:2752-2761.
124. Bruno K, Volkel D, Plaimauer B, et al. Cloning, expression and functional characterization of the full-length murine ADAMTS13. *J Thromb Haemost*. 2005;3:1064-1073.

125. Varadi K, Rottensteiner H, Vejda S, et al. Species-dependent variability of ADAMTS13-mediated proteolysis of human recombinant von Willebrand factor. *J Thromb Haemost.* 2009;7:1134-1142.
126. Banno F, Kaminaka K, Soejima K, Kokame K, Miyata T. Identification of strain-specific variants of mouse Adamts13 gene encoding von Willebrand factor-cleaving protease. *J Biol Chem.* 2004;279:30896-30903.
127. Banno F, Chauhan AK, Kokame K, et al. The distal carboxyl-terminal domains of ADAMTS13 are required for regulation of in vivo thrombus formation. *Blood.* 2009;113:5323-5329.
128. Zhang G, Budker V, Wolff JA. High levels of foreign gene expression in hepatocytes after tail vein injections of naked plasmid DNA. *Hum Gene Ther.* 1999;10:1735-1737.
129. Sebestyen MG, Budker VG, Budker T, et al. Mechanism of plasmid delivery by hydrodynamic tail vein injection. I. Hepatocyte uptake of various molecules. *J Gene Med.* 2006;8:852-873.
130. Budker VG, Subbotin VM, Budker T, Sebestyen MG, Zhang G, Wolff JA. Mechanism of plasmid delivery by hydrodynamic tail vein injection. II. Morphological studies. *J Gene Med.* 2006;8:874-888.
131. Pergolizzi RG, Jin G, Chan D, et al. Correction of a murine model of von Willebrand disease by gene transfer. *Blood.* 2006;108:862-869.
132. Lenting PJ, de Groot PG, De Meyer SF, et al. Correction of the bleeding time in von Willebrand factor (VWF)-deficient mice using murine VWF. *Blood.* 2007;109:2267-2268.
133. Marx I, Lenting PJ, Adler T, Pendu R, Christophe OD, Denis CV. Correction of bleeding symptoms in von Willebrand factor-deficient mice by liver-expressed von Willebrand factor mutants. *Arterioscler Thromb Vasc Biol.* 2008;28:419-424.

134. De Meyer SF, Vandeputte N, Pareyn I, et al. Restoration of plasma von Willebrand factor deficiency is sufficient to correct thrombus formation after gene therapy for severe von Willebrand disease. *Arterioscler Thromb Vasc Biol.* 2008;28:1621-1626.
135. Marx I, Christophe OD, Lenting PJ, et al. Altered thrombus formation in von Willebrand factor-deficient mice expressing von Willebrand factor variants with defective binding to collagen or GPIIbIIIa. *Blood.* 2008;112:603-609.
136. Golder M, Pruss CM, Hegadorn C, et al. Mutation-specific hemostatic variability in mice expressing common type 2B von Willebrand disease substitutions. *Blood.* 2010;115(23):4862-9.
137. Dubois C, Panicot-Dubois L, Merrill-Skoloff G, Furie B, Furie BC. Glycoprotein VI-dependent and -independent pathways of thrombus formation in vivo. *Blood.* 2006;107:3902-3906.
138. Gavins FN and Chatterjee BE. Intravital microscopy for the study of mouse microcirculation in anti-inflammatory drug research: focus on the mesentery and cremaster preparations. *J Pharmacol Toxicol Methods.* 2004;49:1-14.
139. Rayes J, Hommais A, Legendre P, et al. Effect of von Willebrand disease type 2B and type 2M mutations on the susceptibility of von Willebrand factor to ADAMTS-13. *J Thromb Haemost.* 2007;5:321-328.
140. Zanardelli S, Crawley JT, Chion CK, Lam JK, Preston RJ, Lane DA. ADAMTS13 Substrate Recognition of von Willebrand Factor A2 Domain. *J Biol Chem.* 2006;281:1555-1563.
141. O'Brien LA, James PD, Othman M, et al. Founder von Willebrand factor haplotype associated with type 1 von Willebrand disease. *Blood.* 2003;102:549-557.

142. Stakiw J, Bowman M, Hegadorn C, et al. The effect of exercise on von Willebrand factor and ADAMTS-13 in individuals with type 1 and type 2B von Willebrand disease. *J Thromb Haemost.* 2008;6:90-96.
143. Cruz MA, Diacovo TG, Emsley J, Liddington R, Handin RI. Mapping the glycoprotein Ib-binding site in the von willebrand factor A1 domain. *J Biol Chem.* 2000;275:19098-19105.
144. Davies JA and Bowen DJ. The association between the L1565 variant of von Willebrand factor and susceptibility to proteolysis by ADAMTS13. *Haematologica.* 2007;92:240-243.
145. Sutherland JJ, O'Brien LA, Lillicrap D, Weaver DF. Molecular modeling of the von Willebrand factor A2 Domain and the effects of associated type 2A von Willebrand disease mutations. *J Mol Model (Online).* 2004;10:259-270.
146. Baronciani L, Federici AB, Cozzi G, Canciani MT, Mannucci PM. von Willebrand factor collagen binding assay in von Willebrand disease type 2A, 2B, and 2M. *J Thromb Haemost.* 2006;4:2088-2090.
147. Wu JJ, Fujikawa K, McMullen BA, Chung DW. Characterization of a core binding site for ADAMTS-13 in the A2 domain of von Willebrand factor. *Proc Natl Acad Sci U S A.* 2006;103:18470-18474.
148. Obert B, Tout H, Veyradier A, Fressinaud E, Meyer D, Girma JP. Estimation of the von Willebrand factor-cleaving protease in plasma using monoclonal antibodies to vWF. *Thromb Haemost.* 1999;82:1382-1385.
149. Desch KC and Ginsburg D. Mutations that render von Willebrand Factor (VWF) resistant to ADAMTS13 cleavage. *J Thromb Haemost.* 2007;5:O-M-069.
150. Pruss CM, Notley CR, Hegadorn CA, O'Brien LA, Lillicrap D. ADAMTS13 cleavage efficiency is altered by mutagenic and, to a lesser extent, polymorphic sequence changes in the A1 and A2 domains of von Willebrand factor. *Br J Haematol.* 2008;143:552-558.

151. Lyons SE, Bruck ME, Bowie EJ, Ginsburg D. Impaired intracellular transport produced by a subset of type IIA von Willebrand disease mutations. *J Biol Chem.* 1992;267:4424-4430.
152. Rayes J, Hollestelle MJ, Legendre P, et al. Mutation & ADAMTS13-dependent modulation of disease severity in a mouse model for von Willebrand disease type 2B. *Blood.* 2010;115(23):4870-7.
153. Shi CX, Graham FL, Hitt MM. A convenient plasmid system for construction of helper-dependent adenoviral vectors and its application for analysis of the breast-cancer-specific mammaglobin promoter. *J Gene Med.* 2006.
154. Vigna E, Amendola M, Benedicenti F, Simmons AD, Follenzi A, Naldini L. Efficient Tet-dependent expression of human factor IX in vivo by a new self-regulating lentiviral vector. *Mol Ther.* 2005;11:763-775.
155. Casonato A, Pontara E, Sartorello F, et al. Identifying type Vicenza von Willebrand disease. *J Lab Clin Med.* 2006;147:96-102.
156. d'Alessio PA, Castaman G, Rodeghiero F, et al. In vivo experiments indicate that relatively high platelet deposition in von Willebrand's disease 'Vicenza' is caused by normal platelet-VWF levels rather than by high VWF-multimers in plasma. *Thromb Res.* 1992;65:221-228.
157. Bowman M, Mundell G, Grabell J, et al. Generation and validation of the Condensed MCMDM-1VWD Bleeding Questionnaire for von Willebrand disease. *J Thromb Haemost.* 2008;6:2062-2066.
158. Tosetto A, Rodeghiero F, Castaman G, et al. A quantitative analysis of bleeding symptoms in type 1 von Willebrand disease: results from a multicenter European study (MCMDM-1 VWD). *J Thromb Haemost.* 2006;4:766-773.
159. Mannucci PM, Lombardi R, Castaman G, et al. von Willebrand disease "Vicenza" with larger-than-normal (supranormal) von Willebrand factor multimers. *Blood.* 1988;71:65-70.

160. Gezsi A, Budde U, Deak I, et al. Accelerated clearance alone explains ultralarge multimers in VWD vicenza. *J Thromb Haemost.* 2010;8:1273-1280.
161. Federici AB, Mazurier C, Berntorp E, et al. Biologic response to desmopressin in patients with severe type 1 and type 2 von Willebrand disease: results of a multicenter European study. *Blood.* 2004;103:2032-2038.
162. Castaman G, Lethagen S, Federici AB, et al. Response to desmopressin is influenced by the genotype and phenotype in type 1 von Willebrand disease (VWD): results from the European Study MCMDM-1VWD. *Blood.* 2008;111:3531-3539.
163. Bowen DJ and Collins PW. An amino acid polymorphism in von Willebrand factor correlates with increased susceptibility to proteolysis by ADAMTS13. *Blood.* 2004;103:941-947.
164. Keeney S, Grundy P, Collins PW, Bowen DJ. C1584 in von Willebrand factor is necessary for enhanced proteolysis by ADAMTS13 in vitro. *Haemophilia.* 2007;13:405-408.
165. Baldauf C, Schneppenheim R, Stacklies W, et al. Shear-induced unfolding activates von Willebrand factor A2 domain for proteolysis. *J Thromb Haemost.* 2009;7:2096-2105.
166. Berman HM, Westbrook J, Feng Z, et al. The Protein Data Bank. *Nucleic Acids Res.* 2000;28:235-242.
167. Hodis E, Prilusky J, Martz E, Silman I, Moulton J, Sussman JL. Proteopedia - a scientific 'wiki' bridging the rift between three-dimensional structure and function of biomacromolecules. *Genome Biol.* 2008;9:R121.
168. Flood VH, Gill JC, Morateck PA, et al. Common VWF exon 28 polymorphisms in African Americans affecting the VWF activity assay by ristocetin cofactor. *Blood.* 2010;116:280-6.

169. Wolff LJ, Wolff JA, Sebestyen MG. Effect of tissue-specific promoters and microRNA recognition elements on stability of transgene expression after hydrodynamic naked plasmid DNA delivery. *Hum Gene Ther.* 2009;20:374-388.
170. Kobayashi N, Nishikawa M, Hirata K, Takakura Y. Hydrodynamics-based procedure involves transient hyperpermeability in the hepatic cellular membrane: implication of a nonspecific process in efficient intracellular gene delivery. *J Gene Med.* 2004;6:584-592.
171. Amendola M, Venneri MA, Biffi A, Vigna E, Naldini L. Coordinate dual-gene transgenesis by lentiviral vectors carrying synthetic bidirectional promoters. *Nat Biotechnol.* 2005;23:108-116.
172. Franchini M and Lippi G. Acquired von Willebrand syndrome: an update. *Am J Hematol.* 2007;82:368-375.

## Appendix A

### VWF knockout mice have a low incidence rate of high-titre anti-VWF antibodies post-hydrodynamic injection

#### A.1 Summary

The transgene delivery system of hydrodynamic tail-vein injection using a liver-specific promoter for mouse VWF expression should minimize the host immune response in the VWF knockout mouse. This study uses a screening test for anti-VWF binding antibodies in mouse plasma to determine the rate and magnitude of antibody development. VWF knockout mice received wild type or mutant *Vwf* cDNA, and were monitored longitudinally. Of 34 wild type animals evaluated long term, a total of 10 tested positive. Mutant animals had a higher incidence rate, with R1597W the lowest (2 out of 13), followed by Y1605A/M1606A (2 out of 10) and Y1584C (4 out of 9), and R1205H being the highest at 7 out of 9. However, significantly, only two animals out of the 75 studied showed a strong response with an absorbance greater than 0.250. This absorbance value was much lower than that documented in plasma from mice receiving recombinant mouse VWF administered with Freund's incomplete adjuvant. In addition, antibody positive animals almost always had detectable VWF:Ag, normal VWF multimer structure, and functional VWF in a thrombosis injury model. These results suggest that the anti-VWF immune response is not affecting VWF expression, function or clearance in the majority of animals.

## A.2 Introduction

The success of gene therapy depends on whether the subject's body accepts or rejects the therapeutic gene product. Proteins that the body did not previously encounter are likely to be seen as foreign intruders. The fate of foreign proteins introduced by gene therapy is affected by a large number of factors.

These factors include:

- protein structure
- relative immunogenicity of the protein
- the method of gene delivery,
- cell types that take up and express the gene,
- amount of protein being produced,
- where the protein is expressed in the cell
- where the protein is secreted into the body,
- the genetic background of the host,
- the presence and degree of co-existent inflammation
- the intricate interactions between the protein, cells expressing it, and the host immune system<sup>169</sup>

Hydrodynamic injection of naked plasmid DNA via tail vein in mice is a method that utilizes hydrodynamic pressure to drive the transgene DNA primarily into cells in the liver,<sup>128, 129</sup> although additional expression is observed in other areas of the body, including the kidney, spleen, lung, and heart.<sup>170</sup> By using liver-specific promoters, this method decreases the likelihood of protein expression in antigen presenting cells present in the spleen. The hepatocyte-specific Enhanced murine Transthyretin (ET) promoter has been demonstrated to only express mRNA in the liver, rather than in sites that could produce a deleterious immune response.<sup>154, 171</sup>

This study determines the incidence and severity of the antibody-mediated immune response generated by plasma VWF via hydrodynamic injection of VWF transgenes regulated by the ET promoter. In addition, four mutations within the *Vwf* cDNA are examined to determine if these mutations prove to be more immunogenic than the wild type *Vwf* gene product.

### **A.3 Materials and Methods**

#### **A.3.1 Mice**

Mixed sex C57Bl/6 wild type mice (control animals) or VWF knock out mice<sup>116</sup> on a C57Bl/6 background (The Jackson Laboratory, Bar Harbor, ME, USA) were used in all experiments. All mouse experiments were reviewed and approved by the Queen's University Animal Care Committee.

#### **A.3.2 Hydrodynamic injections**

Plasmid DNA was diluted into lactated Ringer's solution in a volume equivalent to 10% body weight, and injected via tail vein in less than 7 seconds using a 27 gauge needle and 3 ml syringe. VWF knockout mice were both genders and were 8-9 weeks of age at the time of the injections. Wild type, and mutant R1597W, Y1605A/M1606A, R1205H, and Y1584C mice received 100 µg of pSC11-ET-mVWF plasmid.<sup>154</sup>

#### **A.3.3 Blood collection**

Blood was collected using a 70 µl untreated glass capillary tube via the retroorbital plexus under isoflurane/oxygen anesthetic using 10% buffered citrate as anticoagulant. Blood was centrifuged at 11,000g for 5 minutes to generate platelet poor plasma, and samples stored at -80°C until tested.

### **A.3.4 ELISA Assays**

VWF protein concentration (VWF:Ag) was determined by VWF enzyme-linked immunosorbent assay (ELISA) using polyclonal human VWF antibodies A0082 and P0226 (DAKO, Carpinteria, CA, USA). Mouse VWF concentrations were determined using a normal C57Bl/6 plasma pool, consisting of 25 normal eight week old C57Bl/6 mice, with the mean value arbitrarily determined to be 1 U/mL mVWF.

Anti-VWF binding antibodies were measured using an ELISA-based assay.

Recombinant mouse VWF, produced in HEK293T cells and secreted in serum-free medium, was diluted to 0.1 U/mL in 50 mM carbonate buffer, pH 9.6, and 100  $\mu$ l/ well was applied to Immulon 4HBX plates overnight. Plates were washed thrice with PBS (136.9 mM NaCl, 2.68 mM KCl, 10.14 mM Na<sub>2</sub>HPO<sub>4</sub>, 1.17 mM KH<sub>2</sub>PO<sub>4</sub>, pH 7.4)-0.1% Tween-20 wash buffer, and blocked in 2% BSA-PBS for 2 hours. Plates were washed thrice, and 100  $\mu$ l/ well mouse plasma, diluted 1:200 in sample diluent (100 mM HEPES, 100 mM NaCl, 10  $\mu$ M EDTA, 1% BSA, 0.1% Tween-20) was incubated for 2 hours. Plates were washed thrice, and 1:1000 dilution of horseradish peroxidase-conjugated polyclonal rabbit anti-mouse immunoglobulins in sample diluent was incubated for 1 hour. Plates were washed thrice, and developed using OPD (0.667 mg/ml in 34.7 mM citric acid, 66.7 mM Na<sub>2</sub>HPO<sub>4</sub>, 0.41  $\mu$ L/ml 30% H<sub>2</sub>O<sub>2</sub>, pH 5.0). Reactions were stopped at 20 minutes with 1 M H<sub>2</sub>SO<sub>4</sub>. Plates were measured at 492 nm wavelength on a VersaMax plate reader.

An additional comparative antibody control was run by coating wells with different dilutions of purified mouse immunoglobulin IgG rather than recombinant mVWF, and comparing the relative absorbance of plasma samples binding to recombinant mVWF against the known concentrations of the purified mouse immunoglobulins.

### **A.3.5 Control Plasmas**

Anti-VWF antibody positive control plasma was generated by injecting VWF knockout mice subcutaneously with 1 unit recombinant mouse VWF in 50 $\mu$ L Freund's incomplete adjuvant (Sigma, St. Louis, Mo), and harvesting plasma 3 weeks afterwards. Negative control plasma was from naïve normal C57Bl/6 mice.

### **A.3.6 Graphing and Statistical Analysis**

All data and statistical analysis was performed using GraphPad Prism 4.03 for Windows, GraphPad Software, San Diego, CA, USA, [www.graphpad.com](http://www.graphpad.com).

## **A.4 Results**

The anti-VWF antibody ELISA was run in parallel with the VWF:Ag ELISA. A total of 68 naïve C57Bl/6 mice were assayed, with a mean absorbance value of 0.01046, standard deviation of 0.00806, equivalent to 22.9 ng/mL mouse IgG. This generated the assay negative cut off value of 0.035, the mean absorbance value plus 3 standard deviations. The C57Bl/6 normal plasma pool (mean absorbance = 0.007931, equivalent to 21.6 ng/mL, n = 58,) and VWF FIA (mean absorbance = 1.630, equivalent to 4.48  $\mu$ g/mL mouse IgG, n = 56) were run as negative and positive controls respectively for the anti-VWF antibody ELISA on each plate (figure A 1).

VWF knockout mice received plasmid DNA containing the liver-specific ET promoter and mouse *Vwf* cDNA. This results in hepatocyte-specific expression of the mouse VWF protein, which very likely has an altered glycan content compared to normal endothelial and platelet-derived VWF. This transgene delivery method replaces only the plasma component of VWF content in the knockout animals. Mice receiving *Vwf* cDNA via hydrodynamic injection reached peak plasma VWF levels by day 2. These rapidly decayed to a stable plateau phase between days 14 and 42. Wild type mice had an average expression level greater than 1 U/mL until day 42. Of

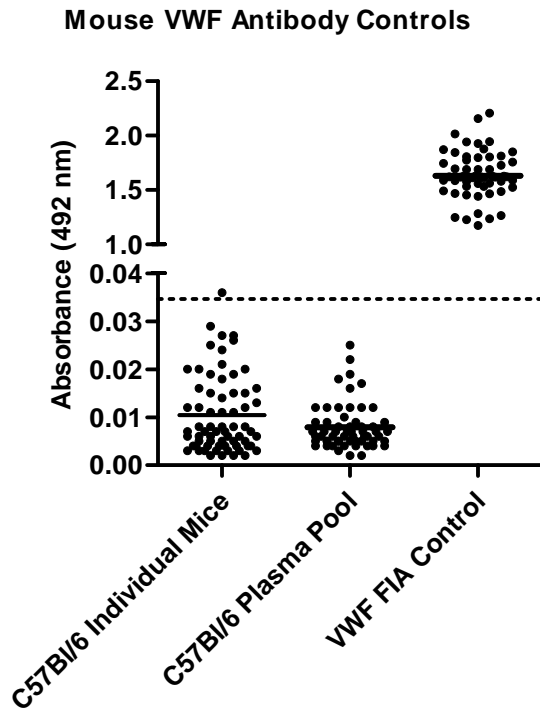


**Figure A 1 Anti-VWF antibody ELISA control plasma results.**

ELISA absorbance results for individual naïve C57Bl/6 mice, C57Bl/6 plasma pool, and positive control plasma from a VWF knockout mouse producing anti-VWF antibodies after receiving SC administered Freund’s incomplete adjuvant with recombinant mVWF protein (FIA). Circles represent individual results, and bars represent the mean. The dotted line at 0.035 absorbance represents the mean plus 3 standard deviations of the C57Bl/6 individual mice (n=56). Values above 0.035 were considered a positive result.

the 34 wild type VWF mice examined in the anti-VWF binding antibody assay, 10 tested positive for antibody (figure A 2). These mice had different profiles regarding antibody expression.

Transient positive results occurred in five animals, with only a single time point being above the negative cut off value of 0.035. One animal had a single positive result at day 14, and all other animals were negative until day 35 or later. Two additional animals only showed positive samples at 1 year or greater. Three animals showed sustained levels of anti-VWF antibodies at

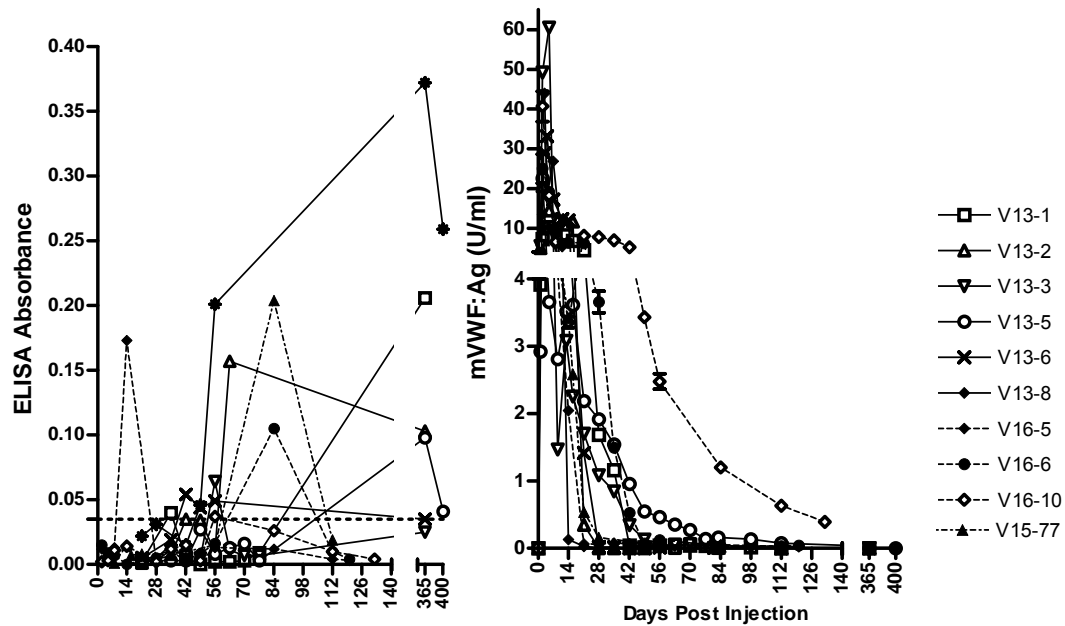


**Figure A 2 Anti-VWF antibody and VWF antigen levels for antibody-positive VWF<sup>(-/-)</sup> mice receiving wild type *Vwf* cDNA.**

Mice having ELISA absorbance values greater than 0.035 (represented as a dotted line) at any time point were considered positive. Each line with symbols represents an individual mouse.

multiple time points. Only V13-8 had absorbance values above 0.250, with a maximum absorbance of 0.372, equivalent to 745 ng/ml mouse IgG. Even this peak value is 4.4-fold lower than that of the FIA positive control plasma.

Four mutations in the *Vwf* cDNA were also examined. R1597W (n = 13) had two positive animals, Y1605A/M1606A (n = 10) had two positive animals, Y1584C (n = 10) was positive in 4 mice (figure A 3). Similar to that of mice expressing wild type VWF, most mice displayed only low level transient antibodies. Three mice had multiple days of positive samples. Only V14-80 (R1597W) had a strong response greater than 0.250, equivalent to approximately 750 ng/ml mouse IgG, that correlated with an abrupt loss of detectable VWF:Ag between day 14 and 21.

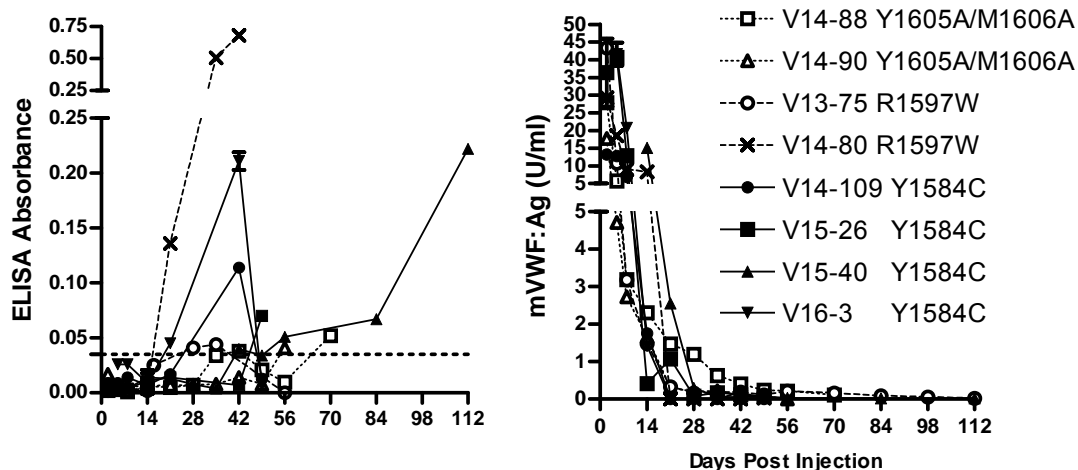


**Figure A 3 Anti-VWF antibody and VWF antigen levels for antibody-positive  $VWF^{(-/-)}$  mice receiving mutant *Vwf* cDNA.**

Mice having ELISA absorbance values greater than 0.035 (represented as a dotted line) at any time point were considered positive. Each line with symbols represents an individual mouse. Dotted lines represent Y1605A/M1606A mutants, dashed lines represent R1597W mutants, and solid lines represent Y1584C.

The type 1 Vicenza mutation, R1205H (n = 9) had the highest positive antibody rate with seven animals (figure A 4). However, no animal had an absorbance greater than 0.110 (330 ng/ml equivalent mouse IgG), 15-fold lower than the FIA positive control. All animals had decreasing antibody response at later time points while still having measureable VWF:Ag levels, and multimer results and a thrombosis injury response that were similar to wild type VWF expressing mice (see Figure 4.6 and 4.7).

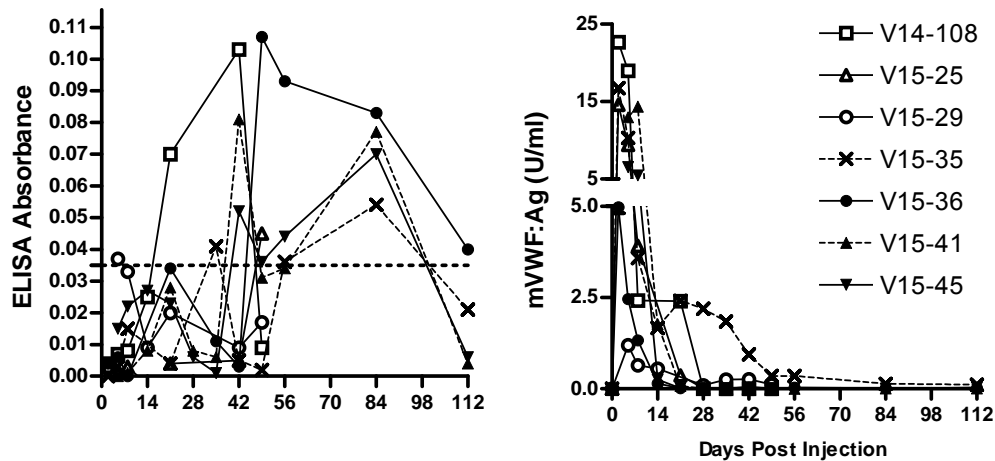


**Figure A 4** Anti-VWF antibody and VWF antigen levels for antibody-positive  $VWF^{(-/-)}$  mice receiving mutant R1205H *Vwf* cDNA.

Mice having ELISA absorbance values greater than 0.035 (represented as a dotted line) at any time point were considered positive. Each line with symbols represents an individual mouse expressing R1205H VWF protein.

## A.5 Discussion

The VWF knockout mice used in this study have a type 3 von Willebrand disease (VWD) phenotype with no detectable plasma VWF, and thus, their immune systems have not previously been exposed to the VWF protein. This leaves the animals with no central immunologic tolerance to the VWF protein, and a susceptibility to developing anti-VWF antibodies.

Wild type-expressing mice had a VWF binding antibody incidence of 8.8% by six weeks, the endpoint of data analysis for chapters 3 and 4 of this thesis. The four mutant proteins studied had higher incidence rates, but were studied in smaller numbers. The R1205H mutation had the highest positive rate, with 7 out of 9 animals developing antibodies. Only 2 out of the 75 total animals had a strong response with abrupt loss of VWF antigen. The remaining plasma samples

tested weakly positive in the anti-VWF antibody ELISA. This was frequently a transient response, and VWF:Ag was still present in most antibody-positive samples.

Due to the limited amounts of plasma remaining after running other assays, there was insufficient plasma to determine antibody isotypes or perform other analyses. Since the majority of animals had undetectable or low anti-VWF antibodies, along with continued VWF:Ag expression and normal VWF function, this suggests that this approach to gene delivery results in a relatively tolerogenic outcome. We suspect that promoter silencing is the most likely mechanism for the loss of VWF expression over time.

Acquired von Willebrand syndrome (aVWS) is a rare bleeding disorder caused by an underlying condition that mimics the congenital form of VWD. Patients have no previous bleeding problems, and produce antibodies against VWF. This can result in a variety of VWF abnormalities. In some patients, the phenotype mimics type 3 VWD with a loss of VWF antigen and lowered FVIII activity. In others, there is the appearance of a type 2A VWD multimer pattern, with loss of high molecular weight material as well as a marked decrease in VWF:Rco and a mild decrease or normal level of FVIII activity.<sup>172</sup>

The antibody-positive R1205H samples exhibited similar multimer patterns compared to wild type VWF, unlike that in patients with aVWS (Figure 4.6). Compared to antibody-negative wild type VWF-expressing animals in a thrombosis injury model, the R1205H expressing animals had no difference in their mean occlusion times. This suggests that the antibodies present did not alter VWF function (Figure 4.7). Since the animals in this study had no differences between antibody-positive and antibody-negative VWF levels or function, the immune response in these animals does not appear to mimic the aVWS disease. Overall, it would appear that our ELISA is detecting predominantly low titer VWF binding antibodies that have no in vivo consequence.

This study demonstrates that the incidence of high-titre anti-VWF antibodies is low in this transgene expression system. Only 2 out of 75 animals tested had antibody results with an absorbance value higher than 0.250. This suggests that the anti-VWF immune response is mild, and probably not the main cause of reduced transgene expression.

## Appendix B

### Thesis Protocols

- B.1. Calcium phosphate transient transfection of HEK293T cells
- B.2. VWF Antigen enzyme-linked immunosorbent assay (ELISA)
- B.3. VWF propeptide ELISA
- B.4. Anti- mouse VWF Antibody ELISA
- B.5. ADAMTS13 Activity ELISA

#### **B.1 HEK293T Calcium Phosphate Transfections**

Purpose: Produce recombinant VWF and ADAMTS13 for other applications.

Reagents: Solutions should be prepared fresh with tissue culture grade reagents and filter sterilized. The pH is very critical for this assay. Solutions can also be made and stored at -20°C.

##### **2X HEPES Buffered Saline (HBS) pH 7.15**

|                  |         |
|------------------|---------|
| 50 mM HEPES      | 0.595 g |
| 280 mM NaCl      | 0.815 g |
| H <sub>2</sub> O | 50 mls  |

pH to 7.15. Filter Sterilize 0.22 µm.

|  |         |
|--|---------|
| <b><u>0.07 M Na<sub>2</sub>HPO<sub>4</sub></u></b> | 0.497 g |
|--|---------|

|                  |        |
|------------------|--------|
| H <sub>2</sub> O | 50 mls |
|------------------|--------|

|                                    |        |
|------------------------------------|--------|
| <b><u>2 M CaCl<sub>2</sub></u></b> | 14.7 g |
|------------------------------------|--------|

|                  |        |
|------------------|--------|
| H <sub>2</sub> O | 50 mls |
|------------------|--------|

## **Day -1: Plating Cells**

Poly-L-Lysine coating to improve cell adhesion (optional but recommended)

Dilute 10 mg/ml Poly-L-Lysine (Sigma P7890) 1:100 in tissue culture grade water. Add 1.5 ml per 10 cm dish, swirl to coat. Incubate 1 hour, room temperature. Wash twice with tissue culture grade water or Hank's balanced salt solution (HBSS, Invitrogen) before plating cells.

Trypsinize cells by washing 2X with 10 ml HBSS and adding 1 ml trypsin. Let sit 2 minutes, add 10 ml DMEM/10%FBS to stop reaction. Pool cells together.

Centrifuge for 8 min at 1000g. Remove supernatant. Resuspend cells in DMEM/10%FBS.

Plate 2-4x10<sup>6</sup> HEK293T cells/100mm dish in 10 ml DMEM/10%FBS/1X P/S/1X L-Glutamine.

(Note: 2x10<sup>6</sup> in morning moving up to 4 x10<sup>6</sup> in the late afternoon-evening)

(COS-7 cells should be 0.5-1x10<sup>6</sup> cells/100mm dish.)

## **Day 0: Transfection**

Cells should be 50-75% confluent. Batch transfections can also be performed, multiply amounts as appropriate, and add 1 ml mix/10cm dish. Use pipette to bubble solution for >30 seconds.

### **1.5 ml DNA TUBES**

Total DNA: 20 µg, use calf thymus DNA to make up difference.

pβgal plasmid: 3.2µg

pCIneo-VWF, pcDNA3.1, etc.: 10 µg

Remember to have 1 negative control plate and 1 pβgal control plate.

Add 20 µg DNA to 1.5 ml eppendorf tube.

Add 440 µl sterile 0.1X sterile TE.

Add 62.5 µl 2 M CaCl<sub>2</sub> to tube. Flick hard to mix.

**5 ml HBS Phosphate TUBES Add:**

500 µl 2x HBS

10 µl 0.07M Na<sub>2</sub>HPO<sub>4</sub>

Add DNA mixture drop-wise to 5 ml tube, and bubble top to bottom at least 10 times.

Let sit 20 minutes. Mild milky appearance will form.

Add 1 ml transfection solution to plates slowly, gently swirl to mix. Medium will be more orange. Fine “grains of salt” precipitate will be visible at highest magnification under the microscope.

**Day 1: Medium Change**

\*No more than 17 hours remove medium.

Add 8-10 ml of 1X PBS (see recipe in B3), 1 mM EGTA to plates.

Wait 2 minutes, swirling periodically to remove precipitate. Aspirate off PBS. Add 10 mL OptiMEM (Invitrogen) with 1X ITS-G, 1X P/S.

**Day 4: Medium and cell harvest**

Pipette off medium into a 15 ml conical tube, labeled. Store at -80°C for later use.

Wash cells twice with 10 ml PBS.

Add 0.625 ml Lysis buffer (0.1 M K<sub>2</sub>HPO<sub>4</sub>, 0.2% TritonX-100, pH 7.8).

Use rubber policeman to scrape off cells into bottom. Pipette into 1.5 ml tube (approximately 1 ml lysate.)

Centrifuge 3 minutes 13,000 g, remove supernatant to fresh tube. Store lysate at -80°C.

## B.2 VWF Antigen ELISA Assay

Purpose: To determine VWF antigen levels in human and mouse plasma.

### Reagents:

**Coating Antibody:** Rabbit Anti-Human von Willebrand Factor, DAKO A0082.

**Detecting Antibody:** Rabbit Anti-Human von Willebrand Factor HRP, DAKO P0226.

**Human Standard Curve Plasma:** Human CryoCheck Reference plasma

**Mouse Standard Curve Plasma:** C57Bl/6 mouse plasma pool

**ELISA Plates:** Immulon 4 HBX, Dynex

This protocol is based upon DAKO recommended conditions. Buffers A, B, and C are stable at 4°C for 2 months. Check for growth before using. Reagent E is stable indefinitely.

### Buffer A: PBS, pH 7.2

10 mM Na<sub>2</sub>HPO<sub>4</sub>                      0.71 g Na<sub>2</sub>HPO<sub>4</sub> or 5 ml 1M solution

145 mM NaCl                      4.238 g NaCl or 14.5 ml 5M solution

500 ml with dH<sub>2</sub>O, pH 7.2

### Buffer B: Washing/Dilution Buffer, PBS 0.5 M NaCl, 0.1% Tween 20, pH 7.2

10 mM Na<sub>2</sub>HPO<sub>4</sub>                      0.71 g Na<sub>2</sub>HPO<sub>4</sub> or 5 ml 1M solution

500 mM NaCl                      14.61 g NaCl or 50 ml 5M solution

0.1% Tween 20                      0.5 ml Tween 20 (cut off end of tip for easier pipetting)

500 ml with dH<sub>2</sub>O, pH 7.2

### 10X Buffer B:

100 mM Na<sub>2</sub>HPO<sub>4</sub>                      8.52 g Na<sub>2</sub>HPO<sub>4</sub>

5 M NaCl                      175.32 g NaCl

1% Tween 20 \_\_\_\_\_ 6 ml Tween 20 (after pHing, will precipitate if hot)  
600 ml with dH<sub>2</sub>O      Microwave 2 minutes to dissolve. pH 6.15 for 1X pH 7.2.

**Buffer C: 0.1 M Citric Acid-Phosphate Buffer, pH 5**

0.0347 M Citric Acid              3.34 g Citric Acid

0.0667M Na<sub>2</sub>HPO<sub>4</sub> \_\_\_\_\_ 4.73 g Na<sub>2</sub>HPO<sub>4</sub>

500 ml with dH<sub>2</sub>O, pH 5.0

**OPD Color Reagent**

7.5 ml Buffer C

5 mg tablet OPD (o-Phenylenediamine) (Dissolve before adding peroxide)

3.1 µl 30% H<sub>2</sub>O<sub>2</sub>

**Stop Solution, 1 M H<sub>2</sub>SO<sub>4</sub>**

5.56 ml 95% H<sub>2</sub>SO<sub>4</sub>, 100 ml with dH<sub>2</sub>O

**Method:**

1. Dilute coating antibody in Buffer A to 10µg/ml. Rabbit Anti-Human von Willebrand Factor, DAKO A0082, 3.1 µg/µl    Add 100 µl/ well, Immulon 4 HBX plate (Dynex).  
Apply plate sealer and store 4°C, Overnight.
2. Dilute samples with Buffer B. Prepare standard curves with reference plasmas. Starting dilutions: Human 1:20, Mouse 1:5. Wash plate 3 times with >250 µL buffer B.
3. Add 100 µL diluted samples/well. Cover plate with plate sealer. Let sit room temperature for at least 2 hours. (4°C overnight if absolutely necessary). Wash plate 3 times with >250 µL buffer B.
4. Dilute detecting antibody Rabbit Anti-Human von Willebrand Factor HRP, DAKO P0226, 1.1 µg/µl, in Buffer B. For human VWF, 1:8000, For mouse VWF, 5 µg/µl. Add

100  $\mu$ l/ well and recover plate. Incubate at least 1 hour room temperature. Wash plate as above 3 times.

5. Add 100  $\mu$ l OPD Color Reagent/well. Cover plate and incubate 12-30 minutes, until standard curve is apparent. This takes ~10 minutes.
6. Stop reaction with 100  $\mu$ l Stop Solution.
7. Read results at 492 nm using the plate reader. 1 minute shake optional.

### **B.3 Mouse VWF Propeptide ELISA protocol**

Purpose: Determine Mouse VWFpp levels in mouse plasma.

Materials:

**Immulon 4HBX Plates** (Dynex)

**349.3 mouse VWFpp Antibody** (provided by Sandra Haberichter)

**349.2 Horseradish peroxidase-labelled VWFpp Antibody** (provided by Sandra Haberichter, HRP labeled in house.)

**Coating buffer** (50 mM Carbonate buffer): 1L

2.93 g NaHCO<sub>3</sub>

1.59 g Na<sub>2</sub>CO<sub>3</sub>

Fill graduated cylinder up to 1 L with dH<sub>2</sub>O, pH 9.6

**PBS pH 7.4** (136.9 mM NaCl, 2.68 mM KCl, 10.14 mM Na<sub>2</sub>HPO<sub>4</sub>, 1.17 mM KH<sub>2</sub>PO<sub>4</sub>)

32 g NaCl

0.8 g KCl

5.76g Na<sub>2</sub>HPO<sub>4</sub>

0.96g KH<sub>2</sub>PO<sub>4</sub>

4L total volume, pH 7.4

**Wash Buffer** (0.1% Tween 20-PBS):

**ELISA Block** PBS w/ 0.05% TWEEN 20 and 1% BSA

**1-Step Ultra TMB-ELISA detection** (34028, Pierce, Rockford IL, USA)

1. Coat Plate with 349.3 (1.3 mg/ml) at 2µg/mL in carbonate coating buffer; 100 µL/well.

Incubate at 4°C over night or over the weekend. Wash plate three times with 250  $\mu\text{L}$ /well ELISA wash buffer.

2. Block Plate with ELISA Block; 200  $\mu\text{L}$ /well. Incubate at least 60 minutes at room temperature. Wash plate three times with 250  $\mu\text{L}$ /well ELISA wash.
3. Plate antigen diluted in ELISA Block or DAKO Buffer B 100 $\mu\text{L}$ /well. Samples are diluted 1:50, standard curve is diluted two-fold starting at 1:5. Incubate at room temperature 2 hours. Wash plate three times with 250  $\mu\text{L}$ /well ELISA wash.
4. Plate Detection Antibody 349.2 HRP (0.5 mg/ml) at 1.0  $\mu\text{g}/\text{mL}$  (1:500) in ELISA Block; 100  $\mu\text{L}$ /well. Incubate at room temperature 2 hours. Wash plate three times with 250  $\mu\text{L}$ /well ELISA wash.
5. 1-Step Ultra TMB-ELISA detection (34028, Pierce, Rockford IL, USA) Plate 1-Step Ultra TMB solution (room temperature); 100  $\mu\text{L}$ /well Incubate 15-30 (~20) minutes, solution turns blue. (absorbs at 370 and 652 nm)
6. Add 1 M  $\text{H}_2\text{SO}_4$ , 100  $\mu\text{L}$ /well, solution turns yellow. (absorbs at 450 nm)
7. Read plate at 450 nm.

## **B.4 Anti-VWF Antibody ELISA Protocol**

**Purpose:** To determine the total anti-VWF antibody titre in mouse plasma.

### **Materials:**

Recombinant mouse VWF

Santa Cruz Mouse IgG 400ug/ml

Polyclonal Rabbit anti-mouse Immunoglobulins HRP (DAKO P0260)

OPD (o-phenylenediamine) substrate reagent

96-well microtiter **Immulon** ELISA plates – **4 HBX**

### **Buffers:**

**1. Coating buffer** (50 mM Carbonate buffer)

**2. Washing buffer** (0.1% Tween 20-PBS)

**3. Blocking buffer** (2% BSA-PBS)

**4. Sample Diluent 250 ml**

5.95 g HEPES

1.46 g NaCl

0.93 g EDTA

2.5 g BSA

2.5 mL 10% Tween-20

Final volume 250 mL dH<sub>2</sub>O, pH 7.2 with NaOH, store at -20°C

**5. OPD Color Reagent** (See protocol B.2)

**6. Stop solution** (1.0 M H<sub>2</sub>SO<sub>4</sub>)

**Method:**

1. Coat a 96-well microtiter plate with 100  $\mu\text{L}$  of recombinant mVWF (**0.1 U/mL**) per well diluted in coating buffer and incubate at 4  $^{\circ}\text{C}$  overnight. For positive control use **1  $\mu\text{L}/2\text{ml}$**  Santa Cruz Mouse IgG 400  $\mu\text{g}/\text{ml}$  = 200  $\text{ng}/\text{ul}$ , 1:3 dilution series, 8 points +blank. Coat last three with VWF as control blank, control medium, positive FIA plasma (V16-13 1-6). Wash plate 3 times with 250  $\mu\text{L}$  of wash buffer.
2. Block plate with 200  $\mu\text{L}$  of blocking buffer for 2 hours at room temperature. Wash plate 3 times with 250  $\mu\text{L}$  of wash buffer.
3. During the incubation in step 3, prepare plasma samples. Dilute plasma samples as required (Normally 1:200 final dilution) with sample diluent. Include C57Bl/6 normal plasma pool negative control and FIA plasma positive control. Load 100  $\mu\text{L}$  of plasma samples in duplicate to the plate. Incubate plasma samples for 2 hours at room temperature. Wash plate 3 times with 250  $\mu\text{L}$  of wash buffer.
4. Dilute Polyclonal Rabbit anti-mouse Immunoglobulins HRP-conjugated (DAKO P0260) in sample diluent, **1 : 1,000**. Add 100  $\mu\text{L}$  of this secondary antibody to each well. Incubate plasma samples for 1 hour at room temperature. Wash plate 4 times with 250  $\mu\text{L}$  of wash buffer.
5. Add 100  $\mu\text{L}$  of OPD color reagent to each well. Gently and evenly tap the sides of the plate to mix. Incubate for 20 minutes, room temperature.
6. Add 100  $\mu\text{L}$  of stop solution. Gently and evenly tap the sides of the plate to mix.
7. Read the optical density at 492 nm on a microplate reader.

## **B.5 ADAMTS13 Activity ELISA Protocol**

**Purpose:** To determine the total ADAMTS13 activity in a sample.

### **Materials:**

Recombinant ADAMTS13 and VWF73 (species specific: human or mouse)

PBS (See protocol B3)

Goat polyclonal GST antibody (Abcam ab6613), 10.0 mg/ml

Rabbit polyclonal VWF Carboxyterminal antibody (Abcam Ab47139)

Polyclonal anti-rabbit Immunoglobulins HRP-conjugated (DAKO P0448)

Protease Inhibitor Cocktail (Sigma P8340, stable 2 months 23°C, store stock at -20°C.)

OPD (o-phenylenediamine) color reagent

96-well microtiter **Immulon** ELISA plates – **4 HBX**

### **Buffers:**

**1. Coating buffer** (50 mM Carbonate buffer)

**2. PBS- 0.1% Tween Washing buffer**

**3. Blocking buffer** (2% BSA-PBS)

**4. ADAMTS13 Digest Buffer**

5 mM BisTris                      2.5 ml 1M

5 mM CaCl<sub>2</sub>                      2.5 ml 1M

0.005% Tween-20              250 µL 10% Tween-20

Final volume 250 mL dH<sub>2</sub>O,

**pH 6.0 at 37°C or 6.1 at room temperature with NaOH or HCl**, store at 4°C

Add 1:200 Protease Inhibitor Cocktail (Sigma, P8340) immediately before digest.

**5. OPD Color Reagent** (see protocol B.2)

**6. Stop solution** (1.0 M H<sub>2</sub>SO<sub>4</sub>)

**Method:**

1. Coat a 96-well microtiter plate with 100 µL of anti-GST antibody (**5 µg/mL, 1:2000**) per well diluted in coating buffer and incubate at 4°C overnight. Wash plate 3 times with 250 µL of wash buffer.
2. Block plate with 200 µL of blocking buffer for at least 1 hour at room temperature. Wash wells 3X 250 µL/well with PBS-T.
3. Coat with mVWF73 (1.95 mg/ml) or hVWF73 (1.61 mg/ml) at 0.5 µg/ml in PBS for 4-6 hours room temperature, or 4°C overnight. **Be sure to leave blanks (A12, B12).**
4. During the incubation in step 3, prepare plasma samples. Dilute plasma samples in ADAMTS13 digest buffer (1:100, but depends on the expected ADAMTS13 activity). Start standard curves at 1:10 (100 mU/ml). Wash plate 3 times with >250 µL of wash buffer PBS-T.
5. Load 100 µL of plasma samples in duplicate to the plate. Incubate plasma samples for 16 hours at 37°C. Wash plate 3 times with 250 µL of wash buffer PBS-T.
6. Dilute Rabbit polyclonal VWF Carboxyterminal antibody Ab47139 in 1:5000 PBS-T. Add 100 µL of this secondary antibody to each well. Incubate 1 hour room temperature. Wash plate 3 times with 250 µL of wash buffer PBS-T.
7. Dilute Polyclonal anti-rabbit Immunoglobulins HRP-conjugated (DAKO P0448) 1:1000 in PBS-T. Add 100 µL of this secondary antibody to each well. Incubate plasma

samples for 1 hour at room temperature. Wash plate 3 times with 250  $\mu$ L of wash buffer PBS-T.

8. Add 100  $\mu$ L of OPD color reagent to each well. Incubate for 20 minutes.
9. Add 100  $\mu$ L of stop solution. Gently and evenly tap the sides of the plate to mix.
10. Read the optical density at 492 nm on a microplate reader.